EFFECTS OF SURFACE ROUGHNESS AND ITS SPATIAL DISTRIBUTION ON RUNOFF HYDROGRAPHS

by
Yao-Huang Wu, Vujica Yevjevich, and
David A. Woolhiser

October 1978

HYDROLOGY PAPERS
COLORADO STATE UNIVERSITY
Fort Collins, Colorado

96

EFFECTS OF SURFACE ROUGHNESS AND ITS SPATIAL DISTRIBUTION ON RUNOFF HYDROGRAPHS

by
Yao-Huang Wu, Vujica Yevjevich, and
David A. Woolhiser

HYDROLOGY PAPERS
COLORADO STATE UNIVERSITY
FORT COLLINS, COLORADO 80523

October 1978

No. 96

TABLE OF CONTENTS

ACKNOWLEDGMENT

This paper is based on the Ph.D. dissertation by Yao-Huang Wu, with Dr. Vujica Yevjevich, Professor of Civil Engineering, serving as major professor and chairman of the graduate study committee. The other members of the committee were: Dr. David A. Woolhiser, Research Hydraulic Engineer, USDA-SEA-AR, and Faculty Affiliate, Civil Engineering Department; Dr. Ruh-Ming Li, Associate Professor of Civil Engineering; Dr. Thomas G. Sanders, Assistant Professor of Civil Engineering; and Dr. Duane C. Boes, Professor of Statistics. Professor Edmund F. Schulz helped Mr. Wu in his initial studies at Colorado State University and kindly guided his course work.

The major financial support for the research leading to this paper was provided by the Colorado State University Experiment Station Projects No. 1114 and 1124 on floods from small watersheds and on rainfall-runoff facility. The Agricultural Research Service, U.S. Department of Agriculture, provided partial support through a cooperative research program with Colorado State University on simulation of hydrologic systems.

ABSTRACT

This paper emphasizes both the selection of the hydraulic resistance model for surfaces of uniform roughness and the estimation of model parameters for hydrograph simulation of watersheds with nonuniform roughness.

The hydraulic resistance modeling of surface roughness is reviewed and discussed in detail. A three-parameter model for hydraulic resistance is designed by assuming a flow through a set of parallel random-width channels with equal water depth in these channels. Numerical methods for solutions of kinematic wave equations for the overland flow are used to simulate the outflow hydrographs of small watersheds. The two-parameter and the three-parameter surface roughness models are used in the optimization of model parameters. These two models are then compared by comparing deviations between the hydrographs simulated with the optimized parameters and the hydrographs observed at the Rainfall-Runoff Experimental Facility at Colorado State University. The results show that the three-parameter model describes more precisely the relationship between the discharge, Q, and the equivalent water depth, h, for various kinds of roughness over a wide range of discharge than does the two-parameter model, $Q=\alpha h^m$. The three-parameter model can be applied in the study of effects of changes in the land use on hydrographs, as well as to determine the precise estimate of sediment transport by the overland flow. When only the high flows of a hydrograph are important in hydrologic analysis, the two-parameter model as simpler and less expensive should be used in hydrograph simulation in comparison with the three-parameter model. The two-parameter model is recommended for high flow application.

Methods of estimation of the lumped parameters of the two-parameter model are in turn developed for watersheds composed of nonuniform roughness elements. For a watershed of nonuniform roughness in the flow direction, the lumped parameters can be estimated by selecting the values of parameters which can reproduce the equilibrium detention storage equivalent to the equilibrium detention storage produced by the watershed with nonuniform roughness. The linear uniformity of roughness in flow direction is much more important than the areal uniformity of roughness for achieving the equivalent uniformity. For a watershed of nonuniform roughness in transverse direction, the hydrographs can be simulated by combining the hydrographs produced by the individual elements.

Chapter I
INTRODUCTION

1.1 General Statement

A great number of factors affect the outflow hydrographs from a watershed, because hydrologic problems usually are very complex. Hydrographs specific to a particular problem can be predicted by using statistical or physically-based deterministic methods or by using a combination of these two methods. However, since too many factors are involved in the generation of a hydrograph, the watershed components are necessarily simplified and model parameters reduced to as few as possible according to accuracy required in practical uses. Physically-based deterministic models have a theoretical structure founded primarily on the laws of conservation of mass, energy, and momentum, and basin output hydrographs can be produced for known initial and boundary conditions and rainfall inputs. This can replace the black-box approach if the model is feasible. Physically-based models of watershed components invariably involve either ordinary or partial differential equations. The solution of these equations frequently requires the use of numerical methods. There have been advanced developments in physically-based deterministic models and in digital computer use in recent decades. During the simulation of hydrographs, adequate selection of the necessary model parameters and adequate simplification of the watershed components are important.

Surface runoff, such as overland or open channel flow, is an important part of the response of a watershed to rainfall. Floods from small watersheds are almost invariably caused by direct surface runoff from rainfall. Therefore, the design of flood control structures or nonstructural measures to reduce flood damage utilizes estimates of flood peaks for given frequencies. As many small rural and urban watersheds do not have discharge records, engineers usually utilize mathematical models along with rainfall data to produce runoff data. The type of hydraulic resistance models and model parameters play an important role in the simulation of the overland flow hydrographs, but the parameters must be determined experimentally. The configuration of natural watersheds is very complex and simplification of watershed components is required. Also, the number of components must be reduced; therefore a component within a watershed simulation model may include many kinds of surfaces with different roughnesses while experiments are mostly restricted to a single surface with a uniform distribution of surface roughness. In order to apply the experimental data to natural watersheds, the hydraulic resistance model must be selected and the representative overall parameters of simplified components estimated.

This study emphasizes both the selection of a hydraulic resistance model for a uniform surface and the estimation of parameters for watershed components which have spatially variable roughness.

1.2 Definition of Basic Concepts and Magnitudes

Surface Roughness

The magnitude, form, and distribution of roughness protrusions have been selected by previous investigators as the parameters of surface roughness for the study of flow over a plane. For a given form and distribution, the magnitude k of the roughness protrusions characterizes the surface conditions. For the natural roughness of most surfaces, k is a random variable and should be treated in statistical terms. In addition to the magnitude k, both the form and distribution of roughness are relevant parameters in describing the hydraulic behavior of flows over various surfaces. Since it is difficult to include all three of these parameters in the general flow formulation, the surface roughness in open channel flow is empirically expressed in the form of resistance coefficients, such as f, C, and n of the Darcy-Weisbach, Chézy, and Manning equations, respectively.

Uniform and Nonuniform Roughness

The roughness in a natural watershed varies with the type of land surface, obstructions and vegetation. Uniformity of roughness is defined herein with respect to a particular path on the watershed surface. If the roughness is a constant along a particular path, the surface is said to have uniform roughness in that direction; if not, it is nonuniform. In this study the uniformity of roughness is expressed in two paths: (i) the flow direction and (ii) the transverse direction, perpendicular to the flow direction. Figure 1-1 shows a scheme of various roughnesses along the flow direction, represented in terms of Manning's n. For the uniform roughness in flow direction the Manning's n is constant along the surface from upstream to downstream. The non-uniform roughness in the flow direction is classified as follows:

(1) Increasing roughness. When the density of vegetation increases in the flow direction, the roughness also increases.

(2) Decreasing roughness. When the density of vegetation decreases in the flow direction, the roughness also decreases. For a sparsely vegetated surface, rills are gradually developed as the water flows downward, with water flow concentrated in the rills of the downstream side, so that the roughness may decrease in downward direction.

(3) Alternating roughness. This kind of surface roughness is often encountered in the agricultural areas of alternating strip croppings for soil conservation purposes. The roughness changes alternatively according to the vegetated crop patterns.

(4) Irregular distribution of roughness. For land surfaces with irregularly distributed obstructions and vegetation, the roughness is also irregularly distributed.

To simulate hydrographs for a watershed with alternating roughness, the watershed can be modeled by a cascade of planes with uniform roughness within each plane. For a watershed with a gradual change or a random distribution of roughness, the watershed can be divided into planes of proper sizes, and the roughness of each plane approximated by a constant value. Usually, man-made experimental surfaces do not have gradual change of roughness, being mostly limited to surfaces of uniform roughness, or with a discrete nonuniform roughness, as shown in (1) and (4) of Fig. 1-1.

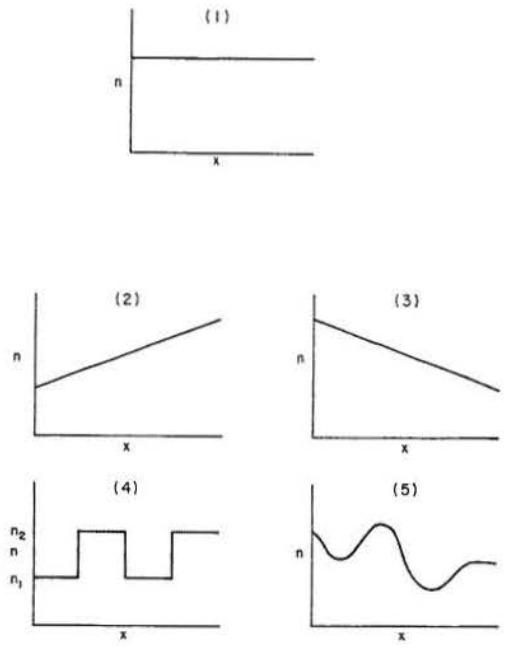

Figure 1-1. Uniform and nonuniform roughness patterns in the flow direction: (1) uniform; (2) increasing Manning roughness coefficient in flow direction; (3) decreasing Manning roughness coefficient in flow direction; (4) alternating (checkered) patterns; (5) irregular variation.

Uniform and nonuniform roughness in the transverse direction can be classified in the same manner as roughness in the flow direction.

Uniform and Nonuniform Roughness of Surfaces

The uniformity of roughness of a surface is classified as follows:

UFUT, meaning uniform roughness in the flow direction and the transverse direction.

UFNT, meaning uniform roughness in the flow direction and nonuniform roughness in the transverse direction.

NFUT, meaning nonuniform roughness in the flow direction and uniform roughness in the transverse direction.

NFNT, meaning the plane has nonuniform roughness in both directions.

This study uses data from an experimental watershed of conic section. Spatial variability was accomplished by utilizing two surface roughnesses--a smooth butyl surface and the butyl surface covered with gravel, subsequently called the butyl and gravel surfaces. Schematic drawings of the experimental watershed configurations are shown in Fig. 1-2. Some of the nonuniform arrangements of roughness surface are systematic while the others are random.

Equivalent Uniform Roughness

Equivalence of two watersheds with identical boundaries can only be defined in terms of their

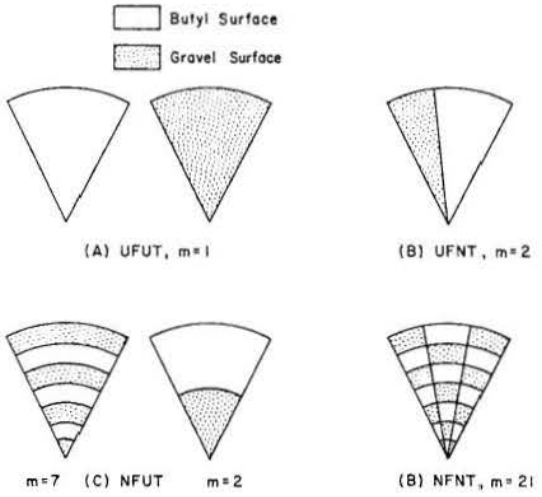

Figure 1-2. Various roughness arrangements on the conic-section surfaces with m = the number of elements.

response to identical rainfall input. Consider hydrographs from two watersheds, A and B, which are identical except that watershed A has nonuniform roughness and watershed B has uniform roughness. From these two hydrographs we can obtain the following index of goodness-of-fit,

$$G = 1 - \frac{D}{2a}, \qquad (1\text{-}1)$$

with G = the goodness-of-fit, D = the absolute value of the deviation of volumes between the two hydrographs from watersheds A and B, and a = the total volume of rainfall input, Fig. 1-3. Theoretically, the goodness-of-fit can be unity if the sizes of roughness elements in watershed A are infinitesimally small and the different kinds of roughness are alternatively arranged. However, from the practical viewpoint, watershed A can be considered as a watershed of uniform roughness if the two hydrographs nearly coincide.

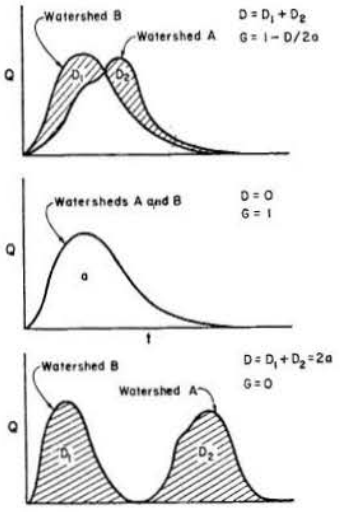

Figure 1-3. Goodness-of-fit measures for two hydrographs from uniform and nonuniform roughness watersheds.

It is conceived in this study that an equivalent uniform roughness exists for a watershed with nonuniform roughness if the hydrographs from both configurations are equivalent for identical rainfall excess patterns. Hydrographs will be considered equivalent when (1) the goodness-of-fit, G, is greater than G_e, and (2) the ratio of difference between hydrograph peaks to the peak of the uniform watershed is less than P_e, where G_e and P_e are the criteria to be used for defining equivalent uniform roughness and will be determined in this investigation. The equivalent uniform roughness may be determined from experiment or by simulation of hydrographs by mathematical models. However, determination by experiment is very time consuming and expensive and simulation of hydrographs by mathematical models is a convenient way to work.

Consider a watershed composed of elements of two kinds of roughness, described by Manning's coefficients n_1 and n_2. An element is defined in this study as a subarea of the watershed which has a defined shape and its surface roughness can be assumed as approximately or truely uniform over it. For NFUT surfaces, the flow is one dimensional because of uniform roughness in the transverse direction. The factors determining whether or not an equivalent uniform roughness exists are: (1) difference between two roughnesses, (2) relative area of two roughness surfaces, and (3) size of elements. The domain of equivalent uniform roughness with respect to those three factors is shown schematically in Fig. 1-4. With only two elements an equivalent uniform roughness can exist only if $n_1 \to n_2$ or the relative area of one roughness is too small to affect the total hydrograph. The locus of points represented by $n_1/n_2 = 1$ obviously defines a region of equivalent uniform roughness as do the left and right boundaries in Fig. 1-4. For a certain area ratio of two roughness surfaces, water flows through the alternate roughnesses more frequently and the hydrograph becomes equivalent to the hydrograph of a uniform surface when the number of elements is greater. The domain of equivalent uniform roughness is enlarged as the number of elements increases.

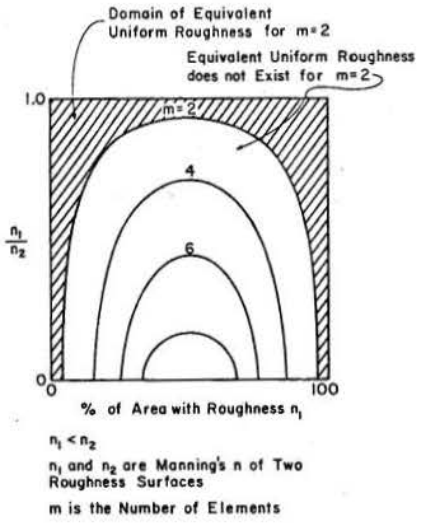

Figure 1-4. Schematic diagram of domain of equivalent uniform roughness.

For UFNT surfaces, it is assumed that the lateral flows will occur since the roughness is not uniform in the transverse direction and the differences in resulting water depths will create then a lateral water surface gradient. The factors affecting uniformity of roughness are the same as those in NFUT surfaces. When only one dimensional flow is considered, the outflow hydrograph from a UFNT watershed of conic section composed of numerous sectors is equivalent to the combination of hydrographs produced by two sectors of different roughness surfaces. The domain of equivalent uniform roughness is bounded by the curve of two elements as shown in Fig. 1-4 regardless of the number of elements. However, in the actual situation, it is postulated that lateral flows will occur and its effect becomes more significant as the size of sectors becomes smaller or the number of sectors increases. Because of mixing of flows from two roughness surfaces, the apparent uniformity of roughness is improved and the domain area increases as the number of elements increases.

It should not be expected often that a natural watershed would have a UFNT surface with numerous small elements of various roughnesses. When the size of elements is not small and the effect of lateral flows is not significant, the outflow hydrographs from UFNT surface can be easily simulated by a combination of hydrographs from various elements. In contrast, NFUT-like surfaces often occur in natural watersheds and the simulation of hydrographs is more complicated.

1.3 Scope and Objectives

Numerical methods for solutions of the kinematic wave equations for overland flow have been used extensively for simulating watershed outflow hydrographs. Before presenting the analysis of these methods, the hydraulic resistance laws are discussed. Alternative two- and three-parameter models for hydraulic resistance are proposed and are tested for their goodness-of-fit by comparing simulated hydrographs with observed hydrographs. Experimental data from the Rainfall-Runoff Experimental Facility at Colorado State University are used for these tests. Finally, the two-parameter model is selected as most feasible for the simulation of hydrographs. The methods of parameter estimation for watersheds with spatial variability of roughness are developed. The objectives of these investigations are:

(i) To select the simplest hydraulic resistance model that adequately describes overland flow for a watershed with uniform roughness in the flow direction and in the transverse direction (UFUT),

(ii) To develop criteria for determining the existence of an equivalent uniform roughness for a watershed with nonuniform roughness and to develop techniques to estimate the parameters for the equivalent uniform roughness, and

(iii) To develop methods for the application of the model to natural watersheds.

Chapter II
LITERATURE REVIEW

2.1 Analytical Models of Hydraulic Resistance on a Uniform Surface

Plane Surface

Many researchers have discovered that three flow regimes--laminar, transitional laminar-to-turbulent, and turbulent--exist in flows over relatively smooth plane surfaces. These regimes are often distinguished from one another by discontinuities in curves which show the relationship between the Darcy-Weisbach friction coefficient, f, and the Reynolds number, Re.

The theoretical equations of uniform laminar flow in open channels, in pipes and between two plates have the same form:

$$V = \frac{gR^2S}{c\nu} \quad , \tag{2-1}$$

with c = a constant, R = the hydraulic radius of flow passage, ν = the kinematic viscosity, g = the gravitational acceleration, and S = the slope of energy gradient.

The resistance to uniform turbulent flow is often expressed by one of the following equations:

Darcy-Weisbach $$S = f \frac{V^2}{8gR} \tag{2-2}$$

Chézy $$V = C\sqrt{RS} \tag{2-3}$$

Manning $$V = \frac{1.486}{n} R^{2/3} S^{1/2} \tag{2-4}$$

with f = the Darcy-Weisbach friction factor, C = Chézy's coefficient, V = the average velocity, and n = the Manning roughness coefficient. Actually, the Chézy formula has the same form as the Darcy-Weisbach formula.

Most investigators have related the Darcy-Weisbach friction coefficient to the Reynolds number. The Reynolds number equation is:

$$Re = \frac{VR}{\nu} \quad . \tag{2-5}$$

Because of difficulties in defining the hydraulic radius of flow passages over or through grass or stems, the water depth, y, has also been used instead of the hydraulic radius, R, in the relationship between f and Re for overland flow. Since the basic approximation made in the kinematic wave equation for overland flow is that the energy slope is equal to the bed slope, the bed slope is used for the energy slope in flow equations.

Numerous studies of hydraulic resistance in open channel and overland flow have been made. The equations for steady uniform laminar flow and for the Reynolds number on smooth surface, wide open channels are:

$$V = \frac{gy^2S}{3\nu} \quad \text{or} \quad S = \frac{3\nu V}{gy^2} \tag{2-6}$$

$$Re = \frac{Vy}{\nu} \tag{2-7}$$

with y = the water depth, equivalent to R. By equating Eq. (2-6) to Eq. (2-2) and making a substitution in Eq. (2-7) the following relation is obtained:

$$f = \frac{24}{Re} \tag{2-8}$$

Many investigators have shown the Darcy-Weisbach f in laminar flows to be

$$f = \frac{C}{Re} \tag{2-9}$$

with C = a constant depending on roughness, cross-sectional shape and channel slope. Theoretically, C = 24 for a wide, smooth-bed channel.

In the turbulent flow regime, the effect of the Reynolds number is smaller than in laminar regime, as the relative roughness becomes important. For low relative roughnesses (k/y small) and fixed rigid boundary conditions, Manning's n becomes practically independent of the water depth in the full turbulent regime. For a comparatively high relative roughness of the fixed rigid boundary condition, the friction coefficient is primarily a function of relative roughness.

Several investigators studied the transition from laminar to turbulent flow in an open channel with smooth boundaries. The critical Re has a considerable variation, from 300 to 1500. Apparently, other factors besides the Reynolds number influence the upper limit for viscous type flow, and the change is from a laminar to an intermediate regime rather than to a strictly turbulent regime (Kruse, et al., 1965; Parson, 1949). The transition regime is intermediate between the laminar and turbulent regimes, and the relationship between f and Re is rather unstable. In general, the range of Re for the transitional regime for rough surfaces is wider than for smooth surfaces. Chen (1976) showed f = C/Re is applicable up to Re = 10^4 for flow on natural turf surfaces which is equivalent to laminar flow.

The upper limit of flow equivalent to laminar flow can be defined in terms of the Reynolds number for which the relationship f(Re) starts to deviate from f = C/Re. It is called the critical Reynolds number. To the left of the discontinuity, the flow is equivalent to laminar; to the right, the flow is transitional, a mixture of laminar and turbulent. The flow with Re exceeding the upper bound of the transitional regime is then fully developed turbulent flow.

The following relationships are valid for open channel turbulent flow if Manning's equation is used:

$$f = \frac{8gyS}{V^2} = \frac{8gyS}{(1.486/n)^2 y^{4/3} S} = \frac{8gn^2}{1.486^2} y^{-1/3} ,$$

$$Re = \frac{Vy}{\nu} = \frac{1}{\nu} \frac{1.486}{n} y^{5/3} S^{1/2} ,$$

and $$f\, Re^{1/5} = \frac{8g}{\nu^{1/5}} \left(\frac{n}{1.486}\right)^{9/5} s^{1/10} . \qquad (2\text{-}10)$$

For flow over a constant slope, f is proportional to $Re^{-1/5}$, therefore, the f vs Re line on log-log paper has a slope of -0.2.

A schematic relationship of f vs Re is shown in Fig. 2-1. This is the model for laminar-turbulent flow on a plane with two parameters, C in f = C/Re and Rc, with Rc the Reynolds number of the transition. This model has been used by many investigators to simulate hydrographs for overland flow. For the Chézy equation, f is constant in the turbulent regime.

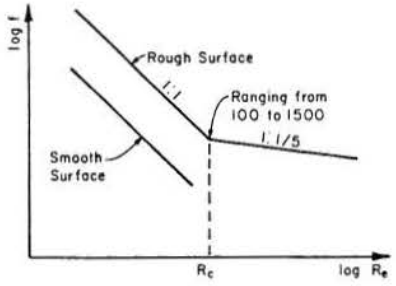

Figure 2-1. Relationship f vs Re for flows on a plane.

Upright Circular Cylinder on a Plane

In studying the effect of tall vegetation on flow and sediment, Li and Shen (1973) proposed a plane surface with vertical circular cylinders on the plane as an analogy. They concluded that the different patterns or groupings of tall vegetation have a significant effect on retardation of flow rates and sediment yields. Equations for the wake spread and decay derived by Petryk (1969) and the linear superposition of velocity effects were used to obtain the mean drag coefficient of individual cylinders among an array of cylinders in an open channel. The equation obtained for the drag force is

$$F_i = \frac{1}{2} \bar{C}_i \rho V_o^2 d\, y, \qquad (2\text{-}11)$$

in which Fi = the drag force for the cylinder at the i^{th} row, $\bar{C}i$ = the computed mean drag coefficient at the i^{th} row, ρ = the water density, V_o = the mean velocity, d = the diameter of cylinders, and y = the water depth. In deriving this equation, the drag coefficient for a single cylinder, C_d, was assumed to be 1.2, which is the drag coefficient for the range of the Reynolds number of 8×10^3 to 2×10^5. The results showed that $\bar{C}_i$ for a high order of rows (beyond the order of seven) tended to be a constant. It was 1.1 for the staggered array and 0.77 for the parallel array when spacing was ten times the cylinder diameter.

For a surface with unsubmerged obstructions the hydraulic resistance force which must be equal to the downslope water weight component consists of bed surface resistance force and drag force due to cylinders.

Porous Medium Flow

Henderson and Wooding (1964) suggested that overland flow over an impermeable surface would be included in one of the following three cases: (1) laminar flow, (2) turbulent flow, and (3) flow in a porous medium. The flow passing through closely growing plants may resemble type (3). They noted that in flow over clipped turf, the fluid motion near the base of the plants may qualitatively resemble type (3) while the motion above the plants may be better described by either type (1) or (2). Because of high hydraulic resistance, porous media flow will rarely reach turbulent range. For a uniform porous medium, the hydraulic radius of flow passage, R, in Eq. (2-1) is a constant regardless of water depth, y. If the energy gradient is approximated by the bed slope for overland flow, the velocity is constant and the Reynolds number, $\frac{Vy}{\nu}$, is proportional to the water depth, y. When y is substituted for R in Eq. (2-2) the Darcy-Weisbach coefficient, f, is also proportional to the water depth, y. The relationship of f vs Re will be a straight line with one to one increasing slope on log-log graph which is completely different from the relationship for flow over a hydraulically smooth plane surface.

Two Parameter Statistical Relationship

Because of viscosity, the flow in a system is either laminar or turbulent, or a combination of both. The selection of the discharge model for the laminar or turbulent flows, which will be used in the simulation of hydrographs, depends mainly on the range of the Reynolds number. For the flow covering a wide range of Reynolds numbers or discharges, both the laminar and turbulent regimes should be investigated. The flow equation can be expressed for either laminar or turbulent flows in the form

$$Q = \alpha h^m , \qquad (2\text{-}12)$$

with Q = the unit width discharge, h = the equivalent water depth (water storage expressed in depth), m = a constant of 3 for the laminar flow and 1.5 (Chézy) or 1.67 (Manning) for the turbulent flow in a wide open channel and 1.0 for the porous media flow, and α = a constant depending on slope, surface roughness and shape of cross section. For the flow at a plane surface, the m value can be fixed in both the laminar or turbulent flow with only a parameter, α, remaining. However, if the flow of interest is mainly in the range of transition or combination of the laminar, turbulent and porous media flow, the m value is between 3.0 and 1.0, and it cannot be fixed in advance. Equation (2-12) is a two-parameter model with two unknown parameters, α and m, which are statistically estimated from the observed hydrographs of a watershed.

2.2 Experimental Investigation

Izzard (1944) concluded from a series of experiments that C for shallow flows over paved and turf surfaces departs significantly from the

theoretical value of 24. With a paved surface, he found values for C other than 24, such as 27, 40 and 58, for various bed slopes and rainfall intensities tested. For a turf (Kentucky Blue grass) surface, he obtained C as high as 10,000, which is a few hundred times greater than values for paved surfaces.

Woo and Brater (1961) studied the effect of channel slope on C. For a masonite surface, with 11 channel slopes ranging from .001 to .006 tested, the C values obtained were all approximately equal to 30.8. However, for a glued-sand surface, C increases with an increase of the slope. They also analyzed the data of the Corps of Engineers Laboratory in Vicksburg, Mississippi, for various packed-sand and cement surfaces and found that the finest sand surface acts as a very smooth surface with C = 24, whereas C for the other six sand surfaces are larger than 24, with the largest C being for the roughest sand surface. The ranges of critical Reynolds number were 400 to 900 for the masonite surface, 400 to 800 for the sand surface, and 500 to 1000 for the Vicksburg data. This range varied inversely with the slope.

Emmett (1970) conducted experiments on a smooth plane surface of uniform sand-grain roughness with a median grain diameter of .50 millimeters in a laboratory flume with adjustable slope. From the flow experiments without artificial rainfall, he concluded that extremely shallow uniform flows were characterized by laminar flow at Reynolds numbers of less than 350 (or somewhat greater) and turbulent flow at Reynolds numbers higher than 1,500 (or somewhat smaller). A transitional flow exists between the laminar and turbulent flows. For laminar flow with constant slope, the Darcy-Weisbach friction factor, f, decreases inversely proportional with an increase of Reynolds number, Re. For the turbulent flows, f decreases only slightly with an increase in Re which agrees with the Manning equation. Absolute resistance to flow depends on the magnitude of relative roughness of flume surface. For shallow flow depths, with uniform simulated rainfall over the flume, all flows were in the laminar regime as defined by the Re criterion established for the uniform flow tests without rainfall. However, the flow was not truly laminar, because of the effect of falling raindrops. For disturbed flow compared to uniform flow, Emmett found the falling raindrops roughly double the resistance to flow.

Kouwen and Unny (1973), using flexible plastic strips to simulate a vegetated open channel, studied the variation of relative roughness with respect to the stiffness of vegetation. Two widths of the plastic strips were 0.5 cm and 0.75 cm. In experiments with the 0.5 cm plastic strips the space between these strips was 0.5 cm, while the space between the 0.75 cm plastic strips was 0.75 cm. Spaces between the rows were 2.0 and 3.0 cm, respectively. Three basic flow regimes: erect, waving, and prone, were observed. In the erect regime the plastic strips were erect and stationary; in the waving regime the strips underwent a waving motion; in the prone regime the strips were bent over. The plot for the erect and waving regimes of the Darcy-Weisbach f versus Re show that f is mainly a function of the relative roughness, being independent of Re. For k/y = 1 (k = the deflected height of roughness elements, y = the normal depth), f was about 35 for the experiment range of Re between 1000 to 3000.

From experiments on steady uniform flow over a simulated turf surface Phelps (1970) found a marked dissimilarity between the friction coefficient-Reynolds number relationship for the flow over the turf at different depths, when there was only a partial submergence of surface elements. The relative water depth (y/d, y = the mean depth, d = the representative length dimension of the flow passage between leaves) influenced the friction coefficient in the laminar range, namely the friction coefficient increased with an increase of the relative water depth for a constant Reynolds number. For a constant depth of laminar flow, the product C = fRe was not constant, but decreased as Re increased. This result might be explained by postulating changes in the boundary geometry which means that the flexible elements respond to changes in mean velocity. The critical Reynolds number at the upper limit of laminar flow ranging from 100 for y/d in the range 1.39-1.43 to 750 for the maximum y/d of 4.68-4.71.

Chen (1976) conducted a series of experiments in the laminar range for flow on surfaces with a maximum density of Kentucky Blue grass and on surfaces with a maximum density of Bermuda grass. The bed slope ranged from .1 percent to 1:1.5. The value of f for laminar flow on the turf surface is a few orders of magnitude higher than the value of f on the glued-sand surface. A best fitting line for each slope was drawn through data points to parallel the theoretical line of f = 24/Re. The relationship between C and S for a given turf was drawn on log-log paper. It appeared that a straight line can be fitted. The f value increases with an increase of bed slope. The friction coefficient for shallow flow over the natural surface was expressed as $f = 510{,}000\ S^{.662}/Re$.

Kowobari, et al. (1970), by using different arrangements of 3/32 and 9/32 inch diameter upright aluminum rods on a 44 ft long by 18 inch width flume, studied the relationship of the Manning's resistance coefficient to the size of roughness elements, the pattern of arrangement and the density of rods. The depth of flow in the channel was such as to keep the roughness element unsubmerged for a better understanding of the retardation for flow through upright rods. They concluded that the resistance to flow decreases with an increase of the discharge under smooth channel conditions, but that it increases with an increase of the discharge when the channel contains the roughness elements. The Reynolds number in this experiment ranged from 700 to 20,000.

From the above literature review, the previous investigators obtained, in general, f·Re = constant, which is valid for the laminar flow in wide open channels. However, C = f·Re increases with an increase of roughness. Woo and Brater (1961) showed that C increases with an increase of the channel slope for the flow over glued-sand surfaces, while Chen (1976) showed the same phenomena for the flow over turf surfaces. All the previous investigators used the water depth for R in the Darcy-Weisbach equation and the Reynolds equation (Eqs. 2-2 and 2-5). Most flows on turf surface are in laminar and transition regimes. Only the experiment conducted by Kowobari, et al. (1970) for a surface with rigid upright stems showed that the resistance to flow increases with an increase of the discharge. This is reasonable if the upright elements are not flexible.

2.3 Kinematic Wave Theory

Theory and Analytical Solution for the Rectangular Plane

As shown in Fig. 2-2, a plane of unit width, length L_o, and slope S_o, receives rainfall at a rate $i(x, t)$ per unit area, which is a function of distance x and time t. Water is infiltrating at the rate $i_r(x, t)$. The net lateral inflow is $q(x,t) = i(x,t) - i_r(x,t)$. For simplification of analysis, i is assumed constant, with experiments conducted for an impervious plane. In this case, the lateral inflow is a constant i. Flow is assumed to be one-dimensional, and the dependent variables are the local mean velocity, V, and the local depth, h. The continuity and momentum equations are

$$\frac{\partial h}{\partial t} + \frac{\partial (Vh)}{\partial x} = i(x, t) \qquad (2\text{-}13)$$

$$\frac{\partial V}{\partial t} + V \frac{\partial V}{\partial x} + g \frac{\partial h}{\partial x} = g(S_o - S_f) - i(x,t) \frac{(V - V_\ell)}{h} \qquad (2\text{-}14)$$

with Sf = the friction slope, and V_ℓ = the x-component of the velocity of the lateral inflow. V_ℓ is zero when the downward momentum introduced by rainfall is negligible, and the velocity component of the rainfall in the x-direction is assumed to be zero. The usual basic assumptions, that the sine of the slope angle, θ, is approximately equal to the tangent and that the velocity distribution coefficient, β, is equal to one, are also applied herein.

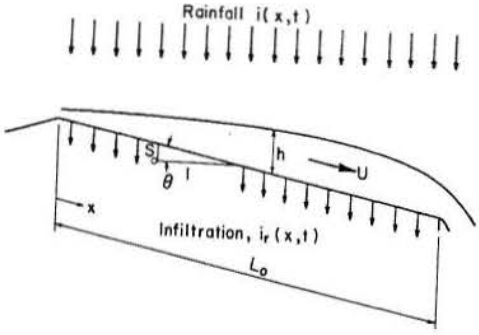

Figure 2-2. Definition sketch of overland flow on a plane.

In the kinematic wave approximation of overland flow, all terms in the momentum equation, except the term involving the bed slope and friction slope, are assumed to be negligible. Equation (2-14) then becomes

$$S_f = S_o. \qquad (2\text{-}15)$$

If the bed slope is constant, the friction slope over the plane must also be constant. Then the unit width discharge and the velocity equations can be written as Eq. (2-12),

$$Q = \alpha h^m \quad \text{and} \quad V = \alpha h^{m-1} \qquad (2\text{-}16)$$

Equation (2-16) can be substituted in Eq. (2-13) to produce a partial differential equation with one dependent variable

$$\frac{\partial h}{\partial t} + \alpha \frac{\partial h^m}{\partial x} = i(x, t) \qquad (2\text{-}17)$$

or

$$\frac{\partial h}{\partial t} + \alpha m h^{m-1} \frac{\partial h}{\partial x} = i(x, t). \qquad (2\text{-}18)$$

The total differential of h(x, t) is

$$dt \frac{\partial h}{\partial t} + dx \frac{\partial h}{\partial x} = dh. \qquad (2\text{-}19)$$

It may be assumed that the flood wave is composed of infinitesimal discontinuous surges (Chow, 1959), and the values of $\partial h/\partial x = 0/0$ and $\partial h/\partial t = 0/0$. The characteristic equations are

$$\frac{dx}{dt} = \alpha m h^{m-1} \qquad (2\text{-}20)$$

and

$$\frac{dh}{dt} = i(x, t) \qquad (2\text{-}21)$$

Let us consider the simple case of a spatially invariant rainfall on an impervious surface, beginning at a constant rate, i, at time t = 0, and continuing until an equilibrium condition is reached, and boundary conditions of h(0, t) = 0 and h(x, 0) = 0. The discharge equations for the rising limb of the hydrograph and at the equilibrium can then be obtained by integration as (Woolhiser, 1975)

$$Q = \alpha(it)^m \; ; \quad 0 \le t \le \left(\frac{L_o}{\alpha i^{m-1}}\right)^{1/m} = t_e$$

$$Q = iL_o \; ; \quad \left(\frac{L_o}{\alpha i^{m-1}}\right)^{1/m} < t < t_o \qquad (2\text{-}22)$$

in which L_o = the length of the plane, Q = the outflow discharge per unit width, te = time to equilibrium, and to = duration of rainfall. The hydrograph of the recession from the equilibrium can be found by assuming that at some time, $t_o > t_e$, the inflow ceases. The relationship between discharge and time for the recession becomes

$$Q - iL_o + im\alpha^{1/m} Q^{\frac{m-1}{m}} (t - t_o) = 0 \; ; \quad t_o < t. \qquad (2\text{-}23)$$

When the duration of rainfall is shorter than the equilibrium time, a partial equilibrium hydrograph results. Supposing that rainfall begins at rate i at t = 0, and continues until t = D, the relationships between discharge and time are (Woolhiser, 1975)

$$Q = \alpha(it)m; \quad 0 \le t \le D$$

$$Q = \alpha(iD)^m; \quad D \le t \le D + \frac{L_o(iD)^{1-m}}{\alpha m} - \frac{D}{m} \qquad (2\text{-}24)$$

$$Q - iL_o + im\alpha^{1/m} Q^{\frac{m-1}{m}} (t-d) = 0; \; D + \frac{L_o(iD)^{1-m}}{\alpha m} - \frac{D}{m} < t$$

The above equations are for the case in which α and m are constant over the plane and invariant for all depths.

Numerical Methods for Solving the Kinematic Equation and Its Application on a Conic Section

Although the kinematic wave equations can be solved analytically for constant values of α and m, numerical solutions are more convenient when i, α and m are not constants over the area and time. Kibler and Woolhiser (1970) compared three finite-difference schemes, namely single step Lax-Wendroff, upstream differencing, and Brakensiek's four-point implicit schemes, for the kinematic wave equations with the input pulse duration equal to the time to reach equilibrium on the two-plane cascade. The result showed that the second-order Lax-Wendroff method gives the best approximation. For experimental watersheds or plots that have geometries other than a plane, the use of the kinematic cascade to simulate surface runoff may also be applied. Kibler and Woolhiser (1970) compared the kinematic cascade solution with the kinematic solutions for a conic section by using the second-order Lax-Wendroff scheme. In approximating the converging section, two variables, the number of rectangular cascade planes, n, and the number of Δx increments in each plane, B, were used (Fig. 2-3). The examination showed that the error index decreased as nB increased for any n, but that very little accuracy was gained by increasing nB from 15 to 20. In general, the results indicated that the kinematic cascade approach effectively reduces the geometric complexity and accurately simulates the overland flow derived from rather complex shapes.

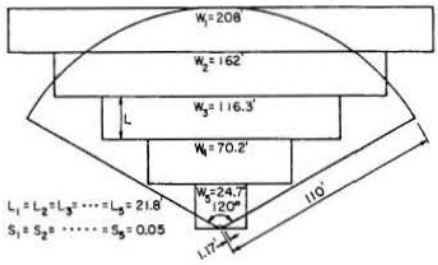

Figure 2-3. Cascade approximation of converging section (after Kilber and Woolhiser, 1970).

2.4 Parameter Estimation Techniques

If the two-parameter model, $Q = \alpha h^m$, is effective over the plane watershed, i.e., α and m are constant through the flow direction, the values of parameters can be easily estimated from experiments (Woolhiser, 1975). The steady-state detention storage can be measured experimentally by integrating the measured recession hydrograph. The mean detention depth, $\bar{h}$, can be also analytically expressed as:

$$\bar{h} = \frac{1}{L_o}\int_o^{L_o} \left(\frac{ix}{\alpha}\right)^{1/m} dx = \left(\frac{i}{\alpha}\right)^{1/m} \left(\frac{m}{m+1}\right) L_o^{1/m}. \qquad (2\text{-}25)$$

Substituting measured detention storage for $\bar{h}$ and using the assumed value of m in Eq. (2-25), α can be obtained.

The α and m can also be simultaneously estimated from the rising hydrograph from a plane surface for a constant lateral inflow rate. Equation (2-22) shows that $Q = \alpha(it)^m$ for the rising limb of the hydrograph. If Q and t obtained from experimental data are plotted on logarithmic graph paper, α and m can be obtained graphically.

For experimental watersheds or plots, geometries are usually other than a plane, the hydraulic resistance model has a complex form and the rainfall excess rate is time-varying. The rising hydrograph and the equilibrium detention are, therefore, very complex and optimization techniques must be utilized for parameter estimation. In this method the hydraulic resistance model is assumed and starting parameter values are estimated. Equation (2-18) is then solved numerically and an objective function is evaluated. The parameters are then adjusted by some optimization scheme until the objective function is minimized.

Two objective functions which are frequently used are:

A. Sum of Squares of Deviations:

$$F = \sum_{i=1}^{n} [Q_o(i\Delta t) - Q_c(i\Delta t)]^2 \qquad (2\text{-}26)$$

with F = the objective function, with the subscripts o and c referring to observed and computed discharge, respectively, and Δt = a fixed time increment. F is the function of parameters in the hydraulic resistance model. Mathematically speaking, equal weights are placed on all of the observations. However, since the absolute difference between the estimated value and the observed value is usually greater for the observation with a greater quantity, in reality, a greater weight is placed on high flows.

B. Sum of Square of Logarithms of Deviations:

$$F = \sum_{i=1}^{n} [\log(Q_o(i\Delta t) - \log(Q_c(i\Delta t))]^2 \qquad (2\text{-}27)$$

$$= \sum_{i=1}^{n} [\log \frac{Qo(i\Delta t)}{Q_c(i\Delta t)}]^2$$

This second objective function transfers the difference between the observed and calculated discharge to their ratio. The estimated errors on all points are more nearly equal in percentage than in absolute values. This is desirable when the small observed values are equally as important as the large values.

For the hydrograph study, the flood peak may be more important than the low flows. Therefore, the sum of squares of deviations is often used for the objective function.

Ibbitt (1970) reported nine optimization echniques applicable to hydrologic models. He concluded that Rosenbrock's method (1960) was the best to use. This method is an iterative procedure in which small steps are taken during the search in orthogonal coordinates. Instead of continually searching the coordinates corresponding to the directions of the independent variables, an improvement of the search is made after one cycle of coordinate search, by lining the search directions up into an orthogonal system, with the overall step of the previous stage as the first building block for the new search coordinates.

Simons and Li (1976) modified Rosenbrock's method by coupling Powell's unidimensional minimization (1964, 1965) and by considering the constrained minimization problems. They noted that the number of function evaluations for the Rosenbrock's function was reduced to 30 in their approach in comparison with the 206 function evaluations needed in the original Rosenbrock's method.

Chapter III
THREE-PARAMETER VERSUS TWO-PARAMETER MODEL FOR HYDRAULIC RESISTANCE

3.1 Three-Parameter, Parallel Channel Model with Random Widths

In this section a model of parallel channels with random widths is proposed as a better physical analogy of flow over natural vegetated surfaces than the commonly assumed plane. As a simple approximation, channels are assumed random with a negative exponential width distribution (Fig. 3-1). Fundamentally, the Boussinesq equation is used for the laminar flow and Manning for the turbulent flow. In 1868, Boussinesq derived the velocity equation of laminar flow for smooth surface with respect to x, y coordinates in a rectangular pipe. Because the flow pattern in a rectangular pipe is symmetrical about the horizontal center line, the Boussinesq equation may be applied to a rectangular channel of width b and depth y to obtain the following expression for the average velocity (Woo and Brater, 1961).

$$V = \frac{gSy^2}{3\nu}\left[1 - \frac{384}{\pi^5}\,\frac{y}{b}\sum_{n=1}^{\infty}\frac{1}{(2n+1)^5}\tanh\frac{2n+1}{4}\frac{\pi b}{y}\right] \tag{3-1}$$

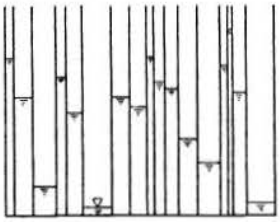

Figure 3-1. Random width parallel channel model.

For a channel of infinite width, Eq. (3-1) reduces to Eq. (2-6)

$$V = \frac{gSy^2}{3\nu}\,.$$

Woo and Brater (1961) evaluated the importance of side wall effect by

$$k = 1 - \frac{384}{\pi^5}\,\frac{y}{b}\sum_{n=1}^{\infty}\frac{1}{(2n+1)^5}\tanh\frac{2n+1}{4}\,\frac{b}{\pi y} \tag{3-2}$$

$$V = k\,\frac{gSy^2}{3\nu}\,, \qquad S = \frac{3\nu V}{kgy^2}$$

with $k = 1$ for $b = \infty$ and $k < 1$ for $b < \infty$. Equating Eqs. (2-2) and (3-2) gives

$$f = \frac{24\nu}{kVy} = \frac{24}{k}\,\frac{1}{Re} = \frac{C}{Re} \tag{3-3}$$

where

$$C = \frac{24}{k} \tag{3-4}$$

Various values of C were plotted against b/y as shown in Fig. 3-2, from which the effect of side walls can be estimated. For example, for b/y = 25, C differs from 24 by less than 5 percent.

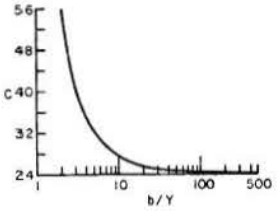

Figure 3-2. Variation of C with b/Y (after Woo and Brater, 1961).

One can use Eq. (3-1) for calculating the discharge of individual channels with smooth surface in a set of isolated channels separated by infinitesimally thin walls as shown in Fig. 3-1.

As an example, the following assumptions were made: S = 0.005, ν = 0.00001, L = length of channels = 1000 ft. The Boussinesq equation is assumed valid in laminar regime for Re < 600, and the Manning equation in turbulent regime for Re > 600 (Re = VR/ν). Manning's n for an individual channel is determined by substituting discharge and depth obtained from the Boussinesq equation at Re = 600 in the Manning's equation, and is assumed constant for Re > 600.

Single Rectangular Channel

The f vs Re (=Vy/ν) relationships have been computed in this study for single rectangular channels with widths of 1/5, 1/10, 1/25, 1/50, 1/100 and 1/200 ft. Results are plotted on a log-log graph paper in Fig. 3-3.

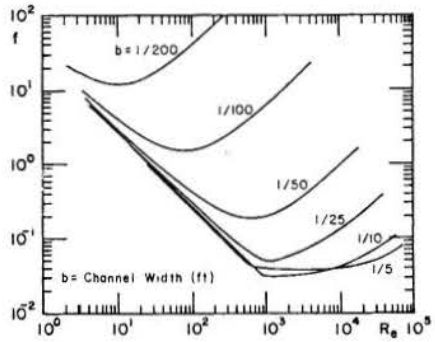

Figure 3-3. Relationship f vs Re for a single channel.

For a single channel of 1/5 ft width, the channel is relatively wide and the Reynolds numbers Re = Vy/ν are close to Re = VR/ν. Since the Manning equation is assumed to be valid for Re = VR/ν exceeding 600, the f vs Re curve deviates from the straight line of the laminar flow regime at around Re = Vy/ν = 600. For the channel of 1/10 ft width, even though Re = Vy/ν exceeds 600, Re = VR/ν is still less than 600 and the

transition occurs at about $Re = Vy/\nu = 850$. All computations have been made up to the depth of .32 ft. Within this range, all the flows in the channels of width less than 1/50 ft are laminar. Because of the narrow width of channels, the velocity increases much more slowly with an increase of the depth. For high Reynolds numbers, V is almost constant with an increase of y. This is the reason why the friction factor $f = 8gSy/V^2$ increases with an increase of y at high Reynolds numbers.

Model of Isolated Parallel Channels

The relationships of f vs Re are obtained from the rising limb of hydrographs of 100 random-width channels by using the kinematic wave equation. Rainfall intensity, i, is assumed to be constant and equal to 1 in/hr. The distribution of the width is assumed to be a negative exponential,

$$f_B(b) = \lambda e^{-b\lambda}, \quad \mu_B = \frac{1}{\lambda} \text{ (ft)} \qquad (3\text{-}5)$$

One hundred random values are considered sufficient for simulating a negative exponential distribution. This distribution seems well fitted, since widths of natural rills or spaces between obstructions for a natural vegetated watershed have high densities of small widths. The average velocity V and the average depth y of 100 channels at outlets are used in calculating f and Re. The analytical solution of kinematic wave equations for the rising limb of hydrographs gives:

$$y_{it} = it, \quad \text{for } t < t_{eqi} \qquad (3\text{-}6)$$

then, $Q_{it} = f(y_{it}, b_i)$, where f is given by Boussinesq, Eq. (3-1) if $Re = VR/\nu < 600$ or by the Manning Eq. (2-4) if $Re > 600$. The subscript "it" is for the i^{th} channel at time t; the subscript "eqi" is for the equilibrium of flow in the i^{th} channel. The equilibrium discharge in the i^{th} channel is then

$$Q_{eqi} = i\, b_i\, L. \qquad (3\text{-}7)$$

Since Q_{eqi} is known, y_{eqi} can be determined from the flow equation. Time to equilibrium is $t_{eqi} = y_{eqi}/i$, and the depth and discharge will be constant after the time of equilibrium. For determining f and Re at time t, the following equations are used.

$$Q_t = \sum_{i=1}^{100} Q_{it}, \quad Y_t = \frac{\sum_i^{100} b_i\, y_{it}}{\sum_i^{100} b_i}, \quad V_t = \frac{Q_t}{Y_t \sum_1^{100} b_i}$$

$$f = \frac{8gSY_t}{V_t^2}, \qquad Re = \frac{V_t\, Y_t}{\nu}.$$

Therefore, a series of f vs Re can be determined for different times t. The λ's of the negative exponential distribution are assumed to be 5, 10, 25, 50, 100 and 200, and mean widths 1/5, 1/10, 1/25, 1/50, 1/100 and 1/200 ft, respectively. The computed results are plotted in Fig. 3-4. To visualize the differences in depth between channels, the water depth in each channel for $\lambda = 100$ at $t = 16{,}000$ sec is computed, showing a large variation of depths, ranging from 0.0277 ft to 0.370 ft. Figure 3-4 shows the limit Reynolds number of around 2,000. At this point, f increases rapidly to high values with an increase of Re. A certain period after rainfall starts, the larger channels attain equilibrium conditions, with a constant depth after that, while in the small channels the water depths are still rising. Increases of depths and cross section areas of small channels decrease the average velocity, since high velocities of large channels keep constant. The increase of y compensates in $Re = Vy/\nu$ for the decrease of V, and Re is almost constant. However, for the Darcy-Weisbach equation, $f = 8gSy/V^2$, V decreases as y increases, causing a rapid increase of f.

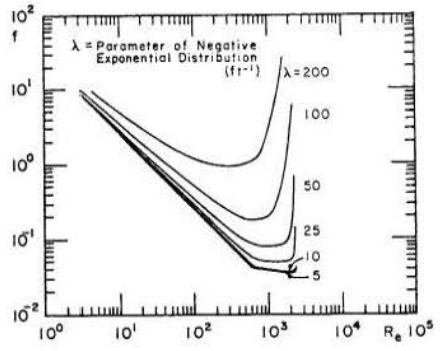

Figure 3-4. Relationship f vs Re for rising hydrographs of isolated channels, with λ = the parameter of negative exponential distribution (ft^{-1}).

Model of Parallel Channels with Equal Water Depths

Because the large difference in depth as shown for the model of isolated parallel channels does not seem appropriate, it is assumed that the channels are interconnected with the shallow flow passing through the spaces between gravel, grass or through rills. If a set of parallel channels with negative exponentially distributed widths but of the same water depths is assumed, then for y = the equal water depth for all the channels and $Q_i = f(y, b_i)$, f is that given by the Boussinesq, Eq. (3-1), if $Re = VR/\nu < 600$, or by the Manning, Eq. (2-4), if $Re > 600$, and

$$Q = \sum_{i=1}^{100} Q_i, \qquad V = \frac{Q}{y \sum_1^{100} b_i}$$

$$f = \frac{8gSy}{V^2}, \quad \text{and} \quad Re = \frac{Vy}{\nu}.$$

The relationships of f to Re for λ = 5, 10, 25, 50, 100 and 200, or the mean width of 1/5, 1/10, 1/25, 1/50, 1/100 and 1/200 ft are plotted on the log-log graphs as shown in Fig. 3-5.

Because of the assumption of an equal water depth in all channels, the average velocity increases with an increase of y. At the high Reynolds numbers, f increases with an increase of Re, but with no rapid increase of f in comparison with the f curves obtained for the rising limb of hydrographs in case of the model of isolated channels. The curves do not

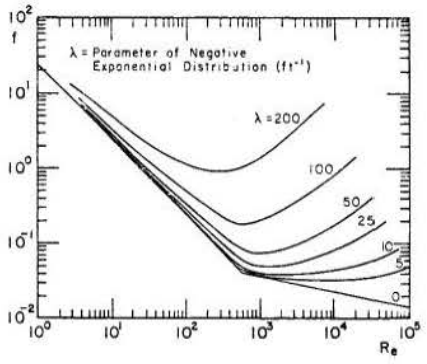

Figure 3-5. Relationship f to Re for parallel channel model of equal water depths, with λ = the parameter of negative exponential distribution (ft^{-1}).

intersect like those of single channels because of negative exponential distribution of the channel width. The curves continuously change in shape from high λ values to low λ values. Kowobari's experiment (1970) on the upright stems showed an increase in the resistance to flow with an increase in discharge for the turbulent flow range. Thus, the proposed model is consistent with his experimental results.

f vs Re Relationship from Balance of Forces

In a previous section, the friction law for parallel channels was derived from the Boussinesq's equation for flow in rectangular ducts. To develop a more general f to Re relationship, the concept of balance of forces by considering the drag force is applied in this section.

For flow passing through the obstructions at the surface, a plane surface with vertical cylinders erected on the plane is assumed. The factors affecting the resistance are the friction of the bed and the drag on the cylinders. Assuming that these factors are mutually independent, the sum of these two forces should be equal to the flow direction component of the weight of flow mass:

$$(F_x)_{\text{Downslope Water Weight Component}} = (F_s)_{\text{Bed Surface Resistance Force}} + (F_b)_{\text{Drag Forces Due to Cylinders}} \qquad (3\text{-}8)$$

with

$$\frac{F_x}{A} = \gamma y S_o \qquad (3\text{-}9)$$

$$\frac{F_s}{A} = \gamma y S_f \qquad (3\text{-}10)$$

and

$$\frac{F_b}{n} = \frac{1}{2}\bar{C}_d\,\rho V_o^2\,d\,y, \qquad (3\text{-}11)$$

in which A = the area of bed surface excluding the area occupied by cylinders, γ = the unit volume weight of water, n = the number of cylinders, y = the water depth, S_o = the bed slope, S_f = the plane surface friction slope $\bar{C}_d$ = the mean drag coefficient of cylinders, ρ = the water density, V_o = the mean velocity based on channel flow area, and d = the diameter of cylinders. By assuming that the drag coefficient for a single cylinder, C_d=12, Li and Shen (1973) obtained the mean drag coefficient $\bar{C}_d$, for an array of cylinders. It was 1.1 for the staggered array and 0.77 for the parcel array. In this trial computation, the C_d values from the graph of the C_d to Re relationship, as reported in standard text books such as Schlichting (1968), are used for the wide range of the Reynolds number. $\bar{C}_d$ in Eq. (3-11) is determined by $\bar{C}_d = 1.0C_d/1.2$, where 1.0 is the approximate value between the parallel array and the staggered array.

The overall Darcy-Weisbach friction coefficient is $f = 8gyS_o/V^2$. By substituting $S_o = f\,V^2/8gy$ in Eq. (3-9), then

$$\frac{F_x}{A} = \frac{1}{8} f\,\rho V_o^2 . \qquad (3\text{-}12)$$

Similarly,

$$\frac{F_s}{A} = \frac{1}{8} f_s\,\rho V^2 \qquad (3\text{-}13)$$

in which V = the velocity of flow through spaces between the cylinders and f_s = Darcy-Weisbach friction coefficient for the plane surface. Expressing the density of cylinders as n cylinders per unit area, the drag force per unit area becomes

$$\frac{F_b}{A_t} = \frac{1}{2} n\,\bar{C}_d\,\rho V_o^2\,d\,y \qquad (3\text{-}14)$$

in which A_t = the area of bed surface including the area occupied by cylinders. From Eq. (3-8), it follows

$$\frac{1}{8} f\rho V_o^2\left(1-n\frac{\pi d^2}{4}\right) = \frac{1}{8} f_s\rho V^2\left(1-n\frac{\pi d^2}{4}\right) + \frac{1}{2} n\,\bar{C}_d\rho V_o^2\,d\,y,$$

or

$$f = f_s\,\frac{V^2}{V_o^2}\,\frac{4n\bar{C}_d d\,y}{\left(1-n\frac{\pi d^2}{4}\right)} .$$

Considering the continuity equation, it can be assumed that $V/Vo = 1/(1-n\pi d^2/4)$, the above equation becomes

$$f = f_s\,\frac{1}{\left(1-n\frac{\pi d^2}{4}\right)^2}\,\frac{4n\bar{C}_d d\,y}{\left(1-n\frac{\pi d^2}{4}\right)} , \qquad (3\text{-}15)$$

for $$f = \frac{8gyS_o}{V_o^2} = \frac{8gS_o}{Q^2}\,y^3 ,$$

then $$\frac{8gS_o}{Q^2}\,y^3 - \frac{4nd}{1-n\frac{\pi d^2}{4}}\,\bar{C}_d y - f_s\,\frac{1}{\left(1-n\frac{\pi d^2}{4}\right)^2} = 0 , \qquad (3\text{-}16)$$

in which Q = the unit width discharge. With known Q, f_s can be obtained from the friction law of a wide open channel flow for smooth surfaces by using Re = $Vy/\nu = Q/\nu\ (1-n\pi d^2/4)$, and $\bar{C}_d$ can be determined by $\bar{C}_d = 1.0C_d/1.2$, and C_d from the C_d to Re curve given in the text, by using $Re = V_o d/\nu = Qd/y\nu$. Equation (3-16) has only one unknown, y, and it can be solved. The parameter f is determined by substituting y in Eq. (3-15). In this test computation, the following values were used: S = 0.005; n = 2, 5, 10, 20, and 50; ν = 0.00001, and d = 1.5/12 ft.

The computational results of the f to Re relationship are shown in Fig. 3-6. The shapes of curves obtained from the balance of forces are quite similar to those obtained from the Boussinesq equation.

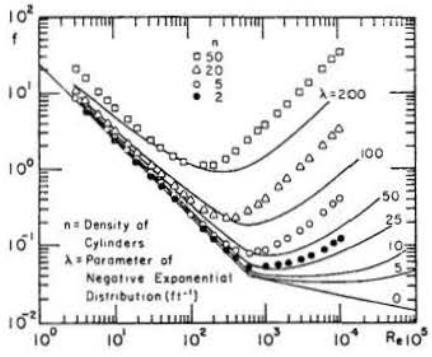

Figure 3-6. Relationship f to Re for balance of force in upright cylinders in comparison with that of the parallel channel model, with n = the density of cylinders, and λ = the parameter of negative exponential distribution (ft^{-1}).

Darcy-Weisbach Friction Coefficient

The analysis of the f vs Re relationship by a balance of forces showed that the model of random width parallel channels with equal water depths gives the relationship close to that for the flow passing through the spaces between obstructions. Furthermore, a set of curves for the f vs Re relationship (Fig. 3-5), derived from this model, can cover the flow phenomena from flow on a smooth plane with $\lambda = 0$ to flow in porous media with a high value of λ. The model of random width parallel channels with equal water depths is considered herein as a feasible model.

For application of the model of random width parallel channels to the natural watershed, the thickness, W, of the walls which separate the parallel channels must be taken into account. Assume that n = the number of channels, W_c = the sum of channel widths, W_w = the sum of wall widths = nW, Q_t = the total discharge in n channels, Q_c = the mean discharge per unit width of channels, Q = the mean discharge per unit width of a watershed, including channel and wall widths, V_c = the average velocity in the channel, V = the average velocity in the watershed = Q/y, and y = depth of flow in channels, then

$$Re = \frac{Vy}{\nu} = \frac{Q}{\nu} = \frac{1}{\nu}\frac{Q_t}{W_c + W_w} = \frac{Q_c}{\nu}\frac{W_c}{W_c + W_w}$$

and

$$f = \frac{8gyS}{V^2} = \frac{8gyS}{V_c^2}\left(\frac{Wc + Ww}{W_c}\right)^2,$$

with

$$\log Re = \log\frac{Q_c}{\nu} - [-\log W_c + \log(W_c + W_w)] \quad (3\text{-}17)$$

and

$$\log f = \log\frac{8gyS}{V_c^2} + 2[-\log W_c + \log(W_c + W_w)]. \quad (3\text{-}18)$$

The first terms at the right sides of Eqs. (3-17) and (3-18) are log Re and log f of channels without a consideration of the wall thickness. By considering the wall thickness, the f to Re relationship shifts diagonally in the direction parallel to the slope of 1:2 in log-log paper. Other factors such as slope, surface roughness, and the Reynolds number at the transition will also affect the position of this curve; however, there will only be a slight change in the shapes of these curves. Since the discharge is often expressed as a function of water storage in the analysis of overland flow, the effect of those factors will be discussed in more detail in the next section, in which the discharge is expressed as a function of water storage. The friction coefficient derived for the model in this section will be compared with data obtained by previous investigators.

The friction coefficient obtained by using the approach of parallel channels with an equal water depth in channels shows that the friction coefficient decreases with an increase of the Reynolds number in the range of low values of the Reynolds number, but increases with an increase of the Reynolds number in the range of high values of the Reynolds number. Many investigators have shown that the friction coefficients decrease with an increase of the Reynolds number in the range of low values of the Reynolds number, but the experimental data presented by Kowobari, et al. (1970) are the only set that show an increase of the friction coefficient in the range of high values of the Reynolds number.

Experimental data of Kowobari, et al. (1970), Ree (1939), Ree and Palmer (1949), and Chen (1976) are plotted on a graph along with the friction coefficient for the parallel channel approach for comparison purposes, as shown in Fig. 3-7. Kowobari, et al. studied the variation of Manning's n for a smooth rectangular channel, fitted with different sizes of unsubmerged artificial roughness elements. The data obtained from a square grid spacing of 9/32 inch diameter cylinders was shown in their table. The computed n and $n/R^{1/6}$ were also given. By equating Manning's equation to the Darcy-Weisbach equation, the Darcy-Weisbach friction factor can be determined. The f to Re relationship shows that data of Kowobari, et al. agree with the friction law obtained for the parallel channel approach.

W. O. Ree (1939) conducted experiments on flows in a channel which had a trapezoidal cross-section and a slope of 3 percent, lined with the Bermuda

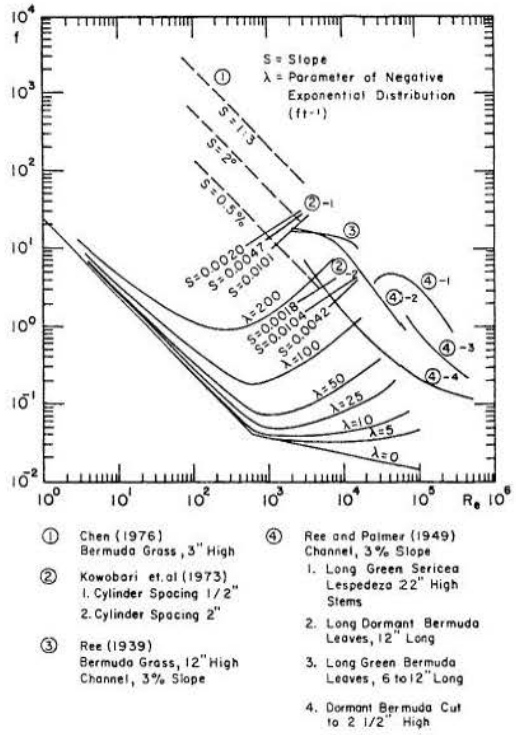

Figure 3-7. The f vs Re relationships for the model of parallel channels in comparison with data given by Ree, Kowobari, and Chen; with S = the slope and λ = the parameter of negative exponential distribution (ft^{-1}).

grass sod 12 inches high with 350 stems per square foot. Five different flow discharges were used in that study. At the time of the tests the grass was bent over, forming a loose mat. For the first four tests, the depths of flow were less than the height of the grass cover, with the flow entirely hidden from view. During Test 5, with the highest discharge, the flow produced a depth and velocity sufficient to submerge about 30 percent of the cover. This resulted in a change in hydraulic characteristics of the test waterway, which is reflected in the sudden drop in the Manning n value. From data shown in that paper, the Reynolds number and the Darcy-Weisbach friction factor were computed by using equations $Re = VR/\nu$ and $f = 8gRS/V^2$, respectively. Their relationships are reproduced in Fig. 3-7.

Ree and Palmer (1949) presented the results of a study in an outdoor hydraulic laboratory, concerned principally with the effects of vegetation linings on the capacity and stability of small channels. Experiments were carried out with Bermuda grass, Lespedeza, Sericea Lespedeza and a mixture of orchard grass. From the computed Manning n, as shown in tables of that paper, the Reynolds number and the Darcy-Weisbach friction factor were computed by using equations $Re = VR/\nu$ and $f = (8g/1.486^2)\ (n^2/R^{1/3})$, respectively. The f to Re relationships for dormant Bermuda grass, dormant Bermuda grass cut to 2-1/2 in. high, long green Bermuda grass, and long green Serica Lespedeza with a bed slope of 3 percent are also reproduced in Fig. 3-7. Water flowing at a slight depth through the vegetation encounters the resistance of stalks, stems and foilage. As depth of the flow increases, the force exerted by the flowing water causes the vegetation to bend, when the bending moment becomes greater than the resistance moment. With highly flexible vegetation such as Bermuda grass (leaf blade height 1" to 4" and flower-bearing branch height 6" to 12"), bending occurs rapidly. When a portion of the cross section of the channel is freed of vegetation obstructions by their bending, the resistance to flow greatly decreases with the result that the friction coefficient also decreases sharply. The f to Re relationship is then the inverse of that for the rigid obstructions, such as the erected cylinders. A good stand of tall green Sericea Lespedeza, averaging 22 inches height, produces another type of resistance change. When the depth of flow becomes greater, therefore, the Reynolds number also becomes greater, with the coefficient being higher. As the submergence further increases, the resistance decreases because of the bending of the stems. Before the bending of stems takes place, the phenomenon is similar to that of flow through cylinders. However, after the bending of stems starts, the flow phenomenon becomes that of the Bermuda grass. It is apparent from these results that the f to Re relationship for vegetation cover is greatly affected by the height and stiffness of the grass.

Chen's (1976) laboratory experiments on Bermuda grass, three inches in height showed that the f-value increases as the bed slope increases, but decreases as the Reynolds number increases. Three representative lines of the f to Re relationship are presented in Fig. 3-7.

One can see from the results of past investigations that the friction law for turf surfaces is very complex. Many factors, such as the density, height, length and stiffness of stems and foilage, structure of vegetation, degree of bending, frequency of vibration, and degree of submergence affect their resistance law. The f to Re relationship curves give convex or concave curves rather than straight lines.

Discharge as a Function of Water Storage and Factors Affecting the Discharge

Many investigations reveal that overland flow can be simulated by using kinematic wave theory. In the kinematic wave equations the friction slope, S_f, is assumed to be equal to the bed slope, so, which is constant during the wave passage. The discharge per unit width is a function of water storage only, i.e. $Q = \alpha h^m$. The ultimate purpose of determining the f to Re relationship is to find the relationship between Q and h with respect to various values of the Reynolds number. The f to Re relationship shows a series of concave curves, complex for analysis. It is, therefore, useful to examine the Q to h relationship in order to find a more convenient method of analysis.

Unit Width Discharge versus Water Depth

Figure 3-8 shows the relationships of unit width discharge, Q, to the actual water depth in channels, y, for the model of parallel channels with the slope of 0.005. The upper part of the figure shows the relationship for channels separated by walls with infinitesimal thickness. When wall thickness is considered, the series of curves will shift downward as shown in the lower part of the figure. Let Q_c = the unit width discharge without considering the wall thickness, Q = the unit width discharge

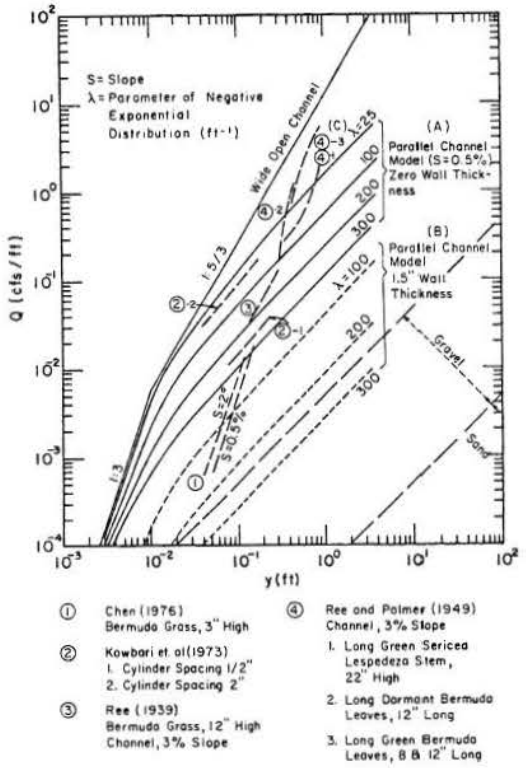

Figure 3-8. The Q to y relationships for parallel channel model; (a) without considering wall thickness, (b) considering wall thickness of 1.5", and (c) comparing with previous investigators' data, with S = the slope, and λ = the parameter of negative exponential distribution (ft^{-1}).

considering the wall thickness W, W_c = the sum of widths of n channels, $Q = Q_c W_c/(W_c + nW)$, and $W_c/(W_c + nW)$ = a constant for λ = a constant. Therefore, Q/Q_c will be a constant for given λ.

For parallel channels, without considering the wall thickness, the Q to y relationship will tend to be a straight line with a 45° slope when the discharge is large. The reason for this is that the velocity tends to be constant in a narrow channel when the discharge is large. If wall thickness is considered, those curves will shift downward and the relationships behave close to the phenomenon of flow in porous media. In other words, the model can represent a wide range of flows between a wide open channel flow and a porous media flow.

Effect of Channel Slope

Previous computations of Q vs y are based on S = 0.005. Since the Rainfall-Runoff Experiment Facility, for which data were used in this study, has a slope of 0.05, Q vs y for parallel channels model was computed for S = 0.05, and shown in Fig. 3-9. The comparison between the Q vs y relationships for these two slopes is shown in Fig. 3-10. The increase of the slope tends to shift the curves to the left, narrowing the range of spacing of curves.

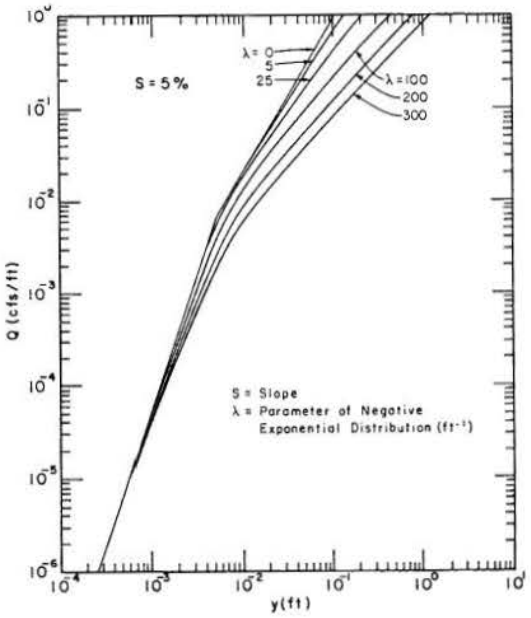

Figure 3-9. The Q vs y relationship for the equal depth parallel channels model, for S = 0.05, with S = the slope and λ = the parameter of negative exponential distribution (ft^{-1}).

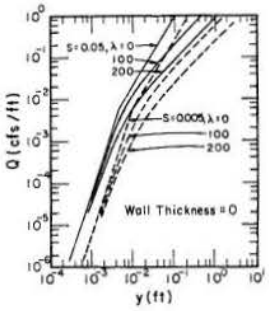

Figure 3-10. The Q vs y relationships for parallel channels, the average unit width discharge, Q, and the equivalent water depth, h, are

Unit Width Discharge versus Equivalent Water Depth, and Effect of Wall Thickness

For an analysis by the kinematic wave equations, flow discharge as a function of water storage should be used. The unit width discharge versus the equivalent water depth for the flow with obstructions is useful. When the wall thickness is considered in the model of parallel channels, the average unit width discharge, Q, and the equivalent water depth, h, are

$$Q = Q_c \frac{W_c}{W_c + nW}, \quad \text{and} \quad h = y \frac{W_c}{W_c + nW} \qquad (3\text{-}19)$$

in which Q_c = the unit width discharge and y = the actual water depth of parallel channels separated by infinitesimally thin walls. On the log-log scale graph, the shifting distances for both Q and h are identical, namely $\log[W_c/(W_c + nW)]$. As shown in Fig. 3-11 the shapes of Q vs h curves for channels for

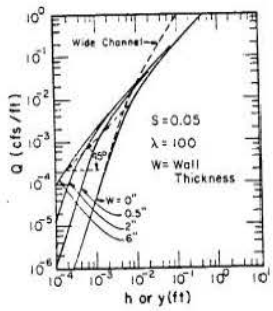

Figure 3-11. The Q vs y relationships for parallel channels, showing effect of wall thickness.

which the wall thickness is considered are identical to shapes of curves without considering the wall thickness; however, the positions are shifted downward diagonally at the slope of 45°.

Effect of Reynolds Number in the Transitional Regime

Previous investigators have shown the various Reynolds numbers for the transitional regime, in general ranging from 100 to 1000. Because of unstable flow phenomena at the transition, this value at transition cannot be precisely determined. With the model of parallel channels, two extreme values of the Reynolds number at transition, namely R_c = 1000 and R_c = 100, were used for computation of the Q vs y relationships. The shapes of curves for these two relationships are similar. The Q vs y relationships for λ = 100, with R_c = 1000 and 100, respectively, are shown in Fig. 3-12. The curve, following a parallel shift of the curve based on λ = 100 and R_c = 1000 to the position of the curve based on λ = 100 and R_c = 100, is shown by a dashed line.

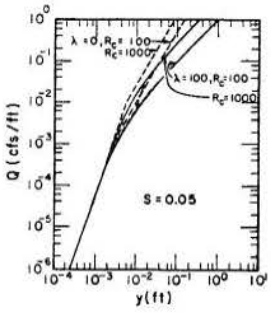

Figure 3-12. The Q vs y relationships for parallel channels, showing effects of Reynolds number at transition.

Since the slopes of curves for different values of the Reynolds number at the transitional regime are similar, the change of the Reynolds number at the transition causes only a parallel shift of curves.

Effect of Surface Roughness

The above computation for the Q vs y relationship refers to the smooth surface. Several investigators showed that a parallel shifting of the log f vs log Re curves for a smooth surface will also fit the relationship for a rough surface. Assuming that this is valid, and that the Reynolds number at the transition from the laminar to the turbulent flow is a constant for all kinds of surface roughness, the distance of the parallel shift in horizontal direction for Q vs y curves can then be estimated. Let f = the Darcy-Weisbach friction coefficient for a smooth surface, f_r = the friction coefficient for a rough surface, y = the depth of water on the smooth surface, and y_r = the depth on the rough surface. For a constant Reynolds number, Re, or for a constant unit width discharge, Q: $f = 8gyS/V^2 = 8gSy^3/Q^2$ and $y_r/y = (f_r/f)^{1/3}$. The ratio f_r/f is equal to the ratio C_r/C, where C_r and C = the C values in f = C/Re for the rough and smooth surfaces, respectively. Therefore, the distance of the horizontal shift becomes

$$r = \log y_r - \log y = \frac{1}{3} \log(C_r/C). \qquad (3\text{-}20)$$

Effect of Tortuosity

Because of various obstructions on the surface of a watershed, tortuosity in flows is a general pattern of natural surfaces. Since the above considered channels were straight, the effect of tortuosity on discharge must be taken into account. If V_t = the average tangential velocity, then mean velocity in the X direction is given by $V_x = V_t L_x/L_t$, with L_x = the distance between the ends of a segment of channel in X direction and L_t = the length of the tortuous channel. The mean slope of the channel is given by $S_t = S_x L_x/L_t$, with S_x = the slope of the watershed in the X direction, and S_t = the slope along the tortuous channel.

The Q vs y curves are derived in previous sections for the flow equation in the laminar flow range, while the Manning n in the turbulent flow range is obtained from the Manning n at the transitional point. For a wide open channel flow, the curve has 1:3 slope in the laminar flow range and 1:(5/3) grade in the turbulent flow range, with the discontinuity at Q = Re X ν = 600 X 0.00001. A horizontal shift of the curve of the laminar flow range causes the horizontal shift of the curve in the turbulent flow range. Let the laminar flow equation be Q = Vy and $V = cy^2S$. The unit width discharge in a straight channel is $Q_x = cy^3S_x$, and in the tortuous channel $Q_x = V_x y_t = V_t(L_x/L_t)y_t = (cy_t^2 S_x L_x/L_t)\ (L_x/L_t)y_t = cy_t^3 S_x (L_x/L_t)^2$. Let Q in both cases be identical, the ratio of the tortuous channel water depth, y_t, to the straight channel water depth, y, is $y_t/y = (L_t/L_x)^{2/3}$. The quantity $(L_t/L_x)^2$ has been called "tortuosity," estimated as 2.0 for the isotropic granular material in porous media flow. This value comes from the statistical mean direction of flow of about 45° with respect to the macroscopic direction of flow. The distance of the horizontal shift of Q vs y curve is, therefore, $\log y_t - \log y = (1/3)\log T$, with $T = (L_t/L_x)^2$. If 2.0 is taken as the T value, the shift on the log scale becomes 0.100.

Comparison with Previous Investigation Data

Data of experiments made by Kowobari, et al. (1970), Ree (1939), Ree and Palmer (1949), and Chen (1976) are plotted in Fig. 2-8 for the comparison with the Q vs y relationship for parallel channels. Kowobari's results show that the parallel channel model fits well the data at high Reynolds numbers. However, the parallel channel model does not fit the turf data well. Chen's data show that the relationship $Q = \alpha y^3$ is applicable for y in the range of 0.02 to 0.20 ft. It follows that the hydraulic radius, R, in $Q = cR^2Sy$ of the laminar flow increases with an increase of the water depth, so that Q is proportional to y^3. The Q vs y curves behave as in the laminar flow though the Reynolds number, Q/ν, is above 600. This may be due to flows passing through spaces between the soft leaves of grass such as the Bermuda grass. For the flow with a high discharge, Ree and Palmer (1949) show that the relationship is much more complex. The height and flexibility of leaves and stems and the degree of bending affect the Q vs y relationship.

Three-Parameter Model

The unit width discharge, Q, versus the equivalent water depth, h, is a more convenient approach than the friction law of the f vs Re relationship in the analysis of overland flow by the kinematic wave theory, and the relationship of Q vs h will be used.

As noted, the curves for a parallel channel model can represent all the smooth surface flows between the open channel and porous media flows. These curves are asymptotes to the laminar flow lines in wide open channels, with slope of 1:3 on the log-log graph in the case the flow is small; they tend to 1:1 slope for a narrow channel of a large flow discharge. The model can be applied to a flat watershed with obstructions, high vegetation or rills. However, the model cannot be applied well to a turf surface. In considering the effects of wall thickness, tortuosity, Reynolds number at transition, and surface roughness, the shapes of curves do not change very much; however, their positions change. The complexity of computations in estimating the parameters through an optimization technique makes it almost impossible to estimate so many parameters. Therefore, the number of parameters must be reduced to as few as feasible. The three parameters approach is selected, with parameters defined as (see Fig. 3-14):

λ = the inverse of mean channel width, which defines the shape of the relationship curve;

V = the vertical shift in the curves with the upward shift as positive; and

H = the horizontal shift in the curve, with the right hand shift as positive.

The observed hydrographs of a specified watershed are used to estimate these three parameters by an optimization technique.

Correia (1972) and Brazil (1976) worked out the Q to h relationships for an impervious rectangular plane having slope of 0.05 in an experiment with the artificial rainfall produced by sprinklers. Under the steady state condition, the unit width discharge was calculated by $Q = ix$ (Fig. 2-2), with the mean velocity, V, measured by the dye injection. The equivalent water depth, h, was computed by $h = Q/V$. The Q vs h relationship was obtained by the regression analysis in using the two-parameter model, $Q = \alpha h^m$. The experiments were made with different rainfall intensities on a butyl rubber surface, a gravel-covered butyl surface and a concrete rill surface. The Q vs h relationships are shown in Fig. 3-13. In every case, the m value was approximately 1.5, although different α values were obtained for various rainfall intensities and roughnesses. The observed data and the Q vs h curve for a concrete rill surface, obtained by Brazil, is plotted in Fig. 3-14. For a trial fit of the parallel channel model to the observed data, the parameters $\lambda = 100$, $V = -.276$, and $H = -1.40$ were used. The curve B of Fig. 3-14, after the vertical and horizontal shifts of the curve for $\lambda = 100$, fits the observed data much better than the straight line obtained by assuming α and m as constants in $Q = \alpha h^m$. This means that the three-parameter model can more precisely model the flow phenomenon over a wide range of discharges than the two-parameter model. In Fig. 3-13 the Q vs h relationships in laminar flow, obtained by Correia (1972) and Brazil (1976) show discharges greater than theoretically possible for the plane surface, as the relationship obtained for a smooth surface by assuming $S_f = S_o$. In other words, the velocity on the experimental watershed is apparently higher than for the smooth surface, while the water depth is smaller than for the smooth surface. The likely explanations of this phenomenon include: (1) Transfer of downstream direction momentum due to the raindrop impact, and (2) Concentration of flow because of an uneven surface. The effect of concentration of flow for the uneven surface has been described as the effect of wall thickness in the section "Model of Isolated Parallel Channels". For a gravel surface, the effect of concentration is more significant than the effect of raindrop impact, or the effect of raindrop impact may be neglected. However, the effect of raindrop impact on the butyl surface may be significant, and therefore must be investigated. The watershed configuration and the sprinkler system used by Brazil were analyzed to determine whether there was a significant raindrop effect in laminar flow in equilibrium for a smooth surface. Brazil made dye injections at the very top of the plane at points 9, 15, and 21 meters from the upstream end (third, fifth, and seventh sections) of the 30 meter section, then evaluated the Q vs h relationship for points at the 4.5, 12, and 18 meters from the upstream end. Since the effect becomes more significant for a shallow flow, the test was carried out for points at the 4.5 and 12 meters from the upstream end for various rainfall intensities. The full momentum equation, Eq. (2-14), was used for the computation of friction slope, S_f, under the raindrop impact, and Eq. (2-6) was used for the computation of velocity at a smooth surface without the raindrop impact. Summation of products of the rainfall intensity and the x-component of velocity for the lateral inflow from all of the sprinklers in operation was taken as the value iV_ℓ of Eq. (2-14). Rainfall intensity and the x-component of velocity for the lateral inflow from each sprinkler are functions of distance and angle of the sprinkler. They were evaluated from data in the test of drop size distribution for sprinklers (M. E. Holland, 1969). The results show that the effect of raindrop impact on the Q vs h relationship is not significant and as such can be neglected. The difference between the bed slope and the friction slope is within 1.5 percent of the bed slope. The difference between the depths of flows with raindrop impact and without it is within

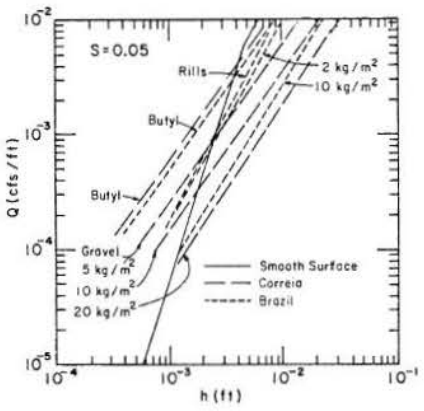

Figure 3-13. The Q vs h relationships after Correia (1972) and Brazil (1976).

Figure 3-13. The Q vs h relationships after Correia (1972) and Brazil (1976).

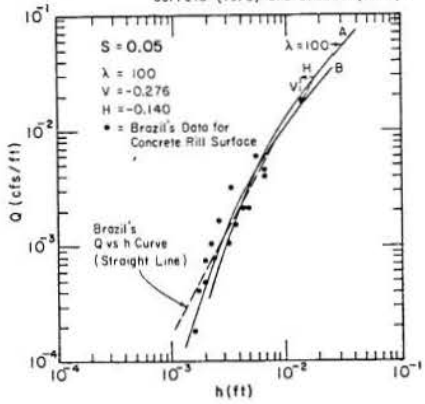

Figure 3-14. The Q vs h relationship for concrete rill surface (Brazil's data, 1976) with three-parameter model.

0.6 percent. Apparently, the reason that the Q vs h relationships in laminar flow exceed the boundary of relationships for plane surfaces is mainly the concentration of flow because of the uneven surface.

3.2 Comparison of Two-Parameter and Three-Parameter Models

Optimization of Parameters with Two-Parameter and Three-Parameter Models

Two-parameter and three-parameter models are used herein for finding the best-fit parameters by minimizing the objective function for various watersheds of this study. An objective function takes into account the sum of squares of deviations between observed and simulated hydrographs with a five second time increment. The model parameters should be determined so that the model can simulate the actual hydrographs as closely as feasible. The observed hydrographs are used for a comparison with hydrographs simulated by the model, with the estimated parameters.

Simulation of hydrographs with estimated parameters are made by using kinematic wave theory and a numerical method, namely the second-order Lax-Wendroff scheme for the interior of each subdivided plane, and the upstream differencing method for the downstream end. Since α and m of $Q = \alpha h^m$ for the three-parameter model are not constant and vary with the depth, h, the schemes used by Kilber and Woolhiser (1970) are rewritten as:

(a) Single Step Lax-Wendroff Scheme

$$h_j^{i+1} = h_j^i - \Delta t \left[\frac{(\alpha_{j+1}^i h_{j+1}^{i\,m_{j+1}^i} - \alpha_{j-1}^i h_{j-1}^{i\,m_{j-1}^i})}{2\Delta x} - \frac{1}{2}(q_{j+1}^i + q_{j-1}^i) \right] +$$

$$\frac{\Delta t^2}{4\Delta x} \left\{ (\alpha_{j+1}^i m_{j+1}^i h_{j+1}^{i\,m_{j+1}^i - 1} + \alpha_j^i m_j^i h_j^{i\,m_j^i - 1}) \left[\frac{(\alpha_{j+1}^i h_{j+1}^{i\,m_{j+1}^i} - \alpha_j^i h_j^{i\,m_j^i})}{\Delta x} - \frac{1}{2}(q_{j+1}^i + q_j^i) \right] \right.$$

$$- (\alpha_j^i m_j^i h_j^{i\,m_j^i - 1} + \alpha_{j-1}^i m_{j-1}^i h_{j-1}^{i\,m_{j-1}^i - 1}) \left[\frac{(\alpha_j^i h_j^{i\,m_j^i} - \alpha_{j-1}^i h_{j-1}^{i\,m_{j-1}^i})}{\Delta x} - \frac{1}{2}(q_j^i + q_{j-1}^i) \right]$$

$$\left. + \frac{2\Delta x}{\Delta t}(q_j^{i+1} - q_j^i) \right\} \qquad (3\text{-}21)$$

and

(b) Upstream Differencing Scheme

$$h_j^{i+1} = h_j^i - \frac{\Delta t}{\Delta x}(\alpha_j^i h_j^{i\,m_j^i} - \alpha_{j-1}^i h_{j-1}^{i\,m_{j-1}^i}) + q_j^i \Delta t. \qquad (3\text{-}22)$$

The notations for finite-difference schemes are defined in Fig. 3-15.

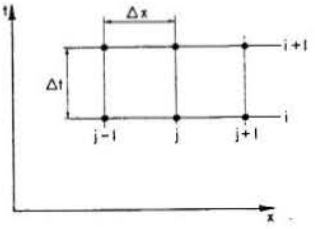

Figure 3-15. Notation for finite-difference schemes.

The data used for the comparison of models are taken from the concrete rill surface with rectangular section 98.4 ft long and 6.6 ft wide and a conic section of 30° central angle with butyl surface covered with uniformly distributed gravel of 20 lbs/yd^2 (configuration 14). Figure 3-16 shows the shapes of the watershed and cascade of planes approximating the conic section for numerical solution of the kinematic wave equation (see section 2.3). Experimental facilities and discharge correction for the data are described in Sections 4.1 and 4.2.

In trial optimization computations, Rosenbrock's method and Simons and Li's modified method were tested. Because of the oscillation of objective functions due to the numerical approximation, the optimization often resulted at the local minimum of the objective function. Finally, the grid method was used for finding the minimum of the objective function. To obtain a graphical representation of the response surface the objective functions are obtained and plotted for a certain grid of points on a graph, with axes of parameters to be estimated. Then the global minimum is determined by search in the area of the possible minima.

Twelve hydrographs were selected for each of two watersheds. Intensities and durations of rainfall inputs of the twelve hydrographs are shown in Table 4-1. These twelve hydrographs cover four rainfall intensities and three rainfall durations. One is a

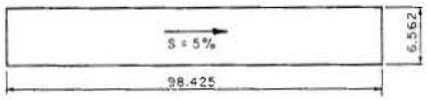

Unit: ft

(a) Concrete Rill Section, Rectangular

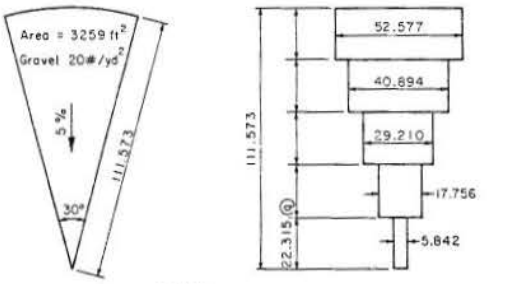

(b) Conic Section and its Approximated Cascade Planes for Numerical Solution by Kinematic Wave Theory

Figure 3-16. Rectangular concrete rill section and conic section with gravel of 20 lbs/ yd^2.

duration long enough to produce the equilibrium hydrograph and the other two are the durations which produce only the partial equilibrium. In order to avoid unnecessary calculations, the computation of the equilibrium hydrograph is limited to the time when the outflow discharge reaches the equilibrium flow. For the partial equilibrium, the hydrograph is limited to the time during recession when the outflow discharge reaches one third of the peak discharge. In numerical computation for the rectangular section, longitudinal distance was divided into ten subdivisions (Δx). For the conic section, the watershed was approximated by a cascade of five rectangular planes and each plane was divided into three subdivisions (Δx). The time increment, Δt, should be within the limit of linear stability which decreases with an increase of the unit width discharge. In order to save computer time, two criteria were used for Δt: (1) to take 90 percent of the maximum allowable Δt, which is restricted by the linear stability criteria of numerical analysis, and (2) to take 5 seconds if the value of (1) exceeds 5 seconds.

In the case of inadequate assumed parameter values, the rising limb of the hydrograph may increase rapidly or the peak may be unreasonably high. This will reduce the magnitude of Δt, and consequently increase the computational time very much. In order to avoid unnecessary computation for unreasonable parameters, the computer program was designed to terminate computation when the number of time increments exceeds 250.

The numerical solution of kinematic wave equations needs α and m values at each Δx increment for each Δt increment. For the three-parameter model of parallel channels, Q vs y relationships for 10 selected λ values, ranging from 0 to 300, were computed and α and m values with respect to 84 various depths, y, were obtained for each λ value. For a given value of λ (other than 10 selected values), α and m with respect to various depths are obtained by interpolation. Then, α and m are adjusted for given V and H. During hydrograph computation, α and m for equivalent water depth, h (other than 84 selected depths), at each Δx, were also obtained by interpolation.

Three-Parameter Model

For the three parameters, λ, V, and H, the objective functions are plotted on the graph V against H for fixed values of λ. The best fit parameters are selected as the set which gives the minimum of the objective function on grid points. Both the sum of squares of hydrograph deviations and the sum of squares of peak deviations are plotted on the graph for comparison.

(1) Gravel Surface with Uniform Distribution of 20 lbs/yd^2, with 30° Conic Section of 110 ft Radius

Values for the objective function are plotted on the graphs with V and H as axes for the given λ values of 200, 100, 50, 25, 10, 4, and 0. The examples are shown in Fig. 3-17. For a given λ, the objective function has a long narrow valley. Comparison of the graph for hydrograph deviations with that for peak deviations, shows that the objective function determined from the hydrograph deviations gives smaller values when the locations of the valleys on both graphs meet. A set of V and H with a minimum of the objective function can be found for each λ value. It was observed that the graph for $\lambda = 25$ has a longer valley with the lowest value of the objective function. The minimum of the objective function is located at the point of V = -1.8 and H = -0.88. Among the seven assumed λ, $\lambda = 25$ is the best value. The Q vs h curve for $\lambda = 25$, V = -1.8 and H = -0.88, is shown in Fig. 3-18. It appears that the Q vs h relationship is almost a straight line for the main range of discharges in the log-log paper.

Because a series of discrete values of λ are used in determining the minimum of the objective function, it is difficult to say definitely whether $\lambda = 25$ is the best value; however, it can be said that the best values of parameters are very close to $\lambda = 25$, V = -1.8, and H = -0.88. To determine the minimum of the objective function with CDC 6400 computer, approximately 200 evaluations would be necessary using 5000 seconds of computer time.

Three of the 12 hydrographs simulated for $\lambda = 25$, V = -1.8, and H = -0.88, are plotted in Fig. 3-19, together with the observed hydrographs. The simulated hydrographs agree very well with the observed hydrographs.

(2) Concrete Rill Surface of Rectangular Section, 98.4 ft Long and 6.6 ft Wide

Values of the objective function are plotted on the graphs with V and H axes for given λ, 100, 50, 25, 10, 4 and 0, as shown in the examples in Fig. 3-20. The same procedures as described above are followed in finding the minimum of the objective function. The best values of the three parameters found are: $\lambda = 0$, V = -1.2, and H = -0.5. The Q vs h curve for these values is shown in Fig. 3-21. Three of the 12 hydrographs simulated with these parameter values are plotted in Fig. 3-22 together with the observed hydrographs. The simulated hydrographs agree well with the observed hydrographs. Around 150 evaluations of

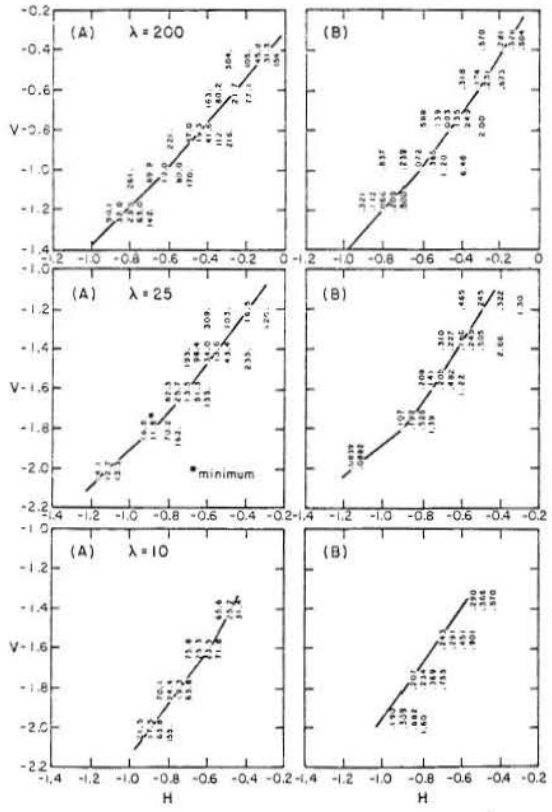

Figure 3-17. Values of objective function of three-parameter model, for gravel conic section surface of 20 lbs/yd^2, (A) hydrograph deviations, (B) peak deviations.

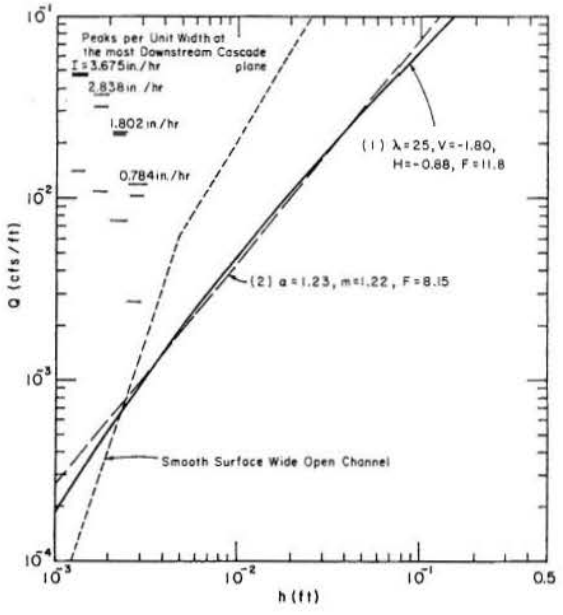

Figure 3-18. The Q vs h curves for gravel 30° conic section surface of 20 lbs/yd^2, 110 ft radius and 5 percent slope: (1) three-parameter model, (2) two-parameter model, with F = the objective function value.

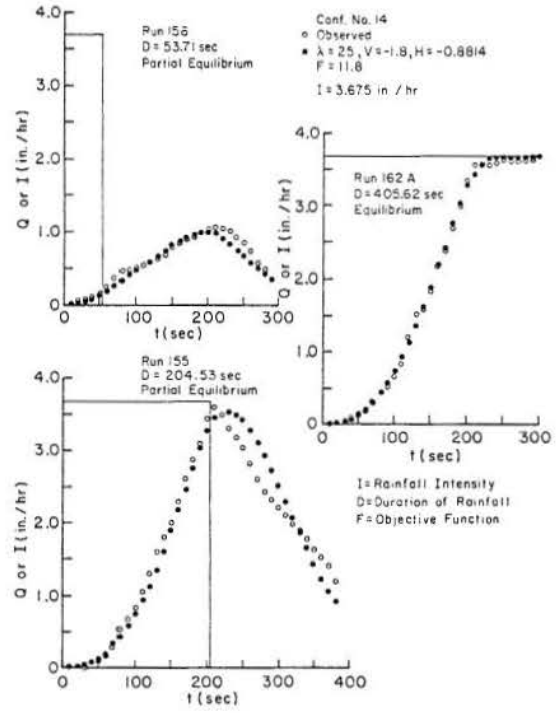

Figure 3-19. Comparison of hydrographs simulated by three-parameter model with observed hydrographs, for gravel 30° conic section surface of 20 lbs/yd^2, 110 ft radius and 5 percent slope.

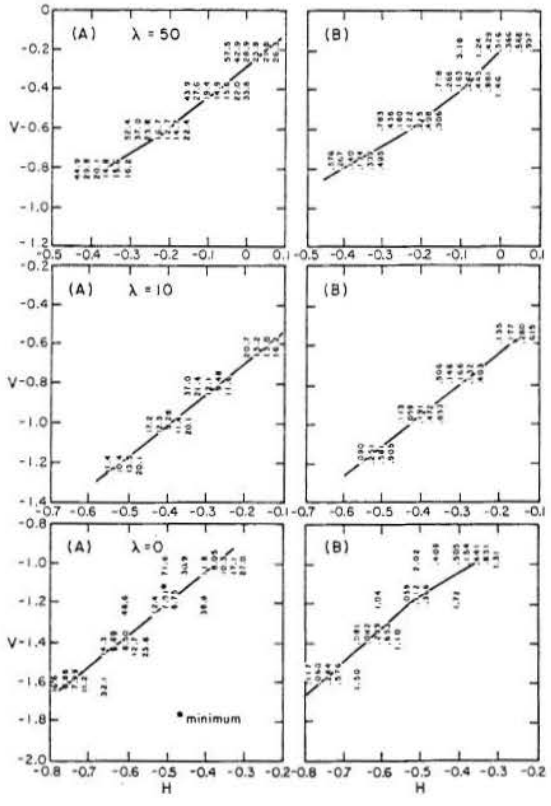

Figure 3-20. Values of objective function of three-parameter model, for concrete rectangular section rill surface: (A) hydrograph deviations, (B) peak deviations.

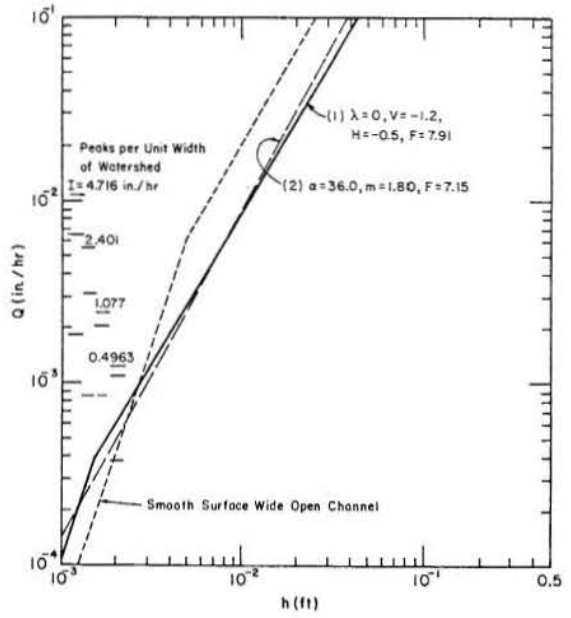

Figure 3-21. The Q vs h curves for concrete rectangular section rill surface, 98.4 ft long, 6.6 ft wide and 5 percent slope: (1) three-parameter model, (2) two-parameter model, with F = objective function value.

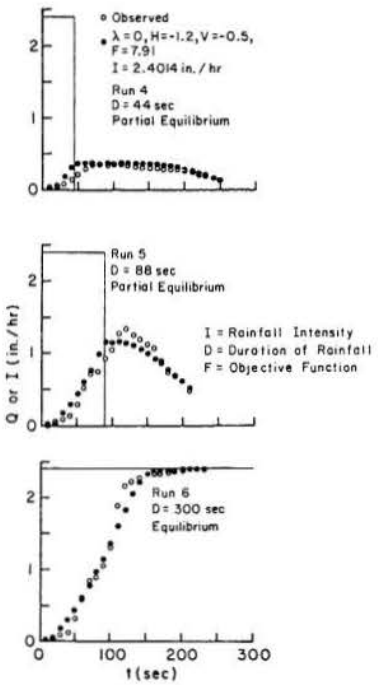

Figure 3-22. Comparison of hydrographs simulated by three-parameter model with observed hydrographs, concrete rectangular section rill surface, with I = the rainfall intensity, D = the duration of rainfall and F = the objective function value.

objective functions are made, with approximately 2300 seconds of computer time used. Since $\lambda = 0$, and the vertical shift of the curve is large, the Q vs h relationship is a straight line for the main range of discharges in the log-log paper.

Two-Parameter Model

(1) Gravel Surface with Uniform Distribution of 20 lbs/yd^2, with 30° Conic Section of 110 ft Radius

Values of the objective function are plotted on the semi-log paper with log α and m axes, as shown in Fig. 3-23. The low values of the objective function lie on a straight line in the semi-log paper. This greatly helps in pre-estimating the location of the minimum. The parameters with a minimum of the objective function are $\alpha = 1.23$ and $m = 1.22$. The values of the objective function vs m are shown in Fig. 3-26.

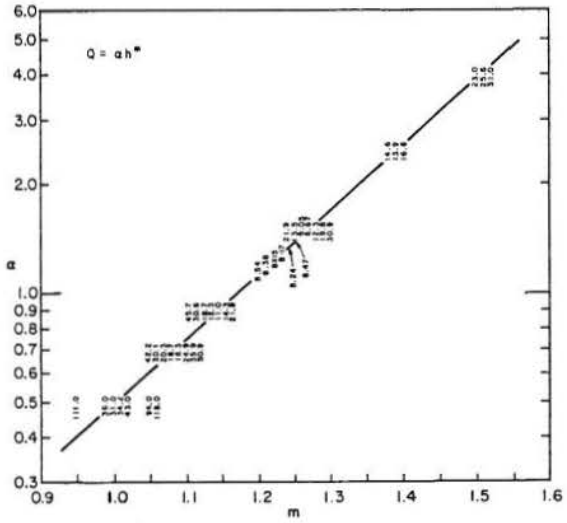

Figure 3-23. Values of the objective function of two-parameter model, for gravel conic section surface of 20 lbs/yd^2.

The Q vs h curve for $\alpha = 1.23$ and $m = 1.22$ is shown in Fig. 3-18 for comparison with the results of the three-parameter model. Three of the 12 simulated hydrographs with $\alpha = 1.23$ and $m = 1.22$ are shown in Fig. 3-24 together with the observed hydrographs. The computed hydrographs agree well with the observed hydrographs.

For obtaining the minimum of the objective function, 45 evaluations of the objective function were made, using approximately 450 seconds of computer time.

The low values of objective functions are located on a straight line in the log α vs m graph (Fig. 3-23). This means that log α and m for the low values of objective function have a linear relationship and can be expressed as $\log \alpha + m \log h = \log Q$, for $Q = \alpha h^m$, with Q and h constant. If the Q vs h relationships for a family of pairs of α and m, located on the straight line, are plotted on the log-log graph, a family of straight lines passing through a fixed point are obtained, as shown in Fig. 3-25. The coordinates of the fixed point in the example of the watershed used are Q = 0.0085 cfs/ft and h = 0.017 ft. In other words, if a Q vs h line passes through that point, the computed hydrograph will be close to the observed

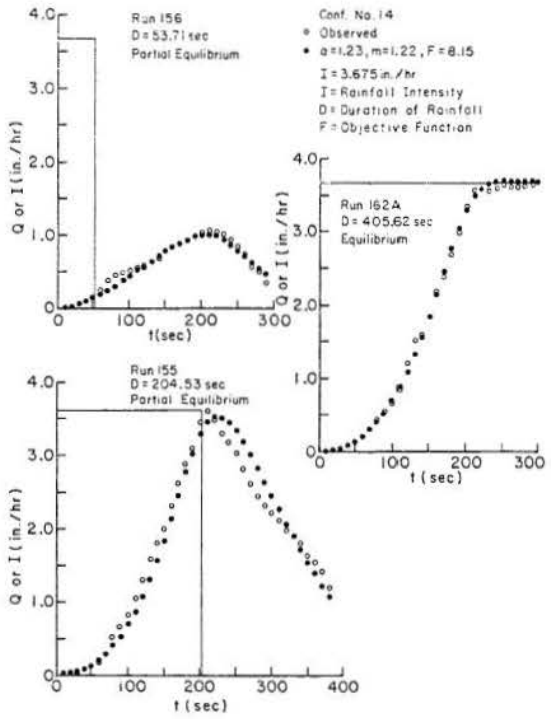

Figure 3-24. Comparison of hydrographs simulated by two-parameter model with observed hydrographs for gravel conic section surface of 20 lbs/yd^2.

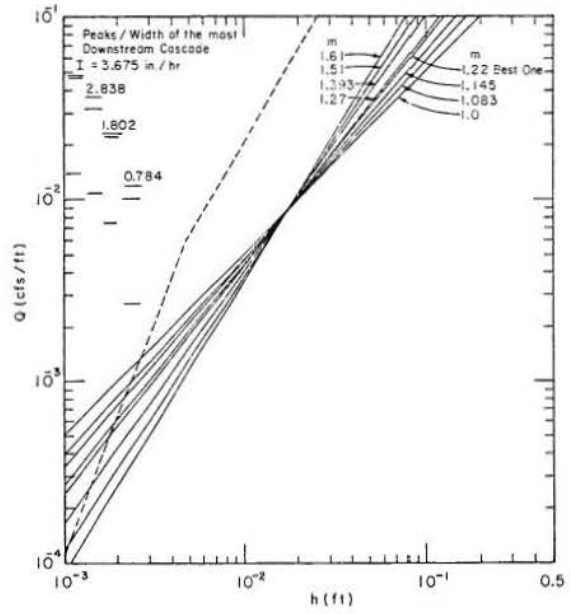

Figure 3-25. A family of Q vs h curves having lower values of objective function of two-parameter model, for gravel 30° conic section surface of 20 lbs/yd^2 with 110 ft radius and 5 percent slope.

hydrograph. This fixed point decides the location of the Q vs h curve while the adjustment of m causes the computed hydrograph to be a best fit for the hydrograph.

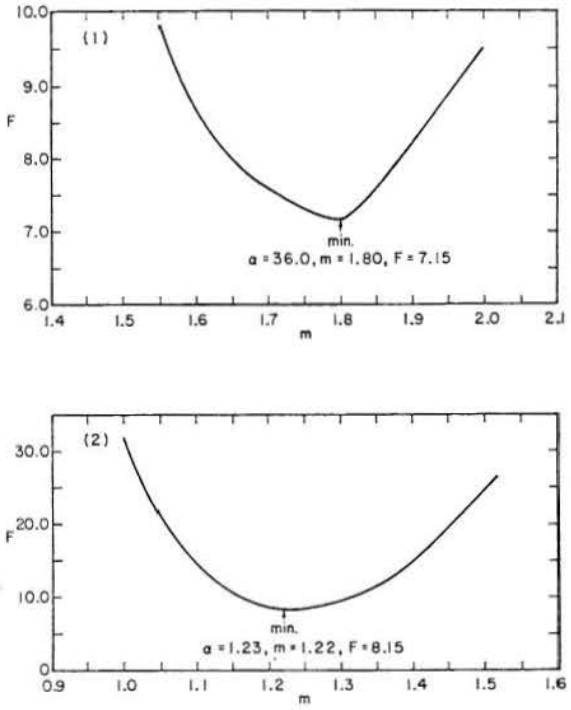

Figure 3-26. Objective function vs m for two-parameter model for: (1) concrete rectangular rill surface and (2) gravel 30° conic section surface of 20 lbs/yd^2.

(2) Concrete Rectangular Section Rill Surface of 98.4 ft Long and 6.6 ft Wide

The values of the objective function for various parameters, three samples of the 12 hydrographs simulated by using the best-fit parameters, α = 36.0 and m = 1.80, and a family of the Q vs h curves for the low values of the objective function are shown in Figs. 3-27, 3-28, and 3-29. The Q vs h curve for the above best-fit parameters is also shown in Fig. 3-21 for comparison with the results of the three-parameter model. The values of the objective function vs m value are shown in Fig. 3-26.

Fifty evaluations are made for obtaining the minimum of the objective function using approximately 250 seconds of computer time.

Table 3-1. Comparison between two-parameter and three-parameter models.

Section Shape	Number of Parameters	Numbers of Evaluation	Computer Time (sec) One	Computer Time (sec) Total	Minimum of Objective Function (in./hr)^2
Conic	3	200	25	5,000	11.8
	2	45	10	450	8.15
Rectangular	3	150	15	2,300	7.91
	2	50	5	250	7.15

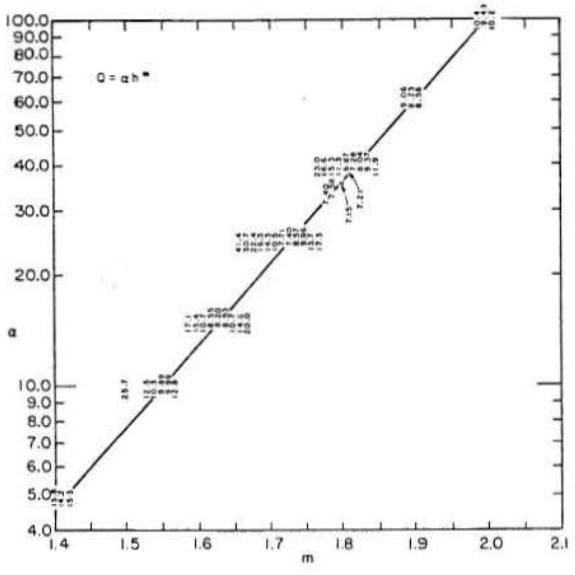

Figure 3-27. Values of objective function of two-parameter model, for concrete rectangular section rill surface.

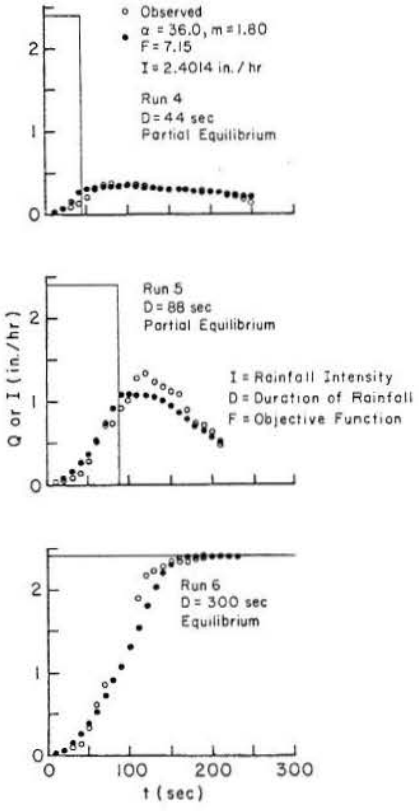

Figure 3-28. Comparison of hydrographs simulated by two-parameter model with observed hydrographs, for concrete rectangular section rill surface, with I = the rainfall intensity, D = the duration of rainfall, and F = the objective function value.

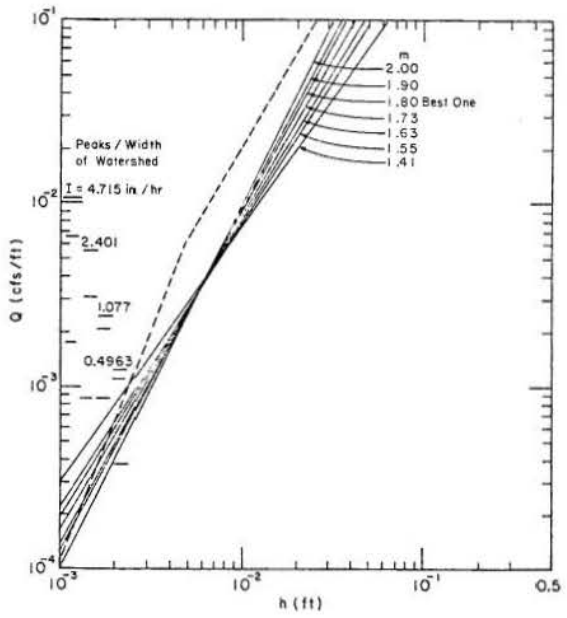

Figure 3-29. A family of Q vs h curves having lower values of objective function of two-parameter model, for concrete rectangular section rill surface 98.4 ft by 6.6 ft and 5 percent slope.

Comparison of Results

Comparison between the computed hydrographs simulated by the three-parameter model and by the two-parameter model shows that both are almost equally good for simulating the observed hydrographs, see Figs. 3-19, 3-22, 2-24 and 3-28. However, the two-parameter model requires substantially less computer time.

The Q vs h curves of the best-fit parameters estimated for the three-parameter model show an almost straight line relationship in the log-log graph for a cycle of log scale representing the main range of discharges of the unit width discharge, as shown in Figs. 3-18 and 3-21. Comparison of the Q vs h relationships for the three-parameter model and the two-parameter model shows that the deviations between these relationships on their extremes, which are outside the main range of discharges, do not significantly affect the hydrograph shapes. Because the main discharge range covers only a limited segment of the Q vs h curve and because the curvature for the three-parameter model is small, the Q vs h curve can be approximated by a straight line which is equivalent to the relationship for the two-parameter model.

From a set of the Q vs h relationships, with low values of objective functions (Figs. 3-25, 3-29), the location of curves on a graph is much more important than the slope of the curves. Once the location is correctly assigned, small changes in m do not affect significantly the hydrograph shape.

Correia (1972) and Brazil (1976) found the relationships of Q vs h for rectangular watersheds using the two-parameter model and the dye-injection method under equilibrium. In this study, these relationships are determined by using the observed hydrographs. Comparison of results are shown in Figs. 3-30

and 3-31. This study used the concrete rill surface watershed that was also used by Brazil. The water depths, h, obtained by Brazil had lower values than the values obtained in this study. The reason for departures is likely the concentration of dye in the rills and the measurement of velocity in dye injection, which tend to give a velocity higher than the average velocity.

In general, the deviations in the Q vs h relationships for the low flow rates cause hydrograph deviations on both its rising and falling limbs. However, the values of low flows for an observed hydrograph are not reliable. The devices used mainly for measuring the peak flows often produce inaccurate results in low flows. Additionally, the low flows of a hydrograph may not be important for flood hydrograph studies. The three-parameter model more precisely describes the relationship of discharge to the equivalent water depth over a wide range of flows. However, from a practical viewpoint, the Q vs h relationship for high flows dominates the hydrograph shape. Then the two-parameter model is sufficient to describe the relationship of discharge to equivalent water depth for the hydrograph simulation.

The two-parameter model requires much less computer time for optimization in comparison with the three-parameter model. The resulting hydrographs fit the observed hydrographs as good as the three-parameter model. Since the low values of objective functions are located on a straight line in the log α vs m graph, it is easy to estimate the α and m parameters. Therefore, the two-parameter model is more efficient in simulation of hydrographs when only the high flow rates are important.

Since the three-parameter model can provide precise relationships of Q vs h over a wide range of flows, this model will be useful when both the high flow and low flow rates are important in hydrological problems. Three-parameter model has significance according to physical principles, therefore, the simulated hydrographs are close to physical reality. The parameter, λ, describes the variation of spaces between obstructions which is the main factor affecting the changing phenomena of flow in the vegetated area. The application of the three-parameter model may lead to study of the effect of changing land use on the flow hydrographs. Sediment transport capacity is proportional to between fourth and sixth power of flow velocity (Simons and Senturk, 1977). If the unit width discharge is constant, 10 percent error in estimate of detention storage will yield 10 percent error in velocity which will cause 45 to 75 percent error in the estimate of sediment transport. The low flow rates at the beginning and ending of the hydrograph are also important in the estimate of sediment transport since the low flow rates may last for a long time. The three-parameter model will produce smaller errors in estimation of detention storage for a wide range of flows, consequently, cause less errors in sediment and erosion analysis.

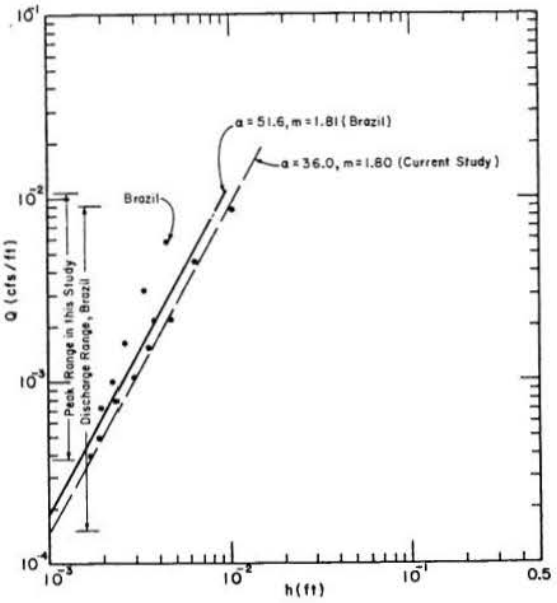

Figure 3-30. Comparison of results obtained in this study with results obtained by dye injection method (Brazil, 1976), for concrete rectangular rill surface.

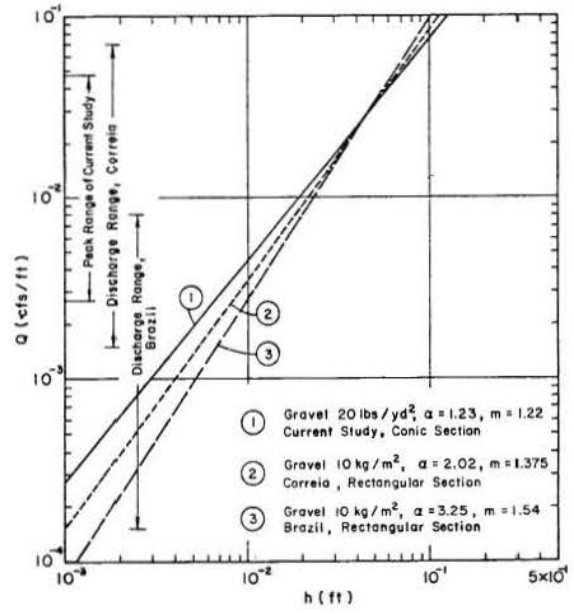

Figure 3-31. Comparison between results obtained by this study and results obtained by Correia (1972) and Brazil (1976) for gravel surface.

Chapter IV
ESTIMATES OF PARAMETERS FOR TWO-PARAMETER MODEL

4.1 Experimental Facilities

The data used in this study are from the Rainfall-Runoff Experimental Facility at Colorado State University. This facility provides a means for conducting controlled experimentation in watershed response. The facility's size is such that it is an intermediate step between laboratory models and natural watersheds; it has the capability of reproducing experiments with consistency, but is not so small as to distort the surface roughness characteristics.

The 25,000 square feet impervious surface has proven particularly useful in simulating urban watersheds where response times are short and infiltration is negligible. Characteristics such as surface roughness and geometry can be changed to represent a wide variety of natural catchments. The consistency with which the facility can be operated and the homogeneity of the surface area allows for test runs to be made where individual parameters can be examined independently. This capability makes the artificial watershed an excellent tool for testing theoretical relationships and mathematical models of runoff from an impervious watershed.

A complete synopsis of the original objectives and design of the facility is given in the paper by Dickenson, Holland and Smith (1967). The shape is two sloping planes, similar to Wooding's model (Wooding, 1965), with an additional upper conical section, Fig. 4-1. This shape can be defined mathematically and allows for simplification of data analysis. The planes slope of five percent in the direction of a line parallel to the straight side boundaries of the conic section. The conic section has a radius of 116 ft and a uniform slope of five percent. The conic section and planes can be divided by walls to make any desirable size of conic section or rectangular section. Water flowing on the conic and plane sections is separated by a six inch high boundary. A similar boundary wall exists around the entire surface.

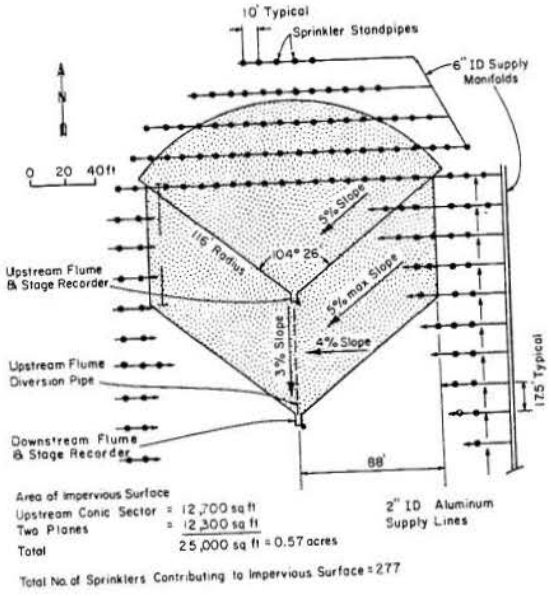

Figure 4-1. Colorado State University Rainfall-Runoff Facility--general arrangement.

The simulated rainfall is generated by 277 sprinklers, each located on top of a 10 ft vertical pipe. Water is supplied to the sprinkler risers by parallel aluminum lines, spaced approximately 17.5 ft apart. Each line has about 20 risers, each spaced 10 ft apart. Various intensities are created by electric solenoid valves operating a different combination of sprinklers. When all sprinklers are running simultaneously, approximately 4 in/hr of rainfall input is being generated. Use of fewer risers will create lower intensities.

Discharge from the watershed is captured and measured by two H flumes; one is a 1.5 ft H flume at the outlet of the conic section, and the other is a 2 ft H flume at the outlet of the plane section of the watershed. The conic and plane sections can be gauged separately or as a single watershed. When flow leaves the conic section, it can be either directed underground and measured separately or added to the flow from the planes and measured through the flume below the planes.

The hydrograph data of the conic section in this study are from experiments conducted during 1969 to 1972. During this period, about 600 runs for about 50 types of configurations with various shapes and sizes of sections and various roughness were conducted. All the data were put on magnetic tapes. The surfaces of various roughness include butyl rubber surfaces, butyl rubber surfaces covered with different densities of uniformly distributed gravel or bricks, and butyl surfaces with different arrangements of gravel covering. The data from the butyl surfaces covered with gravel of 20 lbs/yd^2 are mainly used in analysis, because they give the greatest number of different arrangements of gravel covering for systematic analysis.

The data of concrete rill surface were obtained from the experiment on a rectangular section on sloping plane in 1976. A 0.6 ft HS flume, with a converging section of 2 percent slope was used for measuring discharge at the downstream end.

4.2 Discharge Correction for Experimental Data

Examples of correction for discharge data are made for the two configurations used in Section 3.2, Comparison of Two-Parameter and Three-Parameter Models. They are the concrete rill surface with rectangular section of 98.4 ft long and 6.6 ft wide and a conic section of 30° central angle with butyl surface covered with uniformly distributed gravel of 20 lbs/yd^2 (Configuration 14). For the rectangular section, the time of hydrograph peak should be at the time when rainfall ceases. However, the observed data showed that the peaks were located after the rainfall ceases indicating time lags between the outflow hydrograph and the observed hydrograph. A discharge correction for storage effect in the measuring flume, and lag time correction for the time lag in the transition are required. Since the measuring flume at the end of the conic section does not have a transition, only a discharge correction is required. Figure 3-16 shows the shapes of the rectangular concrete rill section and the conic section with gravel. Figures 4-2 and 4-3 show some of the hydrographs before and after correction for conic and rectangular sections,

respectively. The methods of correction are discussed in Appendix A.

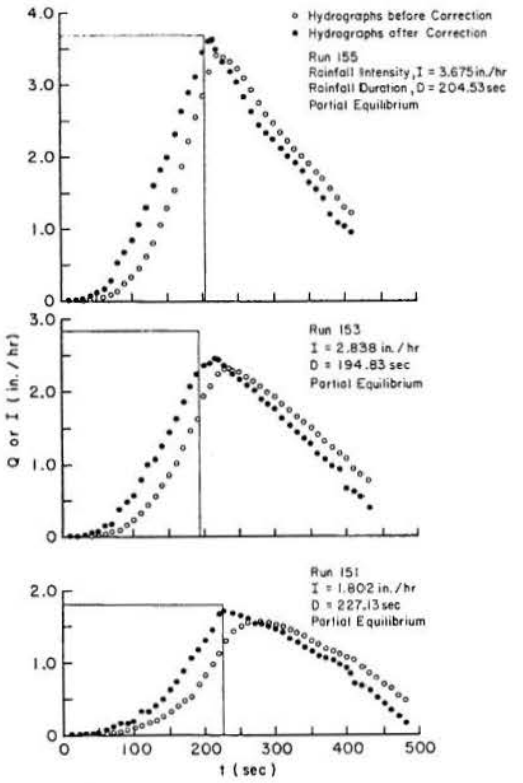

Figure 4-2. Comparison between hydrographs before and after correction, gravel surface of 20 lbs/yd^2, conic section.

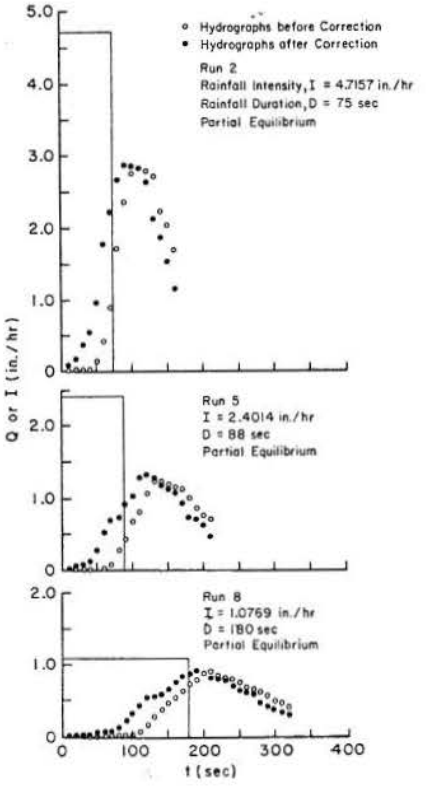

Figure 4-3. Comparison between hydrographs before and after correction, concrete rill surface, rectangular section.

4.3 Parameters for Various Surfaces

As stated in section 4.1, the greatest number of experimental runs were available for the butyl surface covered with 1.50 inch diameter gravel of 20 lbs/yd^2. These experiments provide data that can be used to test the concept of equivalent uniform roughness and to develop short-cut techniques to estimate the roughness parameters for the equivalent uniform surface if it exists.

Seven configurations with different arrangements of gravel surfaces including UFUT, UFNT, NFUT, and NFNT surfaces were chosen. These configurations are shown in Fig. 4-4. Table 4-1 gives rainfall intensities and durations for hydrographs used for each configuration. By assuming the watershed as a lumped system of uniform surface, the two parameter model was used for optimization of parameters. In order to test the assumed equivalent uniform surface, goodness-of-fit and ratio of peak difference were computed by comparing the observed hydrographs with the hydrographs simulated by optimized parameters for the equivalent uniform surface. The optimization results, including the α and m, the minima of objective functions and average values of goodness-of-fit are given in Table 4-2. For the hydrographs which have peaks greater than one inch per hour, Table 4-3 lists the values of goodness-of-fit and ratios of difference between peaks to the peak of uniform surface as defined in section 1.2. Figure 4-7 shows the comparison between the observed and simulated hydrographs by using the optimized parameters. Only a representative hydrograph for each configuration is shown.

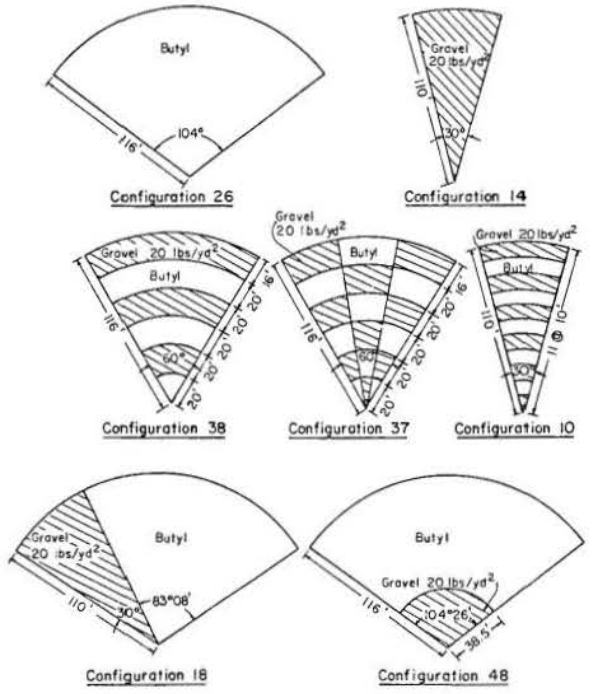

Figure 4-4. Configurations with different arrangements of gravel surfaces of 20 lbs/yd^2 gravel density.

Although configuration 26 is a UFUT surface, the values of goodness-of-fit are between 93 and 96 percent and the ratios of peak difference are between 1 and 25 percent. Errors in data measurement, in the

Table 4-1. Rainfall intensity and duration for hydrographs used in optimization.

Conf. No.	Number of Hydrographs Used	Intensity (In/Hr)	Duration (Sec)	Intensity (In/Hr)	Duration (Sec)	Intensity (In/Hr)	Duration (Sec)	Intensity (In/Hr)	Duration (Sec)
26 1/	12	4.135	53.19* 102.95 232.51e	2.035	45.54 94.69 401.79e	.814	65.58 116.30 293.26e	.415	81.58 126.60 557.67e
14	12	3.675	53.71* 204.53 405.62e	2.838	53.00 194.83 542.69e	1.802	56.98 227.13 462.03e	.784	61.91 272.44 500.87e
38	9	4.073	38.51* 80.12 908.93e	1.807	38.26 99.57 151.99e	.824	52.39 117.57 946.00e		
37	10	3.555	728.79e	1.686	51.24 121.45* 657.01e	.771	49.74 123.87 177.62	.396	51.23 134.35 613.59e
10	8	4.094	69.12* 278.58e	2.374	79.17 715.38e	1.130	124.63 380.20e	.487	161.37 503.91e
18	10	3.739	90.87 131.27* 415.04e	2.073	99.40 143.04 591.91e	.937	94.84 223.76 585.39e	.437	536.93e
48 2/	12	4.401	41.27* 118.85 411.33e	4.337	34.54 103.80 370.63e	1.071	42.88 72.91 92.81 222.20e	.494	32.43 236.81

e Equilibrium Hydrographs
* Representative hydrographs of Fig. 4-7.
1/Including configurations 26, 27, 28, and 29
2/Including configurations 48 and 49.

Table 4-2. Optimized parameters α and m.

Configuration No.	Description of Surface	α	m	Minima of Obj. Fct. F	No. of Hydrographs Used	Average Values of Goodness-of-fit	Equivalent Uniform Roughness
26	UFUT Butyl Surface, Conic Section, L=116 ft.	10.5	1.44	13.90	12	93.8	-
14	UFUT Gravel Surface, 20 lbs/yd^2 Conic Section, L=110 ft.	1.23	1.22	8.15	12	96.2	-
38	NFUT Gravel (20 lbs/yd^2) & Butyl Alternative Strips, 20 ft. width Conic Section, L=116 ft.	3.70	1.35	3.13	9	96.0	Yes
37	NFUT Gravel (20 lbs/yd^2) & Butyl Checkerboard, 20 ft. width Conic Section, L=116 ft.	2.50	1.29	1.80	10	93.8	Yes
10	NFUT Gravel Surface (20 lbs/yd^2) and Butyl Alternate Strips, 10 ft. width Conic Section, L=110 ft.	9.00	1.60	6.21	8	94.0	Yes
18	UFNT Gravel Surface 30° (20 lbs/yd^2) and Butyl Surface 83°, Conic Section, L=110 ft.	10.00	1.46	55.91	10	89.4	No
48	NFUT Upper Portion Butyl & Lower Portion Gravel (20 lbs/yd^2) 30.5 ft., Conic Section L=116 ft.	11.50	1.63	52.26	12	91.1	No

Table 4-3. Goodness-of-fit and peak deviation of hydrographs.

Conf. No.		I (in/hr)	D (sec)	Goodness-of-fit (%)	Ratio of difference Between Peaks to Peak of Uniform Watershed in Percent
26		4.135	53.19	93.6	12.3
		4.135	102.95	95.2	3.6
		2.035	45.54	93.8	24.4
		2.035	94.69	92.7	1.6
	Avg.			93.8	10.5
14		3.675	53.71	96.9	5.0
		3.675	204.53	96.1	2.6
		2.838	194.83	95.6	3.9
		2.838	53.00	96.0	14.8
	Avg.			96.2	6.5
38		4.073	38.51	95.5	7.1
		4.073	80.12	97.3	1.1
		1.807	99.57	96.1	1.0
		1.807	151.99	95.2	6.0
	Avg.			96.0	3.8
37		1.686	51.24	93.3	15.6
		1.686	121.45	95.6	1.7
		.777	177.62	93.1	4.3
		.771	123.87	93.2	5.3
	Avg.			93.8	8.5
10		2.374	79.17	93.7	32.9
		4.094	69.12	95.0	22.8
		1.130	124.63	93.3	25.5
	Avg.			94.0	27.1
18		3.739	90.87	86.5	29.6
		3.739	131.27	92.4	5.1
		2.073	99.40	88.9	18.2
		2.073	143.04	89.7	19.4
	Avg.			89.4	18.1
48		4.401	41.27	91.6	25.8
		4.401	118.85	91.9	8.5
		4.337	34.54	89.2	53.8
		4.337	103.8	91.5	16.7
	Avg.			91.1	26.2

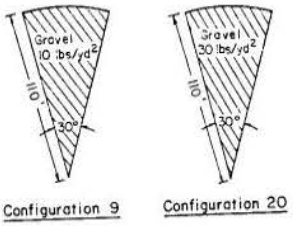

Configuration 9 Configuration 20

Figure 4-5. Configurations with gravel of 10 lbs/yd^2 and 30 lbs/yd^2.

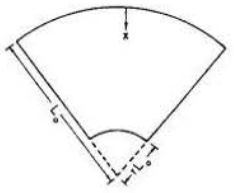

Figure 4-6. Variables used for conic sections.

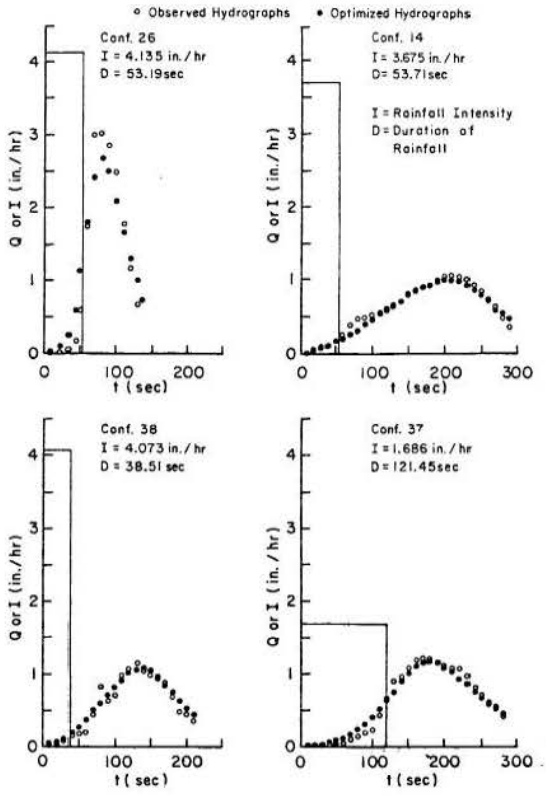

Figure 4-7. Comparison of simulated hydrographs by using optimized parameters with observed hydrographs.

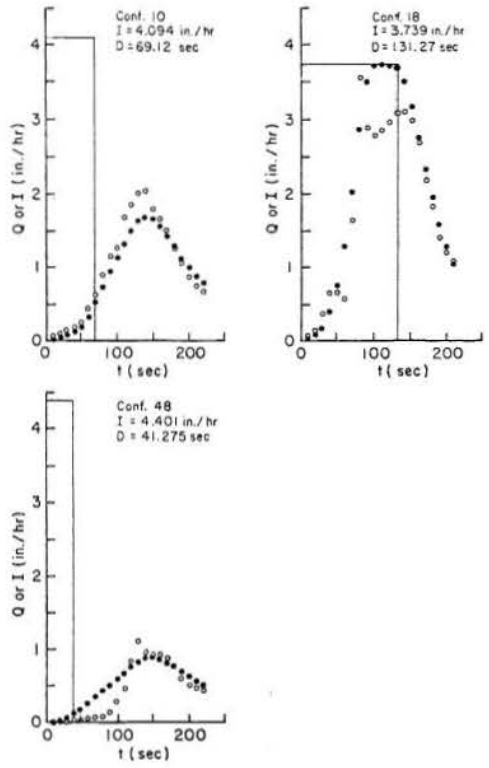

Figure 4-7. (Continued).

selected physical model, and in the numerical solution of kinematic wave equation are unavoidable. The ratios of peak difference are not consistent and deviate a great deal. The reason might be in the difficulties of measuring the discharges of instant peaks. Because of inaccuracy of peak discharge measurement, the criterion of equilibrium uniform roughness might be set at $G_e = 0.93$ without restriction in Pe (see definitions in section 1.2). With this criterion, configurations 26, 14, 38, 37, and 10 are classified as the surfaces of equivalent uniform roughness and configurations 18 and 48 as the surfaces of not equivalent uniform roughness. In general, the simulated hydrographs of configurations 26, 14, 38, 37, and 10 fit well the observed hydrographs. Configuration 18, classified as UFNT, consisted of two conic sections, one a 30 degree gravel conic section and the other an 83 degree butyl section. The observed hydrographs have either comparatively flat peaks or double peaks, because of a combination of two hydrographs from the two sectors. However, the hydrograph simulated from a lumped system of uniform surface can produce only a single peak. This may be the reason why the simulated hydrographs do not fit well the observed hydrographs. Configuration 48, classified as NFUT, consisted of a 116 ft radius conic section with a butyl surface on the upper section and butyl covered by gravel on the downstream section of 38.5 ft. Evidently, the concept of the equivalent uniform roughness could not be used because the observed hydrographs do not agree with the hydrographs of uniform surface.

Since configurations 38, 37 and 10--NFUT and NFNT surfaces composed of alternate roughness of more than six strips--are classified as the equivalent uniform roughness, a watershed composed of alternate roughness may be simulated by an equivalent uniform roughness if the width of strips is less than one sixth of the total flow length. The hydrographs for this kind of watershed can be simulated by using a two parameter model and assuming the system to be a uniform surface. For UFNT surface, it is better to simulate the hydrographs by a distributed system.

4.4 Identification of Watershed Response for Surfaces with the Same Density of Gravel

The parameter optimization technique can be used to determine the roughness parameters for an equivalent uniform surface, however, it is sometimes slow and costly. In this section some techniques for determining equivalency of watershed response are discussed and the experimental watersheds of equivalent uniform roughness with the same density of gravel were used for the test of identification of watershed response. This will help estimation of roughness parameters for watersheds which have the same density of various roughnesses.

(i) By comparison of dimensionless hydrographs:

Woolhiser (1969) introduced the dimensionless hydrographs for the conic section (Fig. 4-6) with the normalized units:

$$Q_* = Q/Q_o \qquad (4\text{-}1)$$

and

$$t_* = t/T_o \qquad (4\text{-}2)$$

with Q* = the dimensionless discharge, t* = the dimensionless time, Q = the outflow discharge, t = the time, Q_o = the normalized discharge at $x = L_o(1-r)$ under steady state conditions, r = the degree of concentration (see Fig. 4-6), T_o = the time required to travel the distance Lo(1-r) at the velocity Vo, given by

$$T_o = \left(\frac{2}{q}r\right)^{\frac{m-1}{m}} \cdot \left(\frac{L_o}{\alpha}\right)^{\frac{1}{m}} \cdot \frac{(1-r)^{\frac{1}{m}}}{(1+r)}, \qquad (4\text{-}3)$$

where V_o = the steady-state normal velocity at x = Lo(1-r), q = the lateral inflow rate, Lo = the radius of conic section and x = the radial distance from the upstream end.

The shape of the rising and recession limbs of a dimensionless equilibrium hydrograph is independent of α and q, but depends on the m and r values. For watersheds with the same r, the shapes of dimensionless hydrographs should be the same if m values are identical. To test if m values are identical, for various watersheds with the same density of gravel, watersheds of configurations 9, 38, and 10 including UFUT and NFUT surfaces were used. Configuration 9 consisted of a 30° conic, butyl covered section, with 1 1/2 inches diameter gravel and a density of 10 lbs/yd^2. Configuration 38 consisted of a 60° conic section of alternate butyl and gravel strips, 20 ft wide, while configuration 10 had a 30° section and alternate strips 10 ft wide. The r values for those configurations are very small and considered as the same. Instead of the time required for water to

travel the distance of $L_o(1-r)$ at the velocity V_o, the water storage at the equilibrium (in inches), divided by the lateral inflow rate (in in/sec), was taken as the normalizing time parameter T_o, since V_o was not measured in experiments. These two normalizing times have a constant ratio for a constant r value, and the change of the normalizing time does not affect the shapes of hydrographs.

Two equilibrium hydrographs are selected for each configuration, with the rising and falling limbs of their dimensionless hydrographs shown in Fig. 4-8. In general, the shapes of superimposed hydrographs are very similar, so there is no reason to reject the hypothesis that m values are identical.

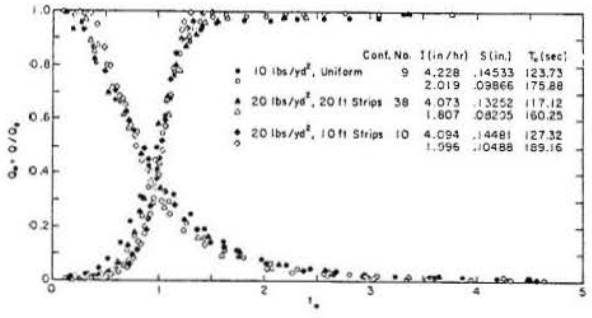

Figure 4-8. Superimposed dimensionless equilibrium hydrographs for configurations 9, 10 and 38.

(ii) By comparison of characteristic time:

The normalizing time, T_o, as the equilibrium storage divided by the lateral inflow rate, is the simplest parameter to measure experimental watershed response. It is called herein the characteristic time. Theoretically, T_o is proportional to $q^{(1-m)/m}(L_o/\alpha)^{1/m}$ if r is constant. When L is a constant, values of α and m are identical if the relationships of observed T_o vs q are identical for the watersheds with the same density of gravel. Configurations 9, 10, 37 and 38, including UFUT, NFUT, and NFNT surfaces, were used for the test. The radii, L_o, of conic sections of these configurations are not the same; two of them are 116 ft and the other two are 110 ft. However, the small difference in L_o will create only around 3.6% error in T_o if m = 1.5. Since the error is not very large, Lo is assumed constant for the test.

The data of T_o vs q are plotted in a log-log graph as shown in Fig. 4-9. Theoretically, log T_o vs log q is a linear relationship and the regression lines can be used for the test of identity of the relationship. Let x = log q and y = log T_o, then the linear models for various watersheds are:

$$\left.\begin{aligned} y &= \beta_{10} + \beta_{11}x \\ y &= \beta_{20} + \beta_{21}x \\ y &= \beta_{30} + \beta_{31}x \\ y &= \beta_{40} + \beta_{41}x \\ &\cdots\cdots\cdots\cdots \end{aligned}\right\} \quad (4\text{-}4)$$

For the test of the equality of these linear models, the hypothesis

$$H_o:\ \beta_{10} = \beta_{20} = \beta_{30} = \beta_{40} = \cdots$$

$$\beta_{11} = \beta_{21} = \beta_{31} = \beta_{41} = \cdots$$

is tested, with the H_o rejected if, and only if, $W > \alpha{:}2(H-1),\ N-2H$, with

$$W = \frac{(S_{yy} - S_{y^2}/N) - \dfrac{(S_{xy} - S_x S_y/N)^2}{S_{xx} - S_x^2/N} - S_{\hat{\sigma}^2}}{S_{\hat{\sigma}^2}} \cdot \frac{N-2H}{2(H-1)}, \quad (4\text{-}5)$$

H = the number of linear models, $N = \sum_{h=1}^{H} n_h$, n_h = the number of observations in model h, α = level of significance,

$$\left.\begin{aligned} &S_y = \sum_{h=1}^{H}\sum_{j=1}^{n_h} y_{hj},\ S_x = \sum_{h=1}^{H}\sum_{j=1}^{n_h} x_{hj},\ S_{yy} = \sum_{h=1}^{H}\sum_{j=1}^{n_h} y_{hj}^2, \\ &S_{xx} = \sum_{h=1}^{H}\sum_{j=1}^{n_h} x_{hj}^2,\ S_{xy} = \sum_{h=1}^{H}\sum_{j=1}^{n_h} x_{hj}\,y_{hj}, \\ &S_{\hat{\sigma}^2} = \sum_{h=1}^{H}\left[\sum_{j=1}^{n_h}(y_{hj}-y_h)^2 - \frac{\left[\sum_{j=1}^{n_h}(y_{hj}-\bar{y}_h)(x_{hj}-\bar{x}_h)\right]^2}{\sum_{j=1}^{n_h}(x_{hj}-\bar{x}_h)^2}\right] = \sum_{h=1}^{H}(n_h-2)\hat{\sigma}_h^2 \end{aligned}\right\} \quad (4\text{-}6)$$

(see F. A. Graybill, "Theory and Application of the Linear Model," 1976, Duxbury (Ch. 8, Sec. 6), "Testing the Equality of a Set of Linear Models"). The computation for the test of equality is shown in Table 4-4(A). Since W is less than $F_{\alpha:2(H-1),\ N-2H}$, there is no reason to reject the hypothesis of identity. By assuming all the linear models to be identical, the regression analysis gives the equation for the characteristic time as $T_o = 206.490\ q^{-0.331203}$, or T_o is proportional to $q^{(1-m)/m}$, and $(1-m)/m = -0.331203$, with m = 1.495.

To test whether or not this technique can discriminate between radically different surfaces, the data from configurations 14 and 20, consisting of gravel of 20 lbs/yd^2 and 30 lbs/yd^2 densities respectively, are included in the test of identity. Computations are shown in Table 4-4(B) and the data points are also plotted in Figure 4-9. Since W is greater than $F_{\alpha:2(H-1),\ N-2H}$, the hypothesis of equality of models is rejected.

Table 4-4. Test of the equality of a set of linear models.

(A) Gravel density of 10 lbs/yd^2

Conf. No.	n_h	$\sum y_{hj}$	$\sum y_{hj}^2$	$\sum x_{hj}$	$\sum x_{hj}^2$	$\sum x_{hj}y_{hj}$	$(n_h-2)\hat{\sigma}_n^2$
9	4	9.112951	20.821835	0.508717	0.616636	0.980432	0.00260811
10	8	18.317541	42.037539	1.150460	0.939900	2.367826	0.00438123
38	3	6.613238	14.615074	0.782799	0.445090	1.631513	0.00000155
37	4	9.043890	20.497972	0.262447	0.529496	0.442415	0.00549366
$\sum$	19	43.087620	97.972420	2.704423	2.531122	5.422186	0.01248455

$H = 4$, $N = 19$, $\alpha = 5\%$, $W = 1.720990 < F_{.05:6,11} = 3.09$

(B) Gravel densities of 10, 20, and 30 lbs/yd^2

Conf. No.	n_h	$\sum y_{hj}$	$\sum y_{hj}^2$	$\sum x_{hj}$	$\sum x_{hj}^2$	$\sum x_{hj}y_{nj}$	$(n_h-2)\hat{\sigma}_n^2$
9,10 38,37	19	43.087620	97.972420	2.704423	2.531122	5.422186	0.01248455
14	4	9.173848	21.048382	1.168340	0.601315	2.634699	0.00077733
20	4	9.466609	22.413930	1.172117	0.577885	2.727485	0.00053139
$\sum$	27	61.728077	141.434732	5.044880	3.710322	10.784370	0.0379327

$H = 6$, $N = 27$, $\alpha = 5\%$, $W = 6.798 > F_{.05:10,15} = 2.04$

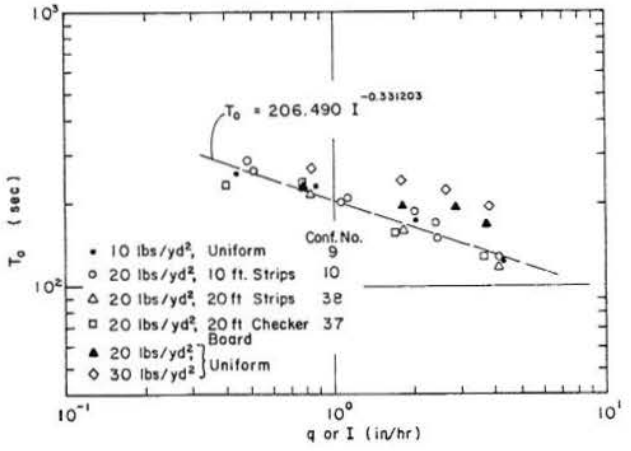

Figure 4-9. Characteristic time vs lateral inflow rate.

The conclusion is that watersheds of the same density of gravel on the butyl surface for which the concept of equivalent uniform roughness is applicable may have the same values of α and m, although the arrangements are different. Furthermore, this technique can discriminate between watersheds with different density of various roughness.

(iii) By comparison of partial equilibrium peaks:

For constant values of m and r, the dimensionless partial equilibrium hydrographs should be identical if the dimensionless durations of lateral inflows are the same. The dimensionless peak increases as the dimensionless duration increases. There is a relationship between the dimensionless peak and the dimensionless duration of lateral inflow if m and r are constant, regardless of the values of α and q. The partial equilibrium hydrograph of the four watersheds with constant r, used in the previous section, are used herein for the test of identity of m. The data of Q_p/Q_e vs D/T_o are plotted in Fig. 4-10, with Q_p = the partial equilibrium peak, Q_e = the equilibrium or steady state discharge, D = the duration of lateral inflow, and T_o = the characteristic time obtained from the regression line of Fig. 4-9. The results show a large scatter of observed values so that it is difficult to say whether the relationships Q_p/Q_e vs D/T_o for the four watersheds are identical or not, or whether the values of m are identical. The reason for the scatter is likely due to the difficulty in measuring the actual peak under the partial equilibrium conditions. Under these conditions the plane surface produces a flat peak hydrograph, while the conic section gives a sharp peak hydrograph. Uneven surface of watersheds and water storage in the measuring flume of the conic section greatly affect the peak values. In addition, the sensitivity of the measuring gage also affects the accuracy of observed peaks.

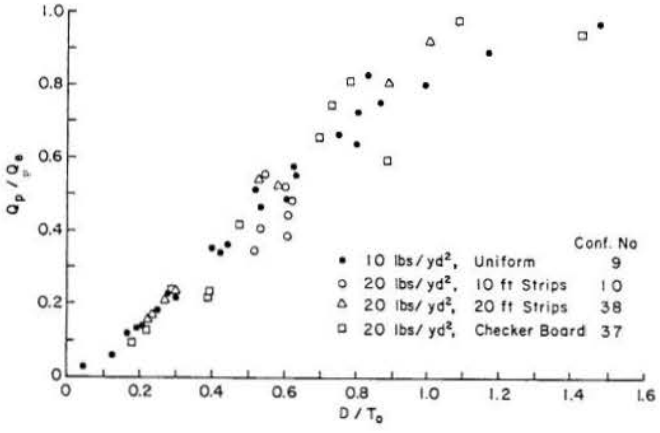

Figure 4-10. The Q_p/Q_e vs D/T_o relationship points.

4.5 Comparison of Hydrographs Obtained by Optimization of Parameters and Hydrographs Simulated by a Distributed System with the Observed Hydrographs

With the optimized values of α and m for a butyl surface (configuration 26) and a gravel surface of 20 lbs/yd^2 density (configuration 14) given in Table 4-2, hydrographs for watersheds of a combination of butyl and gravel surfaces can be simulated by using the numerical scheme of a distributed system. The representative observed hydrographs, simulated hydrographs by using the optimized parameters, and simulated hydrographs in using a distributed system for nonuniform watersheds are superimposed in Fig. 4-11 for comparison. Hydrographs are also simulated for a distributed system by reversing the arrangement of butyl and gravel locations in configurations 37, 38, and 10. The values of the objective function are given in column (4) and (5), Table 4-5.

For configurations 38 and 37, classified as the surfaces of equivalent uniform roughness, the hydrographs are successfully simulated by both the optimization technique and the distributed systems with low values of objective function. The simulated hydrographs obtained by using a distributed system fit the observed hydrographs as well as the optimized hydrographs do. Since the weights of butyl and gravel surfaces are equal in both configurations, the values of objective functions are kept low when the locations of butyl and gravel are reversed. For configuration 18, classified as the surface of not equivalent uniform roughness, the value of objective function is greatly reduced when the distributed system is used for simulating hydrographs. The hydrographs simulated

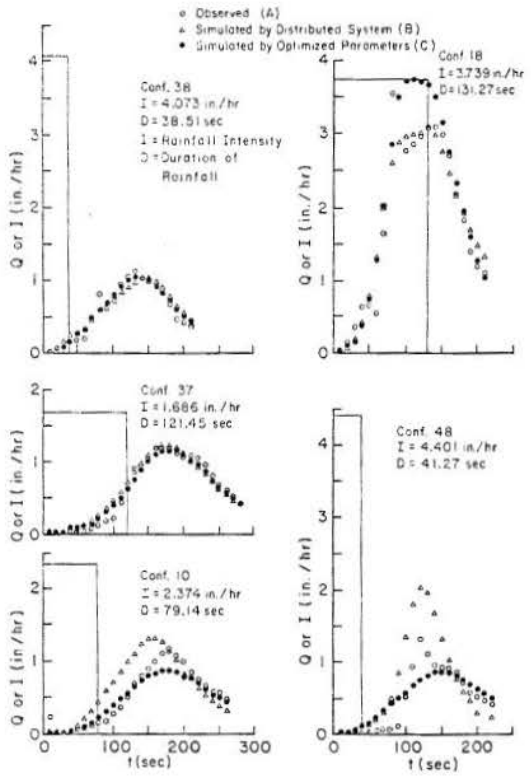

Figure 4-11. Hydrographs for various configurations; (A) observed hydrographs, (B) hydrographs simulated by distributed system, (C) hydrographs simulated by using optimized parameters, with I = the rainfall intensity and D = the duration of rainfall.

Table 4-5. Objective function of simulated hydrographs of watersheds with various arrangements of gravel layers on butyl surface.

Configuration and Classification			Optimized Parameters (2)		Objective Functions $(in/hr)^2$ (Sum of Squares of Deviations)			
	(1)				Optimized Hydrographs (3)	Computed Hydrographs by Numerical Scheme with Distributed System (4)	Same as (4) but Reverse Gravel and Butyl (5)	Computed Hydrographs by Numerical Scheme, Assuming Uniform, α = 2.6826, m = 1.30 (6)*
No.	Configuration	Equivalent Uniform Roughness	α	m				
38	NFUT	Yes	3.70	1.35	3.13	4.42	11.71	6.03
37	NFNT	Yes	2.50	1.29	1.80	2.70	1.87	2.10
10	NFUT	Yes	9.00	1.60	6.21	24.2	30.16	25.1
18	UFNT	No	10.00	1.46	55.90	18.7		
48	NFUT	No	11.50	1.63	52.3	64.4		

*estimations of α and m are described in Section 5.2.

by the distributed system fit the observed hydrographs much better than the optimized hydrographs of a lumped system do. This means that the UFNT surface should not be sumulated by a lumped system but by a distributed system.

In order to avoid the errors resulting from the depression and interception losses at the beginning of rainfall, the observed time of beginning of rainfall excess was corrected at each run by subtracting the time required to fill the amount of depression loss and compensate for the interception loss. The amount of these losses were obtained by subtracting the total outflow volume from the input rainfall. Under the normal conditions, the time correction should be negative, meaning that the time correction should be subtracted from the original time record. However, time corrections in most runs for configurations 48 and 10 were positive. The observed hydrographs might have time errors. The factors that caused these errors are: (1) simulated rainfall at some sprinkler heads was retarded in comparison with the general initiation of rainfall; (2) some of the sprinkler heads could not be shut off immediately at the end of simulated rainfall; and (3) there was some pipe leakage. Since the total volume of outflow was computed from the long duration hydrographs, the factor (3) may have mostly affected the time correction, with the error larger for lower flow rates. The observed hydrographs of configurations 48 and 10 show the low flows to last for a long time at the initiation of runoff output due to errors in time corrections. During the process of minimizing the objective function, the simulated hydrographs were forced to fit the low flows of a long duration at the hydrograph initiation, and become relatively flat and wide hydrographs. In a comparison, the hydrographs generated by a distributed system give sharper high peaks which agree better with the observed peaks. Although the values of objective functions for hydrographs simulated by a distributed system are the same or greater than those for hydrographs simulated by optimized parameters, the simulation by a distributed system is considered to be better. The simulated hydrographs by distributed system should fit the observed hydrographs more closely if the time correction is proper. For NFUT surface composed of large elements of various roughness such as configuration 48, the watershed is classified as the surface of not equivalent uniform roughness, and the simulation by the distributed system is considered much more feasible than the simulation by optimized parameters.

Chapter V
SPATIAL VARIABILITY OF ROUGHNESS

5.1 Uniformity of Roughness

For UFNT watersheds, the outflow hydrographs can be easily simulated by a combination of hydrographs from elements of various roughnesses. However, flow phenomena on NFUT surfaces are more complicated and the application of equivalent uniform roughness for simplification of hydrograph simulation will be necessary. In this section a shortcut method is given for testing whether the equivalent uniform roughness can be used for hypothetical NFUT watersheds composed of alternate elements of butyl and gravel with equal weight along the flow direction. The watersheds are assumed to be the conical sections with a radius of 120 ft and a slope of five percent.

Hydrographs from the two NFUT watersheds A and B, which are identical except that the locations of butyl and gravel elements are reversed, are considered. When the size of elements is sufficiently large, the watersheds do not behave as the surface of equivalent uniform roughness, in which case the two hydrographs simulated for the two watersheds with the same rainfall input will deviate to a great deal. As the size of the elements decreases, the two hydrographs will tend to be closer. When the size of elements become sufficiently small, the two watersheds can be treated as the surfaces of equivalent uniform roughness and the two hydrographs will nearly coincide. The shortcut method for testing the equivalent uniform roughness is to compare the two hydrographs simulated for watersheds A and B. Either the watershed A or the watershed B can be considered as the watershed of equivalent uniform roughness if the two hydrographs from A and B nearly coincide. The goodness-of-fit and ratio of peak difference, as described in section 1.2, are used for the justification of use of the equivalent uniform roughness. When a pair of hydrographs simulated from two NFUT surfaces of reversible roughness arrangements is used to measure the deviations between the hydrographs, the deviations would be double of the deviations between the hydrograph of a nonuniform roughness and the hydrograph of a uniform roughness surface. The criterion of G_e should be smaller than 0.93 used in Chapter IV for comparison between the observed hydrograph of a nonuniform roughness surface and the hydrograph simulated from a uniform roughness surface. However, as there are no observational errors involved in using only the numerical models, the more strict criteria for an equivalent uniform roughness surface are used, i.e., $G_e = 0.93$ and $P_e = 0.05$.

Conical areas (watersheds of curved strips normal to the direction of flow, as shown in Fig. 1.2(C)), composed of 2, 4, 6, 8, and 10 alternate strips either of equal width or equal area are used in these tests. Since hydrograph simulation by the distributed system with kinematic cascade planes can produce hydrographs very close to the observed hydrographs of NFUT surfaces, this method has been used for generation of hydrographs for the considered hypothetical watersheds. Two criteria used for numerical simulation of a cascade of planes are: (1) the number of planes in kinematic cascade is at least five, and (2) the number of Δ increments in each plane is at least three. For each hypothetical configuration, twelve pairs of hydrographs are generated for testing the equivalent uniformity of roughness, namely three durations (one for equilibrium and two for partial equilibrium) for each of the four intensities of 1, 2, 3, and 4 inches of rainfall per hour. Figure 5-1 shows two out of the twelve pairs of hydrographs simulated for the watersheds composed of ten alternate strips of gravel and butyl surfaces. Hydrographs marked 1 and 2 are simulated for watersheds which are divided into ten strips of equal width, and hydrographs 3 and 4 are for watersheds which are divided into ten strips of equal areas. Hydrographs 1 and 3 are simulated for watersheds which have a gravel strip at the upper end, and hydrographs 2 and 4 for watersheds which have a butyl strip at the upper end. The hydrographs simulated for the watersheds with ten equal width strips (1 and 2) are almost identical even though the roughness locations are reversed while the hydrographs (3 and 4) simulated for the watersheds with ten equal area strips, deviate to a great deal when the roughness locations are reversed. Since deviations of partial equilibrium hydrographs are more evident than those of equilibrium hydrographs, only eight pairs of partial equilibrium hydrographs simulated for the reversible arrangements are used for the test of goodness-of-fit. Values of goodness-of-fit and ratios of peak deviation to the lower peak of two hydrographs were computed for eight pairs of hydrographs in each configuration, and their maximum, minimum, and average values are shown in Table 5-1. The average values of goodness-of-fit parameter with respect to the number of strips are plotted on Fig. 5-2. The results show that the surface of watershed with equal width strips can be treated as having an equivalent uniform roughness if the number of strips is greater than six. However, the surface of watershed with equal area strips cannot be treated as having an equivalent uniform roughness even though the number of strips is increased to ten. In one-dimensional flow, the linear uniformity of roughness along the flow direction is much more important than the areal uniformity in meeting the condition of treating it as having equivalent uniform roughness. In other words, when the width of equal width strips is less than one sixth of total flow length, the surface of the watershed can be treated as having an equivalent uniform roughness and may be approximated by a uniform roughness surface. Actually, the width of strips meeting the equivalent uniform roughness condition is related to the difference between the two roughnesses. The larger the width of strips the smaller is the difference between the two roughnesses.

Considering the hydrographs produced by a watershed of ten equal width strips as the hydrographs of a uniform roughness surface the sums of squares of deviations between the 12 pairs of hydrographs simulated from watersheds of ten equal width strips (column A) and hydrographs simulated from watersheds of fewer than ten strips (column B) are shown on Table 5-2. Representative hydrographs are shown in Figs. 5-3, 5-4, and 5-5. It can be inferred from them that the deviations of hydrographs of conical watersheds with equal area strips are larger than the deviations of hydrographs of conical watersheds with equal width strips.

5.2 Estimation of Mean Parameters for the Surface of Equivalent Uniform Roughness

Estimation of Mean Parameters

For the two-parameter model, $Q = \alpha h^m$, it is logical to assume that the regression line of log Q vs log h for a watershed composed of two basic surfaces of different roughnesses, will pass through the intersection point of regression lines for the basic

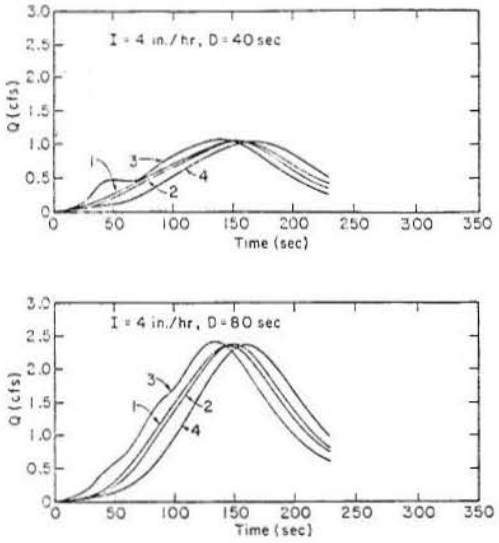

1. 10 Equal Width Strips, Gravel-Butyl-Gravel-Butyl
2. 10 Equal Width Strips, Butyl-Gravel-Butyl-Gravel
3. 10 Equal Area Strips, Gravel-Butyl-Gravel-Butyl
4. 10 Equal Area Strips, Butyl-Gravel-Butyl-Gravel

Figure 5-1. Hydrographs simulated by distributed systems of ten alternate strips of gravel and butyl, L_o = 120 ft.

Table 5-1. Goodness-of-fit parameter and ratio of peak deviation of hydrographs for rever sible watersheds of alternate strips.

Number of Strips	Goodness-of-fit Parameter			Ratio of Peak Deviation		
	Average	Max.	Min.	Average	Max.	Min.
Equal Width Strips						
10	0.963	0.971	0.960	0.0060	0.0176	0.0015
8	0.955	0.962	0.948	0.0106	0.0367	0.0028
6	0.938	0.950	0.931	0.0248	0.0414	0.0035
4	0.874	0.904	0.828	0.0520	0.0986	0.0091
2	0.766	0.800	0.755	0.7554	0.8493	0.6146
Equal Area Strips						
10	0.816	0.851	0.800	0.0251	0.0318	0.0172
8	0.795	0.836	0.775	0.0261	0.0361	0.0028
6	0.767	0.818	0.744	0.0309	0.0614	0.0006
4	0.706	0.763	0.675	0.0816	0.1528	0.0182
2	0.599	0.682	0.562	0.0901	0.1231	0.0307

Goodness-of-fit parameter, $G = 1 - D/2a$.

Ratio of peak deviation, $(P_1 - P_2)/P_2$, with $P_1 > P_2$.

Intensities and durations of eight rainfall inputs:

Rainfall Intensity (In/Hr)	Duration (Sec)	
4	40	80
3	45	90
2	55	110
1	60	120

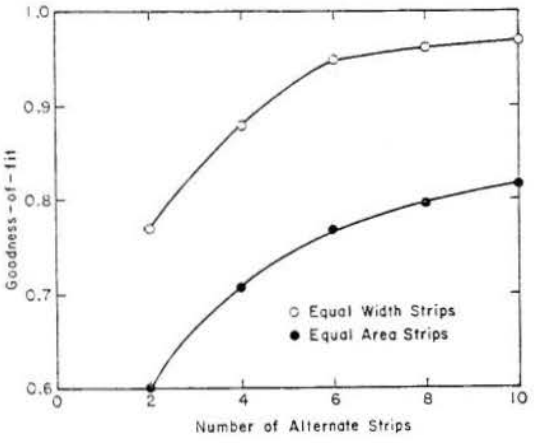

Figure 5-2. Goodness-of-fit parameter versus number of alternate strips.

Table 5-2. Test of feasibility of using the concept of uniform roughness for conical watersheds with gravel strips on a butyl surface.

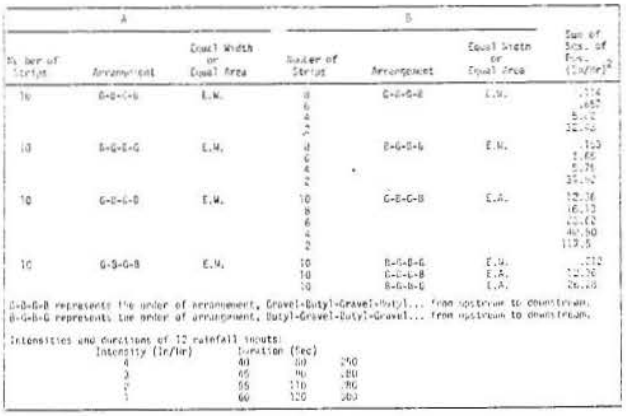

A			B			
No. ber of Strips	Arrangement	Equal Width or Equal Area	Number of Strips	Arrangement	Equal Width or Equal Area	Sum of Sca. Of Peak (In/Hr)²
10	G-B-G-B	E.W.	8	G-B-G-B	E.W.	.1514
			6			1.665
			4			5.412
			2			22.760
10	B-G-B-G	E.W.	8	B-G-B-G	E.W.	.103
			6			1.65
			4			5.71
			2			31.102
10	G-B-G-B	E.W.	10	G-B-G-B	E.A.	12.36
			8			16.13
			6			23.62
			4			46.50
			2			113.5
10	G-B-G-B	E.W.	10	B-G-B-G	E.W.	.212
			10	G-B-G-B	E.A.	12.36
			10	B-G-B-G	E.A.	26.20

G-B-G-B represents the order of arrangement, Gravel-Butyl-Gravel-Butyl... from upstream to downstream.
B-G-B-G represents the order of arrangement, Butyl-Gravel-Butyl-Gravel... from upstream to downstream.

Intensities and durations of 12 rainfall inputs:

Intensity (In/Hr)	Duration (Sec)		
4	40	80	250
3	45	90	280
2	55	110	290
1	60	120	300

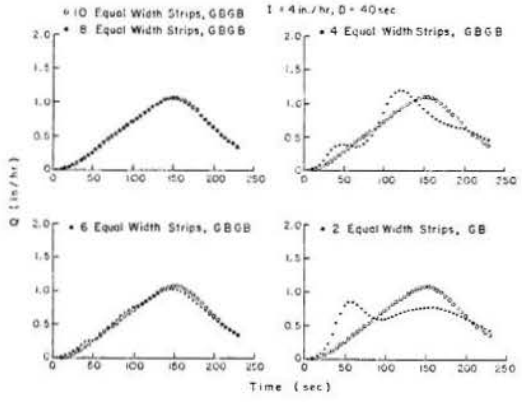

Figure 5-3. Simulated hydrographs for watersheds with equal width strips, with arrangements in order of gravel-butyl-gravel-...

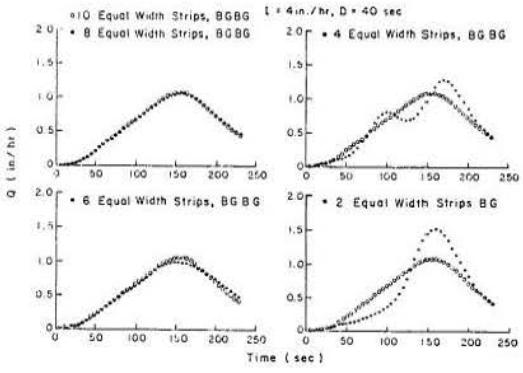

Figure 5-4. Simulated hydrographs for watershed with equal width strips, with arrangements in order of butyl-gravel-butyl-...

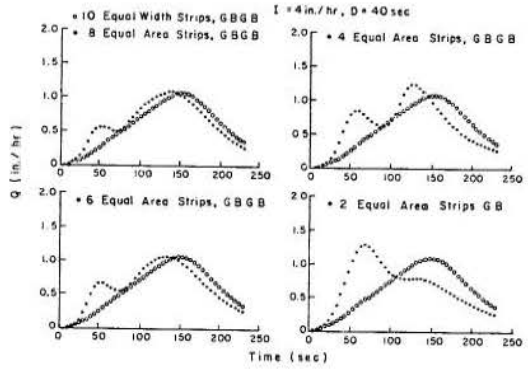

Figure 5-5. Simulated hydrographs for watershed with equal area strips, with arrangements in order of gravel-butyl-gravel-...

surfaces. Letting α and m be the two parameters for this compound watershed, with α_1, m_1 and α_2, m_2 the parameters for two basic surfaces (Fig. 5-6), the coordinate of the intersection point (log h', log Q') can be obtained as

$$\log h' = \frac{\log \alpha_1 - \log \alpha_2}{m_2 - m_1} \quad , \tag{5-1}$$

and

$$\log Q' = \log \alpha_1 + m_1 \log h' \quad ,$$

with

$$\log \alpha = \log Q' - m \log h' \quad . \tag{5-2}$$

With the condition of Eq. (5-2), the number of unknown parameters has been reduced from two to one. Once an m value is obtained, α can be determined from Eq. (5-2). Since the watershed composed of ten equal width alternate strips meets the equivalent uniform roughness conditions and the value of goodness-of-fit parameter is high, the average of two hydrographs simulated for the conical watersheds of ten equal width strips with reversible arrangements of roughness is considered as the hydrograph of the equivalent uniform roughness, as well as the average of detention storages on the uniform surfaces of the two roughnesses considered as the detention storage of the equivalent uniform roughness for the watersheds with

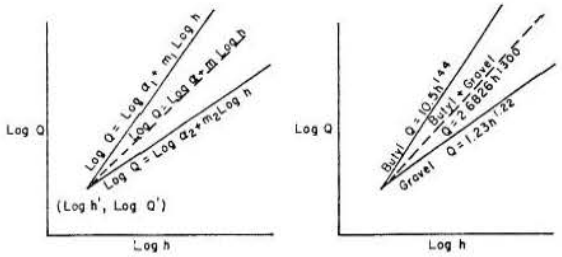

Figure 5-6. Estimation of mean parameters.

equal weight of gravel and butyl surfaces in the following computations. The unknown parameter m can be estimated by an optimization, in two ways:

(i) Obtain m value by minimizing the sum of squares of differences between hydrographs: The objective function used here is the sum of squares of differences between the hydrographs of an equivalent uniform roughness surface and the hydrographs simulated for a watershed considered as a lumped system with assumed values of α and m. Hydrographs simulated for the twelve kinds of rainfall inputs as described in Section 5.1 are used for optimization. But substituting $\alpha_1 = 0.5$ and $m_1 = 1.44$ for butyl surface and $\alpha_2 = 1.23$ and $m_2 = 1.22$ for gravel surface in Eqs. (5-1) and (5-2), α can be expressed as the function of m by $\log \alpha = -5.074489 + 4.23310\ m$. By assuming m, α can be determined and the hydrographs simulated. The best-fit value of m can be obtained by minimizing the objective function as shown in Table 5-3 and Fig. 5-7(A). The minimal value of the objective function is 0.158 $(in/hr)^2$ at $\alpha = 2.683$ and $m = 1.300$. The 12 hydrographs produced with these estimated α and m show that they almost exactly fit the hydrographs of the equivalent uniform roughness.

Table 5-3. Values of objective function for m.

m	1.330	1.320	1.310	1.305	1.300	1.295	1.290	1.280	1.270
α	3.594	3.289	2.957	2.887	2.683	2.555	2.434	2.208	2.002
F $(in/hr)^2$	25.38	14.22	3.89	1.36	.158*	.297	1.99	8.81	23.09

*minimum of the objective function values

(ii) Obtain m by minimizing the water storage deviations: One of the most representative characteristics of watershed response is the water stored at equilibrium. The objective function here is the sum of squares of deviations between the detention storages of an equivalent uniform roughness surface at equilibrium for various rainfall intensities and the detention storages in a watershed of lumped system with assumed m. The best-fit value of m can be obtained by minimizing this objective function.

The detention storage of both the conic section and the rectangular section of uniform roughness are computed as follows:

Storage at equilibrium for a conic section:

For r = the radius, S = the storage/A, A = the area of conic section, Q = the unit width discharge at equilibrium, θ = the central angle in radians, L_o = the radius of conic section, Δr = the increment of

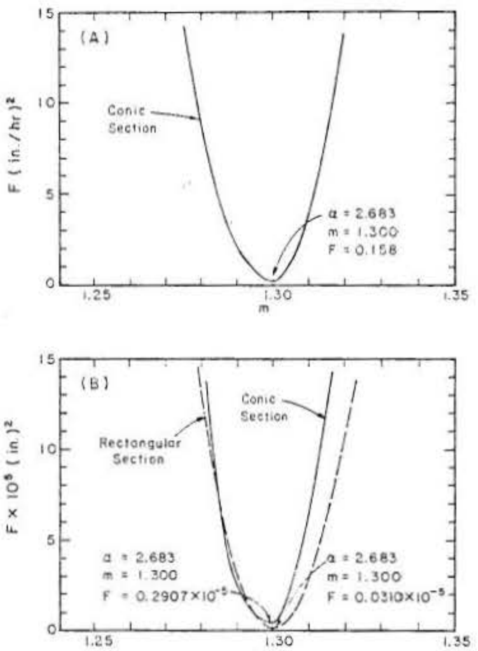

Figure 5-7. Objective functions for m: (A) sum of squares of deviations of hydrographs, (B) sum of squares of deviations of storage values.

radius, and ΔS = the storage increment, then $A = \theta L_o^2/2$, and $Q = q\,\frac{\theta}{2}\,(L_o - r^2)/\theta r = \frac{q}{2}\,\frac{L_o^2 - r^2}{r}$, $h = (\frac{Q}{\alpha})^{1/m} = \left(\frac{q(L_o^2 - r^2)}{2\alpha r}\right)^{1/m}$, $\Delta S = h\theta\Delta r/A =$

$$h\theta\Delta r/(\frac{\theta L_o^2}{2}) = \frac{2rh}{L_o^2}\,\Delta r = \frac{2r}{L_o^2}\left(\frac{q(L_o^2 - r^2)}{2\alpha r}\right)^{1/m}\Delta r =$$

$$\frac{2}{L_o^2}\,(\frac{q}{2\alpha})^{1/m} \cdot r^{1-1/m} \cdot (L_o^2 - r^2)^{1/m}\,\Delta r,$$ with $\Delta S = C\,r^{1-1/m}\,(L_o^2 - r^2)^{1/m}\,\Delta r$, and $S = \Sigma\,\Delta S$, where $C = \frac{2}{L_o^2}\,(\frac{q}{2\alpha})^{1/m}$. The total of detention storage is calculated by computer using 300 Δr increments.

Storage at equilibrium for a rectangular section:

In addition to the notations used above, let x = the distance from upstream end, and L_o = the length of rectangular section, then $Q = qx$,

$$h = (\frac{qx}{\alpha})^{1/m},\quad S = \frac{1}{L_o}\int_o^{L_o} h\,dx = \frac{1}{L_o}\int_o^{L_o} (\frac{qx}{\alpha})^{1/m}\,dx =$$

$$\frac{1}{L_o}\,(\frac{q}{\alpha})^{1/m}\,(\frac{m}{m+1})L_o^{\frac{m+1}{m}} = \frac{m}{m+1}\,(\frac{qL_o}{\alpha})^{1/m}.$$

The dentention storage at equilibrium and the values of the objective function for various values of m are computed and given in Table 5-4. The objective function versus m is shown in Fig. 5-7(B). The best-fit values for α and m are 2.683 and 1.300, respectively. This given the minima of the objective functions for both the rectangular and the conic sections. This pair of values also give the detention storage closest to the detention storage of an equivalent uniform roughness surface for most rainfall intensities. The optimization of parameters by detention storage approach is not affected by differences in shape of watershed or rainfall intensity.

Table 5-4. Detention storage at equilibrium for rectangular and conic sections.

(A) Detention Storage at Equilibrium (in) for the Rectangular Section, L_o = 120 ft.

	Equivalent Uniform Roughness							
α		[illegible]	[illegible]	[illegible]	[illegible]	[illegible]	[illegible]	[illegible]
m		[illegible]	1.290	1.295	[illegible]	[illegible]	[illegible]	[illegible]
1 in/hr	[illegible]	[illegible]	[illegible]	[illegible]	[illegible]	[illegible]*	[illegible]	[illegible]
2 in/hr	[illegible]	[illegible]	[illegible]	[illegible]	[illegible]*	[illegible]	[illegible]	[illegible]
3 in/hr	[illegible]	[illegible]	[illegible]	[illegible]	[illegible]*	[illegible]	[illegible]	[illegible]
4 in/hr	[illegible]	[illegible]	[illegible]	[illegible]	[illegible]*	[illegible]	[illegible]	[illegible]
F(10^{-5})		[illegible]	[illegible]	[illegible]	[illegible]**	[illegible]	[illegible]	[illegible]

(B) Detention Storage at Equilibrium (in) for the Conic Section, L_o = 120 ft.

	Equivalent Uniform Roughness							
α		[illegible]	[illegible]	[illegible]	[illegible]	[illegible]	[illegible]	[illegible]
m		[illegible]	[illegible]	1.295	[illegible]	[illegible]	1.310	1.315
1 in/hr	[illegible]	[illegible]	[illegible]	[illegible]	[illegible]*	[illegible]	[illegible]	[illegible]
2 in/hr	[illegible]	[illegible]	[illegible]	[illegible]	[illegible]*	[illegible]*	[illegible]	[illegible]
3 in/hr	[illegible]	[illegible]	[illegible]	[illegible]	[illegible]*	[illegible]	[illegible]	[illegible]
4 in/hr	[illegible]	[illegible]	[illegible]	[illegible]*	[illegible]	[illegible]	[illegible]	[illegible]
F(10^{-5})		[illegible]	[illegible]	[illegible]	[illegible]**	[illegible]	[illegible]	[illegible]

F = objective function. * Detention storage closest to the detention storage of an equivalent uniform roughness. ** Minimum of the objective function.

Estimation of mean parameters from detention storage:

The result of optimization of m by minimizing the deviations between the detention storages is almost exactly the same as the result of optimization by minimizing the deviations between the hydrographs. In other words, a pair of α and m values which can reproduce the detention storage of the same value as the detention storage on a watershed of equivalent uniform roughness can also reproduce the hydrographs of that watershed.

Assume both hydrographs and detention storage of the equivalent uniform roughness surface were generated by the mathematical simulation for a NFUT conical surface with curved strips with sufficiently small elements of two roughnesses. When the elements of the two roughnesses are so small that the surface is close to a uniform surface of the roughness intermediate between the two basic roughnesses, both the produced hydrographs and detention storages might also be close to the hydrographs and detention storages of an equivalent uniform roughness surface, to be represented by one value of m. Therefore, m opimized from the detention storage might be also m which can reproduce the hydrograph closest to the hydrograph of equivalent uniform roughness surface. However, the deviation between two values of m by the two kinds of optimization will increase as the size of elements increases.

Suppose that α and m are known for two basic surfaces which make a compound watershed. Since the estimation of parameters by detention storage approach does not depend on the difference in the watershed shape or rainfall intensity, α and m can be easily estimated for a compound watershed by letting the detention storage at equilibrium agree with the detention storage of the equivalent uniform roughness surface at equilibrium for a single rectangular section with an assumed rainfall intensity. With estimated α and m, hydrographs for various rainfall

intensities and durations may be then simulated as a lumped system by using the kinematic wave theory.

If m is predetermined as a fixed value, only one parameter α remains to be estimated. Then α for an equivalent uniform roughness surface may be estimated by letting the detention storage at equilibrium agree with the detention storage of an equivalent uniform roughness surface at equilibrium without using Eqs. (5-1) and (5-2).

Comparison of Hydrographs Simulated by Estimated Parameters with Observed Hydrographs

To apply the method of estimating α and m by detention storage approach to a natural watershed, the hydrographs for the experimental watersheds which have the equivalent uniform roughness surface are first simulated by using the estimated parameters and then compared with the observed hydrographs. Some of the simulated hydrographs are compared with the observed hydrographs in Fig. 5-8. The values of objective function are given in column 6, Table 4-5. Hydrographs simulated for configurations 37 and 38 with α and m estimated by detention storage approach fit the observed hydrographs as well as the hydrographs simulated with the optimized parameters or by using the distributed system. Although for configuration 10 the value of objective function resulting from the hydrographs simulated with the mean values of α and m from detention storage estimation is greater than the value of objective function resulting from hydrographs simulated with optimized parameters, the hydrographs simulated with parameters estimated by the detention storage approach agree better in shape with the observed hydrographs than do the hydrographs simulated with optimized parameters. The reason for poor agreement in simulation by using optimization has been stated in Section 4.5: the simulated hydrographs by optimization were forced to fit the low flows of a long duration at the initiation of observed hydrographs, which was caused by errors in time correction. The estimates of α and m by detention storage approach are feasible for the simulation of hydrographs for NFUT surfaces of equivalent uniform roughness surfaces.

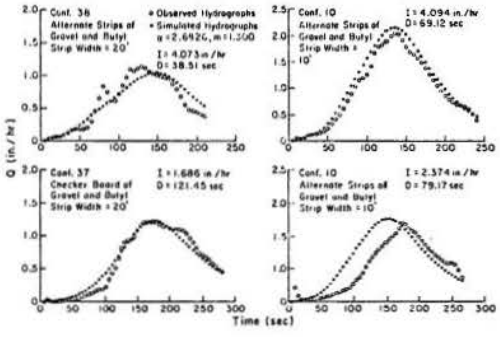

Figure 5-8. Comparison of hydrographs simulated by estimated α and m with observed hydrographs.

5.3 Hydrograph Simulation for Watersheds with Random Distrbution of Surface Roughness

The previous discussion has shown that the linear uniformity of roughness along the flow direction is important in achieving the equivalent uniform roughness for NFUT surfaces. In this section, NFUT surfaces with a random distribution of equal width strips of butyl and gravel are discussed and the reliability of estimating the parameters by detention storage approach is tested. To save computer time, numerical models of watersheds with a radius of 120 ft and a slope of five percent are assumed to be composed of six equal width strips, with three strips of butyl and three strips of gravel. The hydrographs reproduced for a rainfall intensity of 3 in/hr and 90 seconds duration (partial equilibrium) are used for comparison.

The number of combinations of three strips out of the total of six strips is 20 ($_6C_3$). Column 2 in Table 5-5 shows various combinations of butyl and gravel strips. They are represented by symbols 1 and 2, respectively. Column 3 shows the number of runs. A maximal uninterrupted sequence of like symbols is called a run. In Chapter IV it was shown that the hydrographs simulated from the distributed system are closest to the hydrographs observed experimentally from a watershed with random distribution of two types of roughness surfaces. Therefore, the detention storage and hydrographs simulated from the distributed system will be considered as the actual detention storages and hydrographs for a comparison with the other short cut methods used.

Table 5-5. Test of roughness uniformity and estimation of mean parameters for watersheds with random distribution of roughness surfaces.

No. (1)	Combinations[1] (2)	No. of Runs (3)	Storage by Distributed System (4) (in.)	Comparison between hydrographs from the distributed system & hydrograph from an Equiv. Uniform Roughness: G (5)	P (6)	S.S.D. (in./hr)² (7)	Parameters Estimated from Detention Storage: α (8)	m (8)	Comparison between hydrograph from the distribution system and hydrograph from the estimated parameters: G (9)	P (10)	S.S.D. (in./hr)² (11)
1	1 2 1 2 1 2	6	.09478	.968	.004	.3240	2.4335	1.290	.987	.024	.0346
2	2 1 2 1 2 1		.09804	.968	.004	.2063	2.8166	1.305	.983	.040	.0798
3	2 1 1 2 1 2	5	.09934	.937	.172	.9374	2.8116	1.305	.955	.129	.6445
4	2 1 2 1 1 2		.08643	.946	.001	.7568	2.9572	1.310	.978	.055	.2145
5	1 2 2 1 2 1		.09378	.935	.152	1.004	2.4335	1.290	.945	.134	.9473
6	1 2 1 2 2 1		.09639	.948	.002	.9974	2.3177	1.285	.974	.042	.1496
7	1 1 2 2 1 2	4	.09287	.911	.116	3.955	2.2075	1.280	.950	.185	.9705
8	1 1 2 1 2 2		.09991	.909	.146	2.530	2.1025	1.275	.930	.243	1.524
9	1 2 2 1 1 2		.09217	.942	.127	1.691	2.5550	1.295	.943	.126	1.291
10	1 2 1 1 2 2		.09595	.950	.012	.4321	2.3177	1.285	.948	.125	1.101
11	2 2 1 1 2 1		.09399	.910	.010	3.117	1.2600	1.320	.939	.099	1.202
12	2 2 1 2 1 1		.08788	.914	.107	2.648	1.2600	1.320	.921	.187	1.821
13	2 1 1 2 2 1		.09665	.943	.173	.7030	2.6826	1.300	.948	.150	.8055
14	2 1 2 2 1 1		.08697	.953	.019	.8341	2.9672	1.310	.939	.076	1.378
15	1 1 2 2 2 1	3	.10048	.891	.100	4.595	2.1025	1.275	.933	.192	1.284
16	1 2 2 2 1 1		.09271	.901	.140	3.553	2.5550	1.295	.903	.139	2.791
17	2 2 1 1 1 2		.08034	.890	.023	4.545	1.4278	1.325	.927	.087	1.953
18	2 1 1 1 2 2		.09011	.902	.209	2.940	2.6826	1.300	.911	.264	2.958
19	1 1 1 2 2 2	2	.10255	.870	.314	5.992	2.0025	1.270	.834	.453	4.730
20	2 2 2 1 1 1		.08027	.876	.294	5.819	3.5938	1.330	.864	.337	6.279

Conic Section, l_0 = 120 ft, I = 3 in./hr, U = 90 sec.
Detention Storage of an Equivalent Uniform Roughness = $\frac{1}{4}$ (Storage of butyl surf. + Storage of gravel surf.) = 0.09141 in.
1/Combination from upstream to downstream 1 = Butyl, 2 = Gravel.

Uniformity of Roughness

The detention storage and the hydrograph for the surface of equivalent uniform roughness surfaces composed of equal weights of butyl and gravel elements are described in section 5.2. They are considered to be very close to the detention storage and the hydrograph of an equivalent uniform roughness surface. The detention storage and hydrograph produced by the distributed system for a watershed with random distribution of roughness surface are compared with the detention storage and hydrograph of an equivalent uniform roughness surface for the test of equivalent roughness uniformity.

Column 4 of Table 5-5 shows the detention storage at equilibrium for various combinations computed from the distributed system. The deviations of the detention storage from the detention storage of the equivilant uniform roughness show a chance scatter and no general regularity for these deviations can be inferred.

Comparison of hydrographs are shown on Fig. 5-9(A). Columns 5 and 6 of Table 5-5 show the goodness-of-fit parameters, G, and the ratio P_r of difference of two peaks to the peak of the hydrograph of equivalent uniform roughness surface. In accordance with the method used in Section 5.1, G_e and P_r are set at 0.965 and 0.025 respectively. Only the watersheds with alternate strips of butyl and gravel can be classified as the surface of equivalent uniform roughness. The sums of squares of deviations are given in column 7, and the relationships of those values to the number of runs are shown in Fig. 5-10.

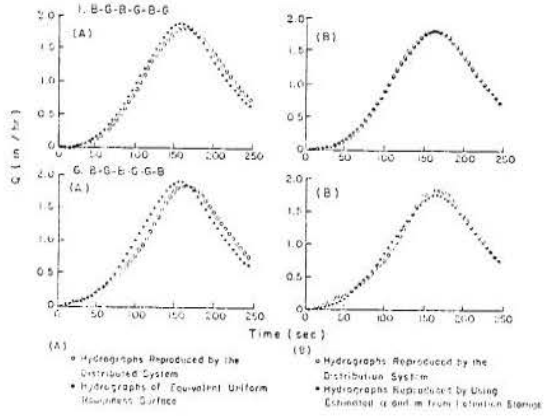

Figure 5-9. Hydrographs of watersheds with randomly distributed roughness, 6 equal width strips, I = 3 in/hr, D = 90 sec.

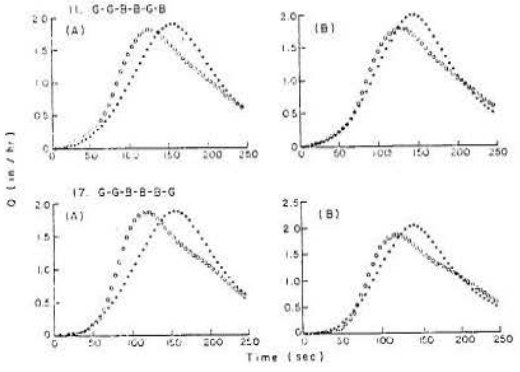

Figure 5-9. (Continued)

Although all of the combinations have an equal weight of butyle and gravel, the hydrographs of an equivalent uniform roughness surface do not fit the actual hydrographs well. The goodness-of-fit parameter increases or the deviation decreases as the number of runs increases, i.e., the roughness uniformity increases as the runs increase.

Reliability of Parameters Estimated by Detention Storage Approach

All the configurations except the configuration with alternate strips of two roughnesses do not correspond to the equivalent uniform roughness surface. The hydrographs produced from these configurations cannot be simulated by a lumped system which considers the watershed as that of an equivalent uniform

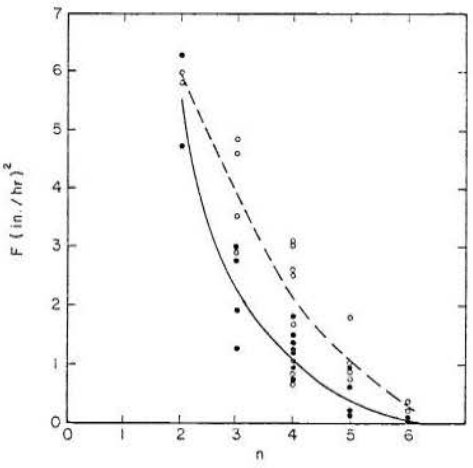

Figure 5-10. Sum of squares of deviations of hydrographs vs number of runs. A maximum uninterrupted subsequence of like symbols of roughness is called a run.

roughness surface. In order to find the reasonable estimate of parameters for the watersheds with random distribution of roughness strips, estimation of parameters by detention storage was first tested.

When the watershed with a random distribution of roughness is considered as a lumped system, two unknown parameters, α and m, may be estimated with the detention storage approach under the two conditions: (1) the regression line of log Q versus log h passes through the intersection point of the two regression lines of basic roughness (log α = -5.074489 + 4.23310 m for the surface composed of butyl and gravel), and (2) the detention storage at equilibrium reproduced by the lumped system with estimated α and m is equivalent to detention storage reproduced by the distributed system. The estimates α and m so obtained are given in column 8 of Table 5-5. To test the reliability of these estimates, hydrographs simulated by α and m are compared with hydrographs simulated by the distributed system as shown in Fig. 5-9(B). The goodness of fit parameter, G, ratio of peak deviation to peak, P_r, and the sums of squares of deviations between hydrographs are given in columns 9, 10, and 11 of Table 5-5. The relationship of the sum of squares of deviations to the number of runs is shown in Fig. 5-10. When hydrographs are simulated by the parameters estimated from detention storage instead of simulation by an equivalent uniform roughness, the sums of squares of deviations are less, thus the values of goodness-of-fit parameter increase. Although these configurations do not meet the equivalent uniform roughness conditions, the simulation of hydrographs by detention storage approach can produce hydrographs very similar to the actual hydrographs. When the number of runs is greater than or equal to four, goodness-of-fit parameter is greater than 0.92 and, in general, the simulated hydrographs can be accepted.

Comparison of Observed Hydrographs with Hydrographs Simulated by Estimated Parameters

Since the Rainfall-Runoff Experimental Facility data did not include NFUT watersheds with random distribution of two types of roughness, NFNT watersheds with random distribution of two types of roughness, Configurations 12 and 13 (Fig. 5-11) are selected for verifying the reliability of α and m estimated from detention storage. They consisted of a 30° conic section with a radius of 110 ft. The conic section was divided into three equal angle sectors, and then into eleven equal width strips along each radial direction, a total of 33 elements with the gravel elements of 20 lbs/yd^2 randomly distributed among the 33 plots, and the numbers of elements of butyl and gravel about the same.

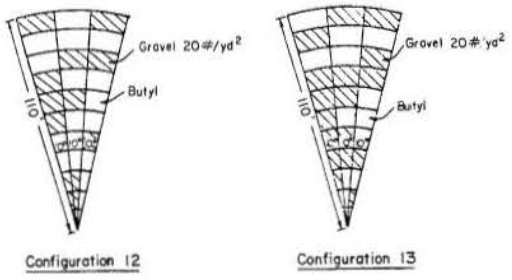

Figure 5-11. Configurations of watersheds with random distribution of roughness.

Estimation of α and m from water storage at equilibrium:

To select α and m which reproduce the detention storage most closely of watershed at equilibrium, four rainfall intensities of 1, 2, 3, and 4 in/hr were used. The total detention storage of a watershed is obtained by summing the corresponding detention storages of butyl and gravel surfaces according to their distribution arrangements. Considering the whole system as a lumped system, detention storages for various values of m (with the condition of $\log \alpha = -5.074489 + 4.23310\ m$) are computed and the best-fit value of m is selected that can reproduce the detention storage closest to the total detention storage of the watershed. The best-fit values of α and m are 2.8166 and 1.305 respectively for Configuration 12, and 2.5550 and 1.295 respectively for Configuration 13. Computation results are summarized in Table 5-6.

Comparison of simulated hydrographs with observed hydrographs:

For Configuration 12, eight hydrographs with various intensities and durations are used for comparison (Table 5-6). The observed hydrographs are well simulated by the estimated α and m. The value of the objective function is only 7.086 (in/hr)^2. Some of the representative hydrographs are shown in Fig. 5-12. The values of goodness-of-fit parameters for partial equilibrium hydrographs which have peaks greater than one inch per hour are greater than 0.92.

For Configuration 13, seven hydrographs with various rainfall intensities and durations are used for comparison (Table 5-6). The hydrographs simulated by the estimated α and m do not fit the observed hydrographs as well as the simulated hydrographs for

Table 5-6. Estimation of parameters for watersheds with random distribution of roughness (Configurations 12 and 13).

Detention Storage at Equilibrium

Configurations	Storages (In) 1 in./hr	2 in./hr	3 in./hr	4 in./hr	Best fit α & m
12	.035162	.060090	.082281	.102872	α = 2.8166, m = 1.305
13	.036415	.062664	.086144	.107999	α = 2.5550, m = 1.295

Uniform System

α	m				
2.4334	1.290	.037652	.064439	.088237	.110282
2.5550	1.295	.037014	.063216	.086458	.107956
2.6826	1.300	.036393	.062026	.084729	.105715
2.8166	1.305	.035787	.060869	.083048	.103531
2.9572	1.310	.035196	.059742	.081415	.101409
3.1049	1.315	.034619	.058646	.079826	.099347

Hydrographs Used in Configuration 12 and 13

Configuration 12								
I(in./hr)	.459	.459	1.094	1.094	2.207	2.207	4.280	4.280
D(Sec)	106.84	563.64	128.63	352.44	93.91	308.47	63.91	285.84
Equil. or Partial Eq.	PE	E	PE	E	PE	E	PE	E
G(%)			92.0		99.5		94.2	
P_r(%)			5.9		2.8		2.9	
Configuration 13								
I(in./hr)	.489	.489	1.069	1.069	2.349	4.361	4.361	
D(Sec)	130.74	447.20	145.03	384.25	303.96	79.61	275.16	
Equil. or Partial Eq.	PE	E	PE	E	E	PE	E	
G(%)			89.38			90.31		
P_r(%)			13.8			19.0		

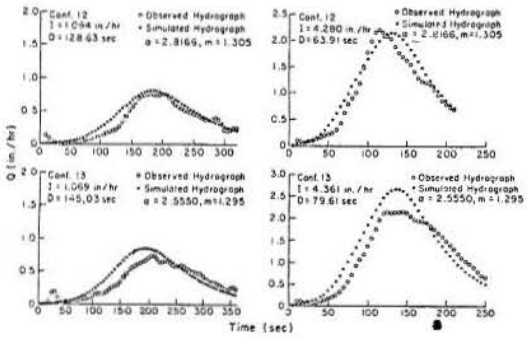

Figure 5-12. Comparison of hydrographs simulated by estimated α and m with observed hydrographs.

Configuration 12, but these fits may still be acceptable. The objective function value is 15.98 (in/hr)^2. Some representative hydrographs are shown in Fig. 5-12. The values of goodness-of-fit parameter for partial equilibrium hydrographs which have peaks greater than one inch per hour are around 0.90.

Chapter VI
APPLICATION OF TWO-PARAMETER MODEL TO NATURAL WATERSHEDS

The results obtained in this study, based on experimental data, are applied to natural watersheds. The two basic results are:

(1) The two-parameter model, $Q = \alpha h^m$, is sufficiently good to simulate well the overland flow hydrographs;

(2) For watersheds consisting of surfaces with various and varying roughnesses, the parameters α and m for the equivalent uniform roughness surface can be estimated by letting the detention storage at the equilibrium, produced by these estimated parameters, be equivalent to the detention storage at equilibrium, produced by the distributed system with known parameters for the surfaces of various and varying roughnesses.

Data available on roughness are in general limited to surfaces of uniform roughness over an area. In simulating the hydrographs of watersheds with random distribution of surfaces of various and varying roughnesses, the method of cascade planes can be applied. However, if a surface consists of a large number of small plots with various and varying roughnesses, the cascade method becomes so complicated that the cost of simulation significantly increases. These kinds of surfaces are often encountered in agricultural land use, such as an area of alternating strip croppings for soil conservation purposes. For this case, results of this study can be applied to obtain the overall parameters by considering the surface as a single system of equivalent and uniform roughness. This approach simplifies to a great extent the computations in simulating the hydrographs of natural watersheds.

To verify the feasibility of this method, a flood event of June 12, 1957 at a watershed near Coshocton, Ohio is used for the test. The data are obtained from "Hydrologic Data for Experimental Agricultural Watersheds in the United States, 1956-1959," published by Agricultural Research Service, USDA. The map of the watershed is shown in Fig. 6-1, with 62.6 percent of the total catchment area under the counter-strip cropped with corn-meadow strips (34 percent) and wheat-meadow strips (28.6 percent). The types of vegetation are given in Table 6-1. The widths of alternate strips for corn-meadow and wheat-meadow were around 100 feet. Program KINGEN75 (Rovey, Woolhiser, and Smith, 1977) was used for the hydrograph simulation. Because sufficient information on the roughness and experimental data for estimating parameters in the two-parameter model for surfaces with various vegetation over the area were not available, the Chézy equation was used in simulating the hydrographs. The values of Chézy's C for surfaces with various vegetation patterns, as given in Table 6-1, were estimated from the data in the table on resistance parameters for overland flow in "Simulation of Unsteady Flow" (Woolhiser, 1975, Unsteady Flow in Open Channels, Chapter 12). Since the flood event occurred in June, and there were legumes, grass and weeds of 5 to 6 inches high between the main crops, lower values of C in the table were chosen.

The watershed was first divided into cascades of 12 rectangular planes contributing to a network of channels as shown in Fig. 6-1. The schematic representation of cascade planes and channels is shown in

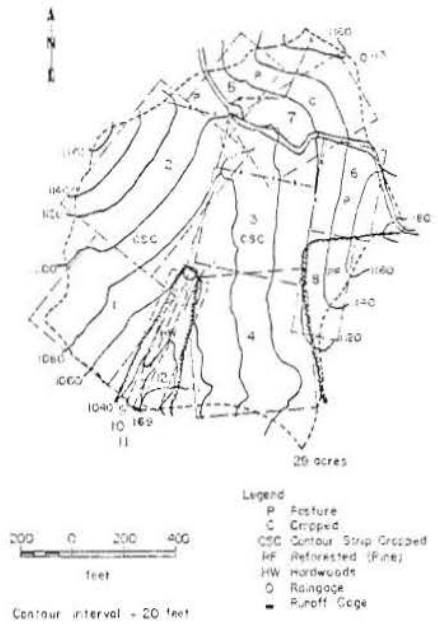

Figure 6-1. Map of Coshocton watershed, Ohio.

Table 6-1. Description of vegetation on the Coshocton watershed, Ohio.

Vegetation	%	Strips	Crops	Height	Estimated Chézy C
Corn-meadow	34	corn	corn	20"	3.6
			weeds	18"	
		meadow	legumes, grass, & weeds	5"	1.9
Wheat-meadow	28.6	wheat	wheat	30"	2.5
			legumes, & grass	5"	
		meadow	legumes, grass, & weeds	6"	1.8
Wheat	6.0		wheat	30"	2.5
Pasture	8.3		legumes & grass	5"	1.9
			weeds	6"	
Hardwood & Orchard	6.4				2.0
Reforested	10				1.8
Miscellaneous	5.9				

Determination of the Overall Discharge Coefficient

Since Chézy formula, $Q = Ch^{3/2}S^{1/2}$, is used in the simulation of hydrographs, α and m in the two-parameter model are then

$$\alpha = CS^{1/2}, \quad \text{and} \quad m = \frac{3}{2}, \tag{6-1}$$

Fig. 6-2. The planes P1 and P2 were the corn-meadow area and the planes P3 and P4 were the wheat-meadow area. Before starting the simulation, the overall discharge coefficient for those four planes should be determined by using the technique described in this study.

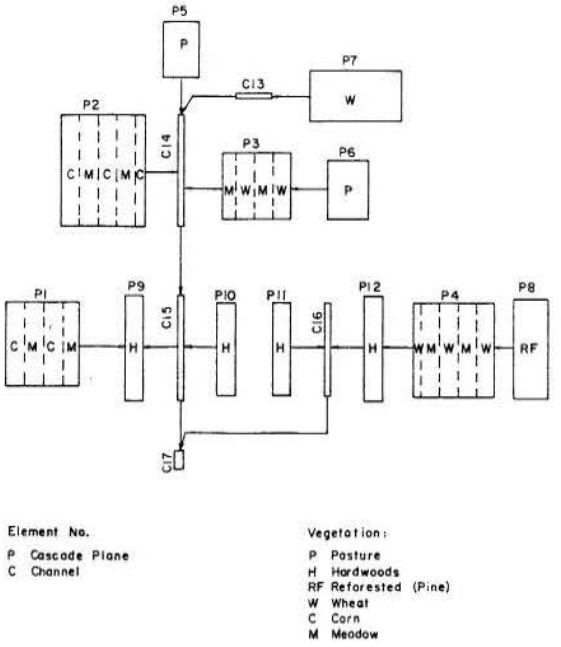

Figure 6-2. Schematic representation of cascade planes and channels.

with S = the slope of the plane, and C = the Chézy coefficient. Only parameter α remains unknown. The overall value of α for a compounded plane can be determined by letting the detention storage of equilibrium, produced by α be equivalent to the accumulated detention storages in subplanes at equilibrium. As stated in Section 5.2, the estimates of parameters from the detention storage are not sensitive to the difference in rainfall intensity. The rainfall intensity of 2 in/hr was used to estimate the overall value of α from the detention storage.

The cascade planes, P1, P2, P3, and P4 were divided into subplanes according to the width of strips, as shown in Fig. 6-2 and given in Table 6-2. The slope of each subplane was measured and the storage in each subplane computed by using the equation

$$\Delta S_t \int_{x_1}^{x_2} \frac{1}{L_o} h\, dx = \frac{m}{L_o(m+1)} \left(\frac{q}{\alpha}\right)^{1/m} \left[x^{\frac{m+1}{m}}\right]_{x_1}^{x_2} =$$

$$k \frac{1}{L_o \alpha^{1/m}} \left[x_2^{\frac{m+1}{m}} - x_1^{\frac{m+1}{m}}\right], \qquad (6\text{-}2)$$

with $k = [m/(m+1)]\, q^{1/m}$, ΔS_t = the storage in a subplane, x = the distance from the upstream end of the plane to the upstream end of the subplane, x_2 = the distance from the upstream end of the plane to the downstream end of the subplane, L_o = the total length of the plane, and q = the lateral inflow rate or the rainfall excess rate. The α value in the above equation for each subplane was obtained from Eq. (6-1). The overall α was obtained by

$$S_t = \Sigma \Delta S_t = K \frac{L_o^{1/m}}{\bar{\alpha}^{1/m}},$$

$$\bar{\alpha} = \left(\frac{k}{S_t}\right)^m L_o . \qquad (6\text{-}3)$$

Table 6-2. Computations of overall parameters for contour-strip cropped planes.

$m = \frac{3}{2}$, $q = 2$ in/hr, $K = \frac{m}{m+1} q^{1/\alpha} = 7.7360 \times 10^{-4}$

Unit: ft

Plane	Section	Crop	C	x_2	S	α	$\alpha^{1/m}$	$x_2^{\frac{m+1}{m}} - x_1^{\frac{m+1}{m}}$	ΔS_t (10^4)	$\bar{\alpha}$	$\bar{C}$
P1 L_o=390	1	Corn	3.6	100	.09	1.080	1.0526	.2154	.00406		
	2	Meadow	1.8	200	.09	.540	.6631	.4686	.01402		
	3	Corn	3.6	300	.18	1.527	1.3260	.6604	.00938		
	4	Meadow	1.8	390	.17	.742	.8196	.7374	.01785		
	Total				.131				.04581	.8559	2.365
P2 L_o=450	1	Corn	3.6	100	.21	1.650	1.3963	.2154	.00765		
	2	Meadow	1.8	200	.19	.705	.8510	.4686	.00947		
	3	Corn	3.6	300	.17	1.484	1.3010	.6604	.00873		
	4	Meadow	1.8	400	.17	.742	.8196	.8271	.01735		
	5	Corn	3.6	450	.14	1.347	1.2197	.4710	.00664		
	Total				.180				.04484	1.0197	2.404
P3 L_o=380	1	Wheat	2.5	100	.17	1.031	1.0206	.2154	.00430		
	2	Meadow	1.8	200	.13	.649	.7496	.4686	.01273		
	3	Wheat	2.5	300	.12	.866	.9085	.6604	.01480		
	4	Meadow	1.8	380	.10	.569	.6868	.6492	.01924		
	Total				.136				.05107	.7085	1.921
P4 L_o=450	1	Wheat	2.5	100	.16	1.000	1.0000	.2154	.00370		
	2	Meadow	1.8	200	.14	.673	.7680	.4686	.01049		
	3	Wheat	2.5	300	.16	1.000	1.0000	.6604	.01135		
	4	Meadow	1.8	400	.14	.673	.7680	.8271	.01861		
	5	Wheat	2.5	450	.18	1.061	1.0403	.4710	.00778		
	Total				.153				.05183	.8206	2.098

The details of computation are given in Table 6-2. The overall Chézy C was obtained by substituting $\bar{\alpha}$ into Eq. (6-1) and then given in Table 6-3.

Table 6-3. Dimensions, areas, slopes, vegetation, and Chézy C for cascade planes and channels.

Element Number*	Length (ft)	Width** (ft)	Area ft^2 (10^4)	Area %	Vegetation	Chézy C***	Slope
P1	390	420	16.380	13.0	Corn-meadow	2.365	.131
P2	450	600	27.000	21.4	Corn-meadow	2.404	.180
P3	380	350	13.300	10.5	Wheat-meadow	1.921	.136
P4	450	500	22.500	17.8	Wheat-meadow	2.098	.153
P5	300	200	6.000	4.8	Pasture	1.8	.182
P6	225	310	6.980	5.5	Pasture	1.8	.200
P7	490	275	13.470	10.7	Wheat	2.5	.160
P8	245	510	12.495	9.9	Reforested	1.8	.267
P9	40	530	2.120	1.7	Hardwoods	2.0	.133
P10	25	470	1.175	.9	Hardwoods	2.0	.100
P11	30	470	1.410	1.1	Hardwoods	2.0	.100
P12	65	530	3.445	2.7	Hardwoods	2.0	.154
C13	130	2.0				20	.08
C14	550	3.0				30	.055
C15	500	4.0				35	.045
C16	500	3.0				20	.055
C17	50	5.0				40	.055
Total			126.3	100			

* P = Plane, C = Channel with 1 to 1 side slope.
** Widths of planes or bottom widths of channels.
*** Estimations of C for P1, P2, P3, and P4 refer to Table 6-2.

Simulation of Hydrographs

Dimensions, areas, slopes, and vegetation, as well as the estimated Chézy C for the elements in the system, are given in Table 6-3. The soil texture consists of 37 percent of mixed silt loams, 26 percent of Keene silt load, 16 percent of Muskingum silt loam, and 21 percent of Muskingum loam. Since no experimental data are available for infiltration, the parameters of infiltration function are assumed and several trial computations made to estimate reasonably the parameters, giving the outflow volume equal to the outflow volume of the observed hydrograph. Definitions of infiltration parameters in KINGEN 75 Program (Rovey, et al., 1977), and the estimated values of parameters are as follows: AL = the exponent parameter for decay curve = 0.6; B = the ponding time parameter = 2.0; C = the infiltration scaling parameter = 3000 min; SI = the initial volumetric relative water content = 0.5; SMAX = the maximum volumetric water content under imbibition = 1.0; ROC = the volumetric relative rock content = 0; and FMIN = the minimum infiltrate rate at steady state condition for a plane = 0.28 in/hr.

The precipitation record and the observed hydrograph, as well as the simulated hydrograph, are shown in Fig. 6-3. The simulated hydrograph fits well the observed hydrograph.

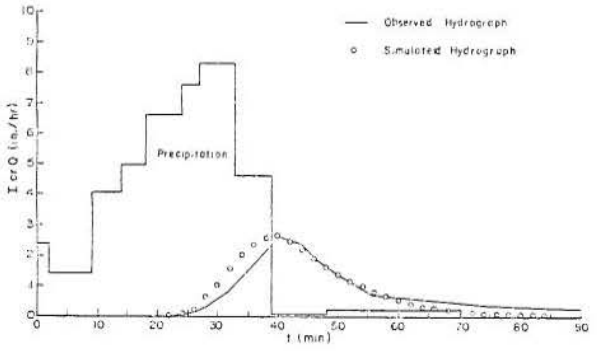

Figure 6-3. Observed and simulated hydrographs of the event of June 12, 1957, Coshocton watershed, Ohio.

Comparison Between the Hydrograph Obtained by the Distributed System and the Hydrograph Obtained by Using the Overall Value of α

Planes P1, P2, P3, and P4 are considered as single planes in the simulation of the above hydrograph. In order to demonstrate the feasibility of the method by using the overall parameter estimated from detention storage, comparisons are made between the hydrographs obtained by the distributed system and the hydrographs obtained by using the overall α, for those four planes, as shown in Fig. 6-4. The results show that the hydrographs simulated by using the overall values of α are almost identical to the hydrographs simulated by the distributed systems. This example demonstrates that the method of obtaining overall parameters from the detention storage is effective. By using the overall parameters, this method greatly simplifies computations in simulating the hydrographs and makes the simulation very efficient.

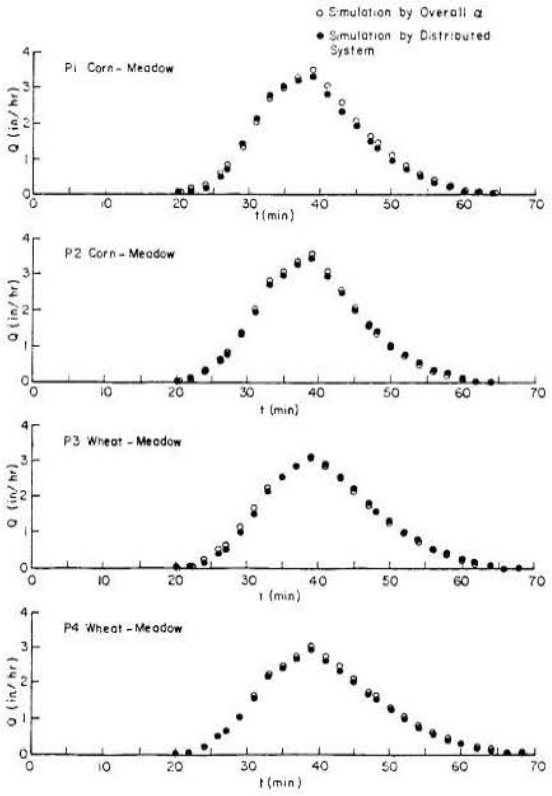

Figure 6-4. Hydrographs simulated by using the overall parameter and by using the distributed system for contour-strip cropped planes.

Chapter VII
CONCLUSIONS AND RECOMMENDATIONS

7.1 Conclusions

(1) A three-parameter model for hydraulic resistance, postulated by assuming a flow through a set of parallel channels with negative exponential distribution of widths and equal water depth in the channels, more precisely describes the relationship between the discharge, Q, and the equivalent water depth, h, for various kinds of roughness over a wide range of discharge than the two-parameter model, $Q = \alpha h^m$, does. The three-parameter model may be applied to the effects on the hydrographs of changing land use, as well as for the precise estimation of sediment transport in overland flow.

(2) The two-parameter model requires much less computer time for simulation of hydrographs in comparison with the three-parameter model. When only the high flows of hydrographs are important in hydrologic analysis, the two-parameter model is simpler and less expensive to use and implement in hydrograph simulation.

(3) An equivalent uniform roughness can be used for a watershed with nonuniform roughness over its surface if the hydrographs from this watershed are proved to be equivalent to the hydrographs of a watershed of equivalent uniform roughness for identical rainfall excess patterns. The factors which affect the application of the equivalent uniform roughness concept are the differences between roughnesses, relative subarea of a given constant roughnesses, and the size of these uniform roughness subareas.

(4) For the experimental watersheds composed of alternating strips of gravel and butyl surfaces, this study shows that the linear uniformity of roughness in flow direction is much more important than the areal uniformity of roughness for applying the equivalent uniform roughness concept.

(5) For a watershed composed of equal width alternate strips of two roughness surfaces along the flow direction, the watershed can be approximated by an equivalent uniform roughness surface, if the width of strips is less than or equal to one-sixth of total flow length.

(6) The lumped parameters α and m of the two-parameter model for a watershed of equivalent uniform roughness surface with equal weights of two roughnesses can be estimated by selecting α and m which reproduce the equilibrium detention storage equivalent to the average of the equilibrium detention storages produced by the two uniform roughness surfaces of the basic roughnesses.

(7) For a watershed composed of randomly distributed surface elements of two roughnesses, α and m can also be approximated by selecting the values of α and m which reproduce the equivalent detention storage matching the equilibrium detention storage produced by the watershed of randomly distributed roughness with distributed system. For a watershed composed of six equal width strips, three gravel strips and three butyl strips, this method is applicable if the number of changes of roughness along the flow direction is greater than three.

(8) For watersheds with nonuniform roughness in the direction normal to the basic flow direction, hydrographs can be simulated by using a distributed system, i.e., by combining the hydrographs produced by the individual surface elements.

7.2 Recommendation for Additional Work

The effects of spatial variability of roughness on the runoff hydrographs have been investigated in this study for watersheds consisting of two roughness surface elements: (1) butyl surface, and (2) surface of 1-1/2" diameter gravel with the density of 20 lbs/yd^2. These two surface elements have significantly different roughnesses. For a watershed with alternate equal width strips of butyl and gravel surface elements, it was shown in this study that the concept of an equivalent uniform roughness surface can be applied, and the hydrographs well simulated by assuming the watershed as having a uniform roughness, when the width of strips is less than or equal one sixth of total flow length. As stated in Section 1.2, the size of strips in applying the concept of an equivalent uniform roughness surface is related to the difference between two roughnesses and to relative weights of two roughnesses. Further investigations might search for the relationship among these three factors.

A runoff hydrograph from a watershed with surface depressions may be much different from a hydrograph from a surface having the upright obstructions. The rising limb of the hydrograph starts late and the flow rapidly increases after depressions are completely filled. A further investigation may search for an adequate hydraulic resistance model for a surface with depressions and determine the effects of its spatial variability on hydrographs. This kind of surface often exists in the area of contour cropping where the contour ridges of farming run along the contour lines of the topography.

In application of the methods used in this study for simulation of hydrographs, the time of travel of overland flow for the watershed with various vegetation strips can be estimated. Consequently, the effect of vegetation management on flow retardation may be investigated. This would provide some useful information for evaluating the effects of vegetation buffer strips in controlling the non-point sources of pollution.

REFERENCES

1. Agricultural Research Service, USDA, 1963, Hydrologic Data for Experimental Agricultural Watershed in the United States, 1956-1959, Miscellaneous Publication No. 945, November.

2. Brazil, Larry E., 1976, A Water Quality Model of Overland Flow, in partial fulfillment of the requirements for the degree of Master of Science, Colorado State University, CET 75-76 LEB 28.

3. Chen, Cheng-Lung, 1976, Flow Resistance in Broad Shallow Grassed Channels, Journal of Hydraulics Division, ASCE, Vol. 102, HY3, March.

4. Chow, Ven Te, 1959, Open Channel Hydraulics, McGraw-Hill, New York.

5. Corey, A. T., 1977, Mechanics of Heterogeneous Fluids in Porous Media, Water Resources Publications, Fort Collins, Colorado (259 pages).

6. Correia, Mario L., 1972, An Experimental Study of the Mean Characteristics of Steady Spatially Varied Overland Flow under Rainfall Impact, in fulfillment of requirement for the course CE-795-C Special Study in Hydrology and Water Resources, Colorado State University, ID-71-72-74.

7. Dickinson, W. T., Holland, M. E., and Smith, G. L., 1967, An Experimental Rainfall-Runoff Facility, Hydrology Paper No. 25, Colorado State University, September.

8. Emmett, William W., 1970, The Hydraulics of Overland Flow on Hillslopes, Geological Survey Professional Paper 662-A, United States Government Printing Office, Washington, D. C.

9. Himmelblau, D. M., 1972. Applied Nonlinear Programming, McGraw-Hill, New York.

10. Henderson, F. M., and Wooding, R. A., 1964, Overland Flow and Groundwater Flow from a Steady Rainfall of Finite Duration, Journal of Geophysical Research, Vol. 69, No. 8, April.

11. Ibbitt, R. P., 1970, Systematic Parameter Fitting for Conceptual Models of Catchment Hydrology, Ph.D. Thesis, Imperial College, University of London.

12. Izzard, C. F., 1944, The Surface-Profile of Overland Flow, Transactions, American Geophysical Union, Vol. 25.

13. Kibler, David F., and Woolhiser, David A., 1970, The Kinematic Cascade as a Hydrologic Model, Colorado State University, Hydrology Paper No. 39.

14. Kouwen, N., and Unny, T. E., 1973, Flexible Roughness in Open Channels, Journal of Hydraulics Division, ASCE, Vol. 102, HY5, May.

15. Kowobari, Timothy S., Rice, Charles E., and Garton, James E., 1970, Effect of Roughness Elements on Hydraulic Resistance for Overland Flow, Paper No. 70-714, for presentation at the 1970 Winter Meeting, ASCE, December.

16. Kruse, E. G., Huntley, C. W., and Robinson, A. R., 1965, Flow Resistance in Simulated Irrigation Borders and Furrows, Conservation Research Report No. 3, Agricultural Research Service, USDA in cooperation with Colorado Agricultural Experiment Station.

17. Li, Ruh-Ming and Shen, Hsieh W., 1973, Effect of Tall Vegetation on Flows and Sediment, Journal of Hydraulics Division, ASCE, Vol. 99, HY5, May.

18. Parson, D. A., 1949, Depths of Overland Flow, SCS-TP-82, Soil Conservation Service Research, USDA in cooperation with the Alabama Agricultural Experiment Station.

19. Petryk, S., 1969, Drag on Cylinders in Open Channel Flow, thesis presented to Colorado State University in partial fulfillment of the requirement for Ph.D.

20. Phelps, H. O., 1970, The Friction Coefficient for Shallow Flows Over a Simulated Turf Surface, Water Resources Research, Vol. 6, No. 4.

21. Ree, W. O., 1939, Some Experiments on Shallow Flows Over a Grassed Slope, American Geophysical Union, Transactions, Vol. 20.

22. Ree, W. O., and Palmer, V. J., 1949, Flow of Water in Channels Protected by Vegetative Linings, USDA Soil Conservation Service, Technical Bulletin No. 967, February.

23. Rosenbrock, H. H., 1960, An Automatic Method for Finding the Greatest of Least Value of a Function, Computer Journal 3.

24. Rovey, Edward W., Woolhiser, David A., and Smith, Roger E., 1977, A Distributed Kinematic Model of Upland Watersheds, Hydrology Paper No. 93.

25. Schlichting, H., 1968, Boundary Layer Theory, 6th Ed., McGraw-Hill Co., New York.

26. Simons, D. B., and Li, R. M., 1976, Procedure for Estimating Model Parameters of Mathematical Model, Paper CER75-76DBS-RML22, Colorado State University, April.

27. Simons, D. B., Li, R. M., and Stevens, M. A., 1975, Development of Models for Predicting Water and Sediment Routing and Yield from Storms on Small Watershed, prepared for USDA Forest Service, Rocky Mountain Forest and Range Experiment Station, Paper CER74-75DBS-RML-MAS24, Colorado State University, August.

28. Simons, Daryl B., and Senturk, Fuat, 1977, Sediment Transport Technology, Water Resources Publications, Fort Collins, Colorado.

29. Singh, Vijay P., 1974, A nonlinear Kinematic Wave Model of Surface Runoff, in partial fulfillment of the requirement for Ph.D., Colorado State University, May.

30. Woo, D. C., and Brater, E. F., 1961, Laminar Flow in Rough Rectangular Channels, Journal of Geophysical Research, Vol. 66, No. 12.

31. Wooding, R. A., 1965, A Hydraulic Model for the Catchment-Stream Problem, Journal of Hydrology, Vol. 3.

32. Woolhiser, David A., 1969, Overland Flow on a Converging Surface, Transactions, ASAE, Vol. 12, No. 4.

33. Woolhiser, David A., Holland, M. E., Smith, G. L., and Smith, R. E., 1971, Experimental Investigation of converging Overland Flow, Transactions, ASAE, Vol. 14, No. 4.

34. Woolhiser, David A., 1975, Simulation of Unsteady Overland Flow, Chapter 12, Unsteady Flow in Open Channels, Edited by K. Mahmood and V. Yevjevich, Water Resources Publication.

APPENDIX A

OUTFLOW DISCHARGE CORRECTION

The outflow systems of the rectangular section and the conic section are shown in Fig. A-1(A) and (C). The outflow hydrograph observed at the end of the measuring flumes should be corrected for storage, so that it becomes the outflow hydrograph at the end of the experimental watershed. Since rectangular watershed has a converging section between the watershed and the flume, the corrections for both the discharge at the converging section and the flume are required. The conic section required only the correction at the flume.

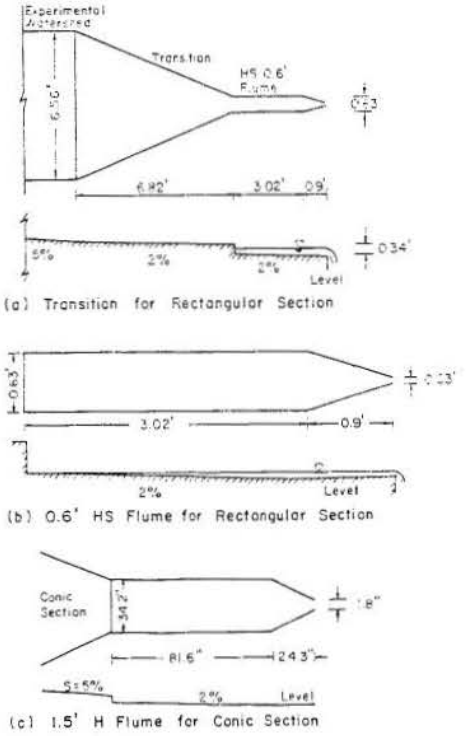

(a) Transition for Rectangular Section

(b) 0.6' HS Flume for Rectangular Section

(c) 1.5' H Flume for Conic Section

Figure A-1. Outflow systems of rectangular and conic section.

A.1 Correction of Discharge for Storage Effect in Flume

The most common reservoir flood routing method is used for this correction, namely

$$I \cdot \Delta t - 0 \cdot \Delta t = \Delta S$$

$$\frac{1}{2} (I_1 + I_2) \Delta t - \frac{1}{2} (0_1 + 0_2) \Delta t = S_2 - S_1$$

$$I_2 = \frac{2}{\Delta t} (S_2 - S_1) + 0_1 + 0_2 - I_1 \qquad (A\text{-}1)$$

in which, I = the inflow rate into the reservoir, 0 = the outflow rate from the reservoir, S = the storage, Δt = the constant time increment in routing, and subscripts 1 and 2 refer to the beginning and the end of a time increment. The difficulties in routing from the downstream hydrograph to the upstream hydrograph are that the routed hydrograph will oscillate strongly if there is a slight oscillation in the relationship of storage versus time due to measurement errors. The storage should be smoothed out first by following Eq. (A-2), as schematically shown in Fig. A-2. Let the subscript n be the index of the time increment,

$$S'_n = \frac{1}{2} \left[\frac{1}{2} (S_{n-1} + S_n) + \frac{1}{2} (S_n + S_{n+1})\right] \qquad (A\text{-}2)$$

with S_n = the storage in the flume from the observed stage in the flume, and S'_n = the corrected storage to be used in the routing. The error in estimation of the inflow at the beginning portion will also cause an exaggeration of the oscillation in the latter portion. In order to avoid an exaggeration of this oscillation, the average of the two successively computed discharges was taken for computation in the next step as follows. The basic equations are:

$$2\Delta t \cdot \frac{1}{2} (I_{n-1} + I_{n+1}) - 2\Delta t \cdot \frac{1}{2} (0_{n-1} + 0_{n+1}) =$$

$$S_{n+1} - S_{n-1}$$

$$I_{n+1} = \frac{1}{\Delta t} (S_{n+1} - S_{n-1}) + 0_{n-1} + 0_{n+1} - I_{n-1}$$

$$I_n = \frac{1}{2} (I_{n-1} + I_{n+1}). \qquad (A\text{-}3)$$

Assuming $I_o = 0$, I'_n = the computed inflow rate before taking the average, I_n = the inflow rate after taking average and to be used in the routing, the steps of computations are as follows:

I_1: $I'_2 = \frac{1}{\Delta t} (S_2 - S_o) + 0_o + 0_2 - I_o$

$I_1 = \frac{1}{2} (I_o - I'_2)$

I_2: $I'_3 = \frac{1}{\Delta t} (S_3 - S_1) + 0_1 + 0_3 - I_1$

$I_2 = \frac{1}{2} (I_1 + I'_3)$

I_3: $I'_4 = \frac{1}{\Delta t} (S_4 - S_2) + 0_2 + 0_4 - I_2$

$I_3 = \frac{1}{2} (I_2 + I'_4)$

and so on. The computation steps are schematically shown in Fig. A-2. The inflow hydrograph so obtained will be the outflow hydrograph of the watershed at the upstream end of the flume.

A.2 Correction of Time Lag in Converging Section

Because the converging section had a cover on it, there was no lateral inflow into the section. The inflow from the upstream end of the converging

section went over the dry surface at the beginning. This caused a surge wave at the very beginning of the hydrograph, for which the analytical solution of the kinematic wave equations may not be applied.

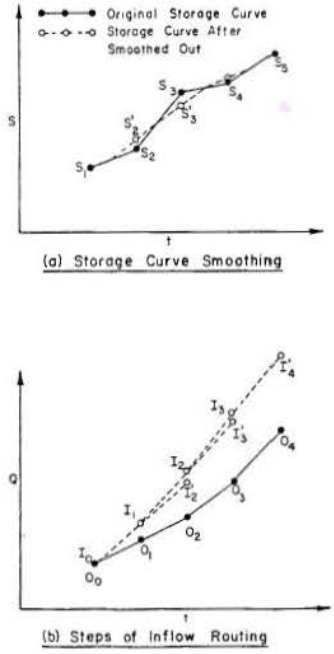

Figure A-2. Schematical representation of storage curve smoothing and steps of inflow routing.

However, considering the whole hydrograph, the analytical solution may be applied because the errors at the very beginning will not affect the total hydrograph very much. The time lag was divided into two parts: the time lag in the converging section, and the time lag in the upstream part of the flume where no storage occurred.

Converging Section

The converging section was approximated by a conic section as shown in Fig. A-3(A). The equation of continuity for the converging section with zero lateral inflow is

$$\frac{\partial h}{\partial t} + \frac{\partial (uh)}{\partial x} = \frac{uh}{(L_o - x)} \qquad \text{(A-4)}$$

and

$$u = \alpha h^{m-1}. \qquad \text{(A-5)}$$

in which, h = the water depth, u = the velocity, α and m = constants, and L_o and x = defined in Fig. A-3(B). The characteristic equations are

$$\frac{dx}{dt} = \alpha m h^{m-1} \qquad \text{(A-6)}$$

and

$$\frac{dh}{dt} = \frac{\alpha h^m}{L_o - x} . \qquad \text{(A-7)}$$

The analytical solution shown above can be employed only when α and m are constant over the surface. Since the laminar-turbulent friction law was used for determining α and m, the length in the x-direction

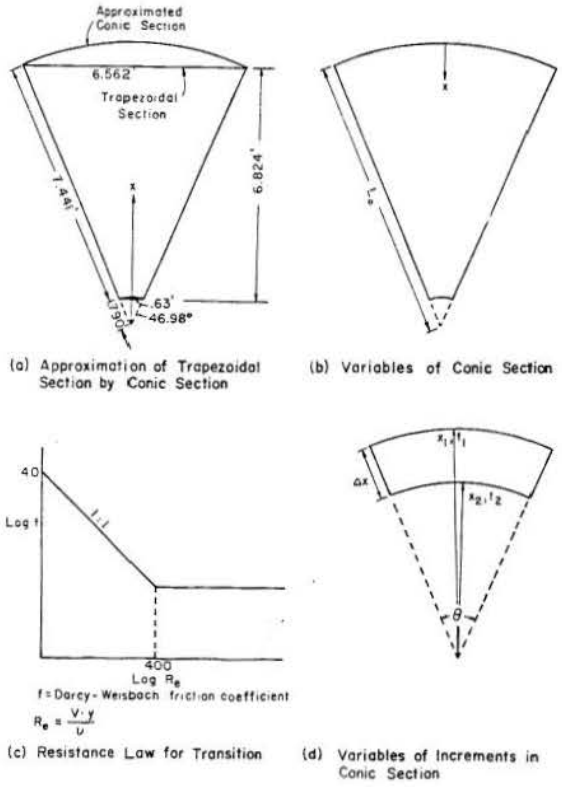

Figure A-3. Resistance law used in the transition for rectangular section.

was divided into small segments for integration. For convenience, $(L_o - x)$ in the above equation is denoted by x in the following computation as shown in Fig. A-3(D). The characteristic equations are:

$$\frac{dx}{dt} = -\alpha m h^{m-1} \qquad \text{(A-8)}$$

$$\frac{dh}{dt} = \frac{\alpha h^m}{x} \qquad \text{(A-9)}$$

$$\frac{dh}{dx} = -\frac{h}{mx} \qquad \text{(A-10)}$$

Taking a section between x_1 and x_2 and integrating Eq. (A-10), then:

$$\frac{h_1^m}{h_2^m} = \frac{x_2}{x_1} \text{ or } x_1 h_1^m = x_2 h_2^m = \text{constant through x along the character line.}$$

$$\alpha\left(\frac{2\pi x_1 \theta}{360}\right) h_1^m = \alpha\left(\frac{2\pi x_2 \theta}{360}\right) h_2^m = \text{Total discharge} = Q_t \qquad \text{(A-11)}$$

Let

$$K = x_1 h_1^m = x_2 h_2^m = \frac{Q_t}{\alpha} \cdot \frac{360}{2\pi\theta} = \frac{Q_t}{C\alpha}, \text{ and } C = \frac{2\pi\theta}{360}, \tag{A-12}$$

$$h = \left(\frac{K}{x}\right)^{1/m} .$$

Substituting Eq. (A-12) into Eq. (A-8), then

$$\frac{dx}{dt} = -\alpha m \left(\frac{K}{x}\right)^{\frac{m-1}{m}}, \quad dt = -\frac{1}{\alpha m K^{\frac{m-1}{m}}} x^{\frac{m-1}{m}} dx$$

$$\int_{t_1}^{t_2} t\, dt = -\frac{1}{\alpha m K^{\frac{m-1}{m}}} \int_{x_2}^{x_2} x^{\frac{m-1}{m}} dx$$

$$t_2 - t_1 = -\frac{1}{m\alpha K^{\frac{m-1}{m}}} \cdot \frac{m}{2m-1} \left(x_2^{\frac{2m-1}{m}} - x_1^{\frac{2m-1}{m}}\right)$$

$$= \frac{1}{(2m-1)\,\alpha K^{\frac{m-1}{m}}} \left(x_1^{\frac{2m-1}{m}} - x_2^{\frac{2m-1}{m}}\right)$$

$$= \frac{1}{(2m-1)\alpha^{1/m}(Q_t/C)^{\frac{m-1}{m}}} \left(x_1^{\frac{2m-1}{m}} - x_2^{\frac{2m-1}{m}}\right)$$

For each segment, the lag time is

$$\Delta t = \frac{1}{(2m-1)\alpha^{1/m}(Q_t/C)^{1-\frac{1}{m}}} \left(x_1^{\frac{2m-1}{m}} - x_2^{\frac{2m-1}{m}}\right) . \tag{A-14}$$

For an outflow discharge Q_t the total time lag in the converging section may be obtained by adding Δt in segments.

Rectangular Section

Because of the concentration of flow in the flume, only the turbulent friction law is used. The characteristic equations for the rectangular section are:

$$\frac{dx}{dt} = \alpha m\, h^{m-1} = \alpha m \left(\frac{Q_t}{W \cdot \alpha}\right)^{\frac{m-1}{m}} = \alpha^{\frac{1}{m}} m \left(\frac{Q_t}{W}\right)^{1-\frac{1}{m}}$$

$$\Delta t = L_o \frac{1}{m\alpha^{1/m}\left(\frac{Q_t}{W}\right)^{1-\frac{1}{m}}} .$$

with W = the width of flume, L_o = the length of flume excluding the part which has storage, and t = the time lag in flume. Computations showed that the time lag in the upstream part of the flume is very small and negligible due to the concentration of the flow.

Key Words: Watershed Response, Hydrographs, Surface Roughness, Kinematic Flow Theory, Modeling Hydrographs.

Abstract: The selection of a hydraulic resistance model for surfaces of uniform roughness and estimation of model parameters for hydrograph simulation for watersheds with nonuniform roughness are the subjects treated in this paper.

A three-parameter model for hydraulic resistance is designed by assuming a flow through a set of parallel random-width channels with equal water depth. Numerical solutions of kinematic wave equations of overland flow are used in simulating the outflow hydrographs. Two-parameter and three-parameter models are used for optimization of model parameters. These two

Key Words: Watershed Response, Hydrographs, Surface Roughness, Kinematic Flow Theory, Modeling Hydrographs.

Abstract: The selection of a hydraulic resistance model for surfaces of uniform roughness and estimation of model parameters for hydrograph simulation for watersheds with nonuniform roughness are the subjects treated in this paper.

A three-parameter model for hydraulic resistance is designed by assuming a flow through a set of parallel random-width channels with equal water depth. Numerical solutions of kinematic wave equations of overland flow are used in simulating the outflow hydrographs. Two-parameter and three-parameter models are used for optimization of model parameters. These two

Key Words: Watershed Response, Hydrographs, Surface Roughness, Kinematic Flow Theory, Modeling Hydrographs.

Abstract: The selection of a hydraulic resistance model for surfaces of uniform roughness and estimation of model parameters for hydrograph simulation for watersheds with nonuniform roughness are the subjects treated in this paper.

A three-parameter model for hydraulic resistance is designed by assuming a flow through a set of parallel random-width channels with equal water depth. Numerical solutions of kinematic wave equations of overland flow are used in simulating the outflow hydrographs. Two-parameter and three-parameter models are used for optimization of model parameters. These two

Key Words: Watershed Response, Hydrographs, Surface Roughness, Kinematic Flow Theory, Modeling Hydrographs.

Abstract: The selection of a hydraulic resistance model for surfaces of uniform roughness and estimation of model parameters for hydrograph simulation for watersheds with nonuniform roughness are the subjects treated in this paper.

A three-parameter model for hydraulic resistance is designed by assuming a flow through a set of parallel random-width channels with equal water depth. Numerical solutions of kinematic wave equations of overland flow are used in simulating the outflow hydrographs. Two-parameter and three-parameter models are used for optimization of model parameters. These two

models are compared by differences of simulated hydrographs with optimized parameters and observed hydrographs at the Rainfall-Runoff Facility at Colorado State University. The results show that the three-parameter model is better over a wide range of discharge than the two-parameter model. When only the flood flows are important in analysis, the two-parameter model is simpler and less expensive to implement.

Reference: Wu, Yao-Huang, Yevjevich, Vujica, and Woolhiser, David A.; Colorado State University, Hydrology Paper No. 96 (October 1978), Effects of Surface Roughness and its Spatial Distribution on Runoff Hydrographs.

models are compared by differences of simulated hydrographs with optimized parameters and observed hydrographs at the Rainfall-Runoff Facility at Colorado State University. The results show that the three-parameter model is better over a wide range of discharge than the two-parameter model. When only the flood flows are important in analysis, the two-parameter model is simpler and less expensive to implement.

Reference: Wu, Yao-Huang, Yevjevich, Vujica, and Woolhiser, David A.; Colorado State University, Hydrology Paper No. 96 (October 1978), Effects of Surface Roughness and its Spatial Distribution on Runoff Hydrographs.

models are compared by differences of simulated hydrographs with optimized parameters and observed hydrographs at the Rainfall-Runoff Facility at Colorado State University. The results show that the three-parameter model is better over a wide range of discharge than the two-parameter model. When only the flood flows are important in analysis, the two-parameter model is simpler and less expensive to implement.

Reference: Wu, Yao-Huang, Yevjevich, Vujica, and Woolhiser, David A.; Colorado State University, Hydrology Paper No. 96 (October 1978), Effects of Surface Roughness and its Spatial Distribution on Runoff Hydrographs.

models are compared by differences of simulated hydrographs with optimized parameters and observed hydrographs at the Rainfall-Runoff Facility at Colorado State University. The results show that the three-parameter model is better over a wide range of discharge than the two-parameter model. When only the flood flows are important in analysis, the two-parameter model is simpler and less expensive to implement.

Reference: Wu, Yao-Huang, Yevjevich, Vujica, and Woolhiser, David A.; Colorado State University, Hydrology Paper No. 96 (October 1978), Effects of Surface Roughness and its Spatial Distribution on Runoff Hydrographs.

LIST OF PREVIOUS 25 PAPERS

No. 71 Determination of Urban Watershed Response Time, by E. F. Schulz, December 1974.

No. 72 generation of Hydrologic Samples, Case Study of the Great Lakes, by V. Yevjevich, May 1975.

No. 73 Extraction of Information on Inorganic Water Quality, by William L. Lane, August 1975.

No. 74 Numerical Model of Flow in Stream-Aquifer System, by Catherine E. Kraeger Rovey, August 1975.

No. 75 Dispersion of Mass in Open-Channel Flow, by William W. Sayre, August 1975.

No. 76 Analysis and Synthesis of Flood Control Measures, by Kon Chin Tai, September 1975.

No. 77 Methodology for the Selection and Timing of Water Resources Projects to Promote National Economic Development, by Wendim-Agegnehu Lemma, August 1975.

No. 78 Two-Dimensional Mass Dispersion in Rivers, by Forrest M. Holly, Jr., September 1975.

No. 79 Range and Deficit Analysis Using Markov Chains, by Francisco Gomide, October 1975.

No. 80 Analysis of Drought Characteristics by the Theory of Run, by Pedro Guerrero-Salazar and Vujica Yevjevich, October 1975.

No. 81 Influence of Simplifications in Watershed Geometry in Simulation of Surface Runoff, by L. J. Lane, D. A. Woolhiser and V. Yevjevich, January 1976.

No. 82 Distributions of Hydrologic Independent Stochastic Components, by Pen-chih Tao, V. Yevjevich and N. Kottegoda, January 1976.

No. 83 Optimal Operation of Physically Coupled Surface and Underground Storage Capacities, by Dragoslav Isailovic, January 1976.

No. 84 A Salinity Management Strategy for Stream-Aquifer Systems, by Otto J. Helweg, and J. Labadie, February 1976.

No. 85 Urban Drainage and Flood Control Projects Economic, Legal and Financial Aspects, by Neil S. Grigg, Leslie H. Botham, Leonard Rice, W. J. Shoemaker, and L. Scott Tucker, February 1976.

No. 86 Reservoir Capacity for Periodic-Stochastic Input and Periodic Output, by Kedar Nath Mutreja, September 1976.

No. 87 Area-Deficit-Intensity Characteristics of Droughts, by Norio Tase, October 1976.

No. 88 Effect of Misestimating Harmonics in Periodic Hydrologic Parameters, by K. L. Bullard, V. Yevjevich, and N. Kottegoda, November 1976.

No. 89 Stochastic Modeling of Hydrologic, Intermittent Daily Processes, by Jerson Kelman, February 1977.

No. 90 Experimental Study of Drainage Basin Evolution and Its Hydrologic Implications, by Randolph S. Parker, June 1977.

No. 91 A Model of Stochastic Structure of Daily Precipitation Series Over an Area, by C. W. Richardson, July 1977.

No. 92 Effects of Forest and Agricultural Land Use on Flood Unit Hydrographs, by Wiroj Sangvaree and Vujica Yevjevich, July 1977.

No. 93 A Distributed Kinematic Model of Upland Watersheds, by Edward W. Rovey, David A. Woolhiser and Roger E. Smith, July 1977.

No. 94 Fluctuations of Wet and Dry Years, an Analysis by Variance Spectrum, by Vujica Yevjevich, August 1977.

No. 95 Mathematical Modeling of Sediment Deposition in Reservoirs, by Jose Luis Lopez S., July 1978.